Reports Control Symbol
OSD 1366

Technical Report ECOM-02246-5

November 1967

MONOPOLE ANTENNA WITH A FINITE GROUND PLANE IN THE PRESENCE OF AN INFINITE GROUND

Report No. 5
Supplemental Technical Report

Contract No. DA 28-043 AMC-02246(E)

DA Project No. 5A6-79191-D902-02-24

Prepared by

Sang-Bin Rhee

COOLEY ELECTRONICS LABORATORY
Department of Electrical Engineering
The University of Michigan
Ann Arbor, Michigan

for

U.S. Army Electronics Command, Fort Monmouth, N.J.

DISTRIBUTION STATEMENT

[redacted]

ABSTRACT

An experimental and theoretical study was made of a monopole antenna mounted on a finite ground plane located above an infinite ground. Circular flat discs and hemispheres were used for the finite ground planes. Experiments were conducted over a 6 to 1 frequency range, with the length of monopole antenna fixed at a quarter wavelength at the upper end of the frequency band. The radii of finite ground planes used for experiments were generally less than a quarter wavelength.

Input impedances were measured as a function of frequency at the base of the antenna, using as variables the radius and the locations of the ground plane with respect to an infinite ground below. Scale models were used to obtain measurements of radiation patterns and antenna current distributions. Results of these measurements are presented graphically.

A theoretical analysis was also made of a monopole with a hemispherical ground plane on an infinite ground. Far-zone electromagnetic fields were calculated as a function of both the ground plane radius and the frequency. Radiation resistances were also calculated.

The results of the study indicate that the radiation resistance of an electrically short antenna may be increased significantly by locating it on a small ground plane above the infinite ground, rather than directly on the infinite ground. This conclusion opens the way for

a more efficient utilization of receiving and transmitting antennas on ground-based vehicles. The impedance characteristics of the antenna system are such as to facilitate its operation over a broad frequency range.

FOREWORD

This report was prepared by the Cooley Electronics Laboratory of The University of Michigan under United States Army Electronics Command Contract No. DA 28-043-AMC-02246(E), Project No. 5A6-79191-D902-02-24, "Improved Antenna Techniques Study."

The research under this contract consists in part of an investigation to develop highly efficient remotely tuned impedance matching coupling networks for electrically short monopoles.

The material reported herein represents a summary of a theoretical and experimental study which was made to determine the input impedance and radiation characteristics of an electrically short monopole over a small ground plane located at various distances above natural ground.

TABLE OF CONTENTS

TABLE OF CONTENTS (Cont.)

LIST OF TABLES

LIST OF SYMBOLS

Symbol	Meaning	First Appeared
δ	electromagnetic waves depth of penetration	10
Z_o	characteristic impedance of a transmission line	14
Z_L	load impedance	14
Z_d	impedance at a distance d from a load	14
λ	free space wavelength	14
d	distance measured from load	14
σ	electric conductivity	21
a	i) distance between an infinite ground plane and a finite ground plane ii) radius of a semisphere	25
R_r	radiation resistance	39
I	input current	39
$\bar{E}$	electric field intensity vector	39
$\bar{H}$	magnetic field intensity vector	39
$\bar{H}^*$	complex conjugate of $\bar{H}$	39
Re	Real part of	39
R_g	ground terminal resistance	40

LIST OF SYMBOLS (Cont.)

Symbol	Meaning	First Appeared
R_t	resistance of tuning units	40
R_i	resistance of equivalent insulation loss	40
R_ω	resistance of equivalent conductor loss	40
R_m	transmission line losses	40
$\bar{i}$	surface current density	42
∇	gradient operator	41
$\frac{\partial}{\partial}$	partial differential operator	41
t	time	41
ω	radian frequency	41
∇ x	curl operator	41
$\nabla \cdot$	divergence operator	41
ρ	electric charge density	41
∇^2	Laplacian operator	41
ϵ	permittivity	41
μ	permeability	41
j	$\sqrt{-1}$	41
i_z	component of surface current density i	48
E_o	electric field intensity on the surface of a conductor	41

LIST OF SYMBOLS (Cont.)

Symbol	Meaning	First Appeared
τ	$\sqrt{j\omega\mu\sigma}$	42
f	frequency	42
J_z	current density per unit length	43
Z_s	surface impedance	43
R_s	surface resistance	43
L_i	internal inductance of a plane conductor	43
r	radial distance in a cylindrical coordinate	45
$\hat{x}, \hat{y}, \hat{z}$	unit vectors	45
A	constant, area of a loop	46
J_n	Bessel function of order n	46
Ber(v)	real part of $J_0(\frac{v}{\sqrt{j}})$	47
$\oint$	closed line integral	48
$\overline{B}^i$	incident magnetic flux density vector	56
$\overline{B}^r$	reradiated magnetic flux density vector	56
c	speed of light	56
e	induced voltage	57
k	free space wave number	57
h_b	effective height of a loop antenna	57

LIST OF SYMBOLS (Cont.)

Symbol	Meaning	First Appeared
Y_o	admittance	57
$d\ell$	incremental length	57
I^o	zero phase sequence current	57
$I^{(1)}$	first phase sequence current	58
h_e	effective height of a dipole antenna	58
K_E	electric sensitivity	59
K_B	magnetic sensitivity	59
D	diameter of a loop	59
$\propto$	proportional to . . .	60
Φ_m	magnetic scalar potentials	111
R', θ', ϕ'	spherical coordinates expressing source points	113
$\bar{N}$	electric radiation vector	115
$\bar{M}$	magnetic radiation vector	115
$\hat{R}, \hat{\theta}, \hat{\phi}$	spherical unit vectors	115
$\bar{N}_t$	transverse electric radiation vector	115
Φ	a scalar function	116
$\bar{M}_t$	transverse magnetic radiation vector	117
$\bar{P}, \bar{Q}$	vector functions of position	117

LIST OF SYMBOLS (Cont.)

Symbol	Meaning	First Appeared
S	surface	117
$\bar{K}_m$	fictitious magnetic current density	125
σ_s	surface electric charge density	125
ϕ	a scalar function	120
r	i) distance between a source point and an observation point	118
R, θ, ϕ	spherical coordinates	118
$\bar{J}_m$	fictitious magnetic current density	118
ρ_m	fictitious magnetic charge density	118
$\bar{E}'$	electric field intensity arising from the actual current and charge	108
$\bar{H}'$	magnetic field intensity arising from the actual current and charge	108
$\bar{E}''$	electric field intensity arising from the fictitious magnetic current and charge	108
$\bar{H}''$	magnetic field intensity arising from the fictitious magnetic current and charge	108
$\bar{A}$	electric vector potential	109
Φ	electric scalar potential	109
G	free space Green's function	110
A_m	magnetic vector potential	111

LIST OF SYMBOLS (Cont.)

Symbol	Meaning	First Appeared
$F(\theta)$	a scalar function	132
u	a scalar function	138
$P_n(\cos\theta)$	Legendre polynomials of order n	138
$\rho_n(kR)$	weighted spherical Hankel function of the second kind with order n	138
$H_n^{(2)}(kR)$	Hankel function of the second kind with order n	139
$h_n^{(2)}(kR)$	spherical Hankel function of the second kind with order n	139
$j_n(kR)$	spherical Bessel function with order n	151
$Y_n(\theta,\phi)$	spherical surface harmonics of degree n	151
!	factorial	151
c_m, d_m	constant coefficients of an infinite series	152
η	temporary variable	154
$P_n^m(\cos\theta)$	associated Legendre functions of the first kind, order n , degree m	154
δ_n	delta function	159

LIST OF ILLUSTRATIONS

LIST OF ILLUSTRATIONS (Cont.)

LIST OF ILLUSTRATIONS (Cont.)

LIST OF ILLUSTRATIONS (Cont.)

LIST OF ILLUSTRATIONS (Cont.)

LIST OF APPENDICES

CHAPTER I

INTRODUCTION

Monopole and dipole antennas over an infinitely large conducting ground plane are two of the oldest types of antennas being used. Their performance characteristics have been thoroughly studied in the past. However, the exact behavior of the antenna over a conducting ground plane of a finite size, and both antenna and finite ground plane over infinite ground with finite conductivity has not been studied heretofore.

1.1 Statement of the Problem

The purpose of this study is to investigate the properties of a vertical monopole antenna and a finite ground plane located above an infinite ground plane. Particular emphasis, in this investigation, is placed upon the study of antenna systems having circular ground planes in which the dimensions of both the ground-plane diameters and the ground-plane heights above infinite ground are smaller than the wavelengths of interest.

The investigation of the properties of this antenna system provides a basis for a detailed comparison with the conventional antenna system of a monopole antenna over an infinite ground plane and for determination of the relative advantages and limitations of this system. In addition, the results of this study will be applied to an investigation of possible performance improvement for a monopole antenna mounted

on a ground-based vehicle, since there is reason to believe that the antenna system proposed for study approximates the vehicular-mounted antenna.

1.2 Topics of Investigation

Since the purpose of this paper is to report a study of the vertical monopole with a finite ground plane in the presence of an infinite ground plane, the following topics are explored:

(1) The experimental measurement of the input impedance of the antenna was carried out over the frequency range of 5 MHz to 30 MHz (a 6 to 1 band) and as a function both of the ground-plane size and of the ground-plane location, relative to an infinite ground.

(2) The experimental measurement of current distribution on the antenna over the frequency range described above was carried out with the ground plane size and its location as the variables.

(3) The radiation pattern was measured and its dependence on the ground plane size and location was studied.

(4) A number of theoretical models was examined to determine a suitable approximation to the given system. Results obtained from the appropriate theoretical model was then compared with the experimental measurements.

One of the theoretical models which was studied is a monopole placed on a semi-spherical conductor, as shown in Fig. 1.

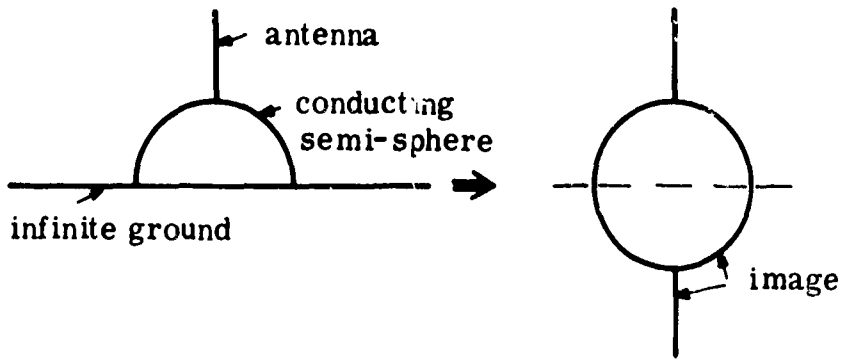

Fig. 1.1. Theoretical models

1.3 Review of the Literature

Many studies of the properties of vertical monopole antennas mounted both on infinite and on finite ground planes have previously been reported in the literature.

Bardeen (Ref. 1), in 1930, studied the diffraction of a circularly symmetrical electromagnetic wave by a circular disc of infinite conductivity. The result of his study has been used in determining the power flow into the earth below a vertical antenna that is grounded by a circular disc lying on the surface. In 1945, Brown and Woodward (Ref. 2), in an experimental study, measured the resistance and reactance of a cylindrical antenna operated against ground. The ground immediately below the antenna had a buried metallic screen of a finite size whose top surface was flush with the rest of the natural ground. A particular emphasis was given to a study of impedance behavior as a function of the antenna length to diameter ratio. Terminal conditions such as capacitance of the base of the antenna to ground were considered.

Later, Meier and Summers (Ref. 2) (1949) performed an experimental study of the impedance characteristics of vertical antennas mounted on finite ground planes. Leitner and Spence (Ref. 3) (1951) confirmed some of these experimental results through the theoretical study of a quarter-wavelength monopole on a finite, circular-disc ground plane. They assumed a sinusoidal current distribution to exist on the antenna. The results of this study showed a marked dependence of the antenna radiation resistance upon the diameter of the disc employed.

This dependence was particularly pronounced for small ground planes. In 1951, Storer (Ref. 4) used a variational method to readily obtain the expression for the dependence of the antenna impedance on the ground plane diameter. Tang (Ref. 5), in 1962, further studied the radiation pattern of this system by using the Babinet principle and the Wiener-Hopf technique.

In each of the above papers, the monopole was considered to be above a finite ground plane suspended in a free space with no direct effect from the infinite ground plane. Solutions by Leitner and Spence (Ref. 3) are mainly for the ground plane diameter smaller than the wavelength of interest. On the other hand, Tang and Storer's solutions can best be applied to the ground plane larger than ten wavelengths in diameter.

Wait and Pope (Ref. 6) in 1955, studied the input resistance of low-frequency, monopole antennas with the radial-wire earth system. The conducting wires were placed radially over the infinite natural ground and the changes in the input resistance ΔR from the input resistance of a monopole with an infinite conducting ground plane was calculated.

Brown (Ref. 7), in 1937, and Abbott (Ref. 8), in 1952, carried out earlier studies of the radial wire system.

1.4 Report Organization

(1) Chapter 2 contains the development of the experimental procedures for the input impedance measurement of the combined antenna and for the ground plane. The results of both actual and scale model

impedance measurements are included. Some discussion of the losses involved in the real part of the impedance is included.

(2) Chapter 3 contains a discussion of the technique for making current measurements on the antennas. Results of the measurements are shown in graphic form. Also, a comparison is made with the sinusoidal current distribution that is ordinarily assumed for a monopole antenna over an infinite conducting ground plane.

(3) Chapter 4 contains a discussion of the technique of radiation-pattern measurements. The pertinent assumptions made in obtaining these patterns are discussed. The results of the experiment are displayed graphically in polar plots that show the dependence of side-lobe levels on the ground plane size and its location.

(4) Chapter 5 contains an analysis of the theoretical model outlined in the topics of investigation. The far-field electric and magnetic fields are calculated for a given current distribution. The radiation resistances are also calculated for different antennas and the results are compared with the experimental ones. The radiation patterns obtained from this theory are also compared with the experimental results.

(5) Chapter 6 contains a summary and conclusions. Suggestions for further research are presented and practical applications using the result of this study are discussed.

The measurement procedure is described in Section 2.2 in which the steps taken to ensure accuracy in the measurement of small input resistances are given. The results determined using this procedure

are reported in some detail in Section 2.3, and compared with the input impedance of a monopole on infinite ground plane. Some additional measurements, which are set out in Section 2.4, were carried out with scale models (1) of the monopole over a small ground plane and both above the infinite ground and (2) of the monopole on a hemispherical ground plane above an infinite ground. Experimental measurements on the latter model were carried out and were compared with the theoretical results in Chapter 5.

CHAPTER II

INPUT IMPEDANCE MEASUREMENT

2.1 Introduction

This chapter contains a discussion of the experimental work carried out to measure the impedance of a monopole antenna that was a quarter-wavelength long at 30 MHz and that was located on a finite ground that, in turn, was located above natural ground. The impedance was measured as a function both of ground plane size and of ground plane location.

Theretofore, no extensive study of such a configuration has been reported. The input impedance characteristics of an antenna which is mounted on an infinite ground plane has been reported by Brown and Woodward (Ref. 2) for a wide variety of antenna lengths and diameters. Both experimental and theoretical studies have been conducted on the input impedance of a monopole antenna mounted on a finite ground plane, having diameters ranging down to wavelength. These studies did not, however, consider the effect of an infinite ground below the finite ground plane.

2.2 Experimental Measurement Procedure

Measurements were conducted with an antenna made of copper pipe one-quarter inch in diameter, which is a quarter-wavelength long at 30 MHz. The antenna was mounted on a non-conducting variable height test stand, shown in Fig. 2.1. With this stand, one

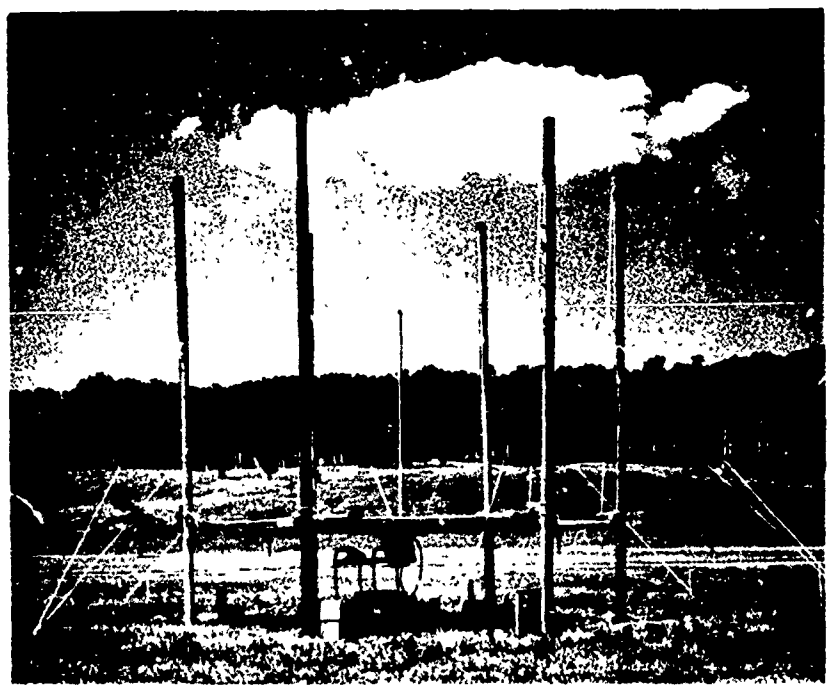

Fig. 2.1. Antenna on the variable height ground plane

can take measurements at heights of from zero to 5 meters above ground within continuous changes, and at the ground plane diameters of from zero to 5 meters.

In order to observe the impedance variation with size and location of the ground plane as measured in terms of wavelength, the size and the location of the finite ground plane was varied in four steps ranging from one-sixteenth of a wavelength to one-half wavelength at 30 MHz

The block diagram in Fig. 2. 2 shows the test set-up. The test equipment was placed just below the ground plane, to minimize the reflection of electromagnetic waves from the equipment. The entire experiment was conducted in a flat field where the nearest building was at least 10 wavelengths away from the test set-up. (See Fig. 2. 3).

Four sizes of ground plane were used in the experiments. A highly conducting 5 mil thick aluminum sheet was chosen for the ground plane material, after considering the skin depth at the frequencies where the measurements were taken.

Because of the provision for variable height and diameter, the total weight of the ground plane is an important factor in designing the experimental set-up. The depth of penetration, δ , for aluminum at frequencies of 5 MHz and 30 MHz is 1. 45 mils and 0. 594 mil, respectively. The thickness chosen was the smallest,but was much thicker than the skin depth in aluminum sheet ground plane. A 5 mil

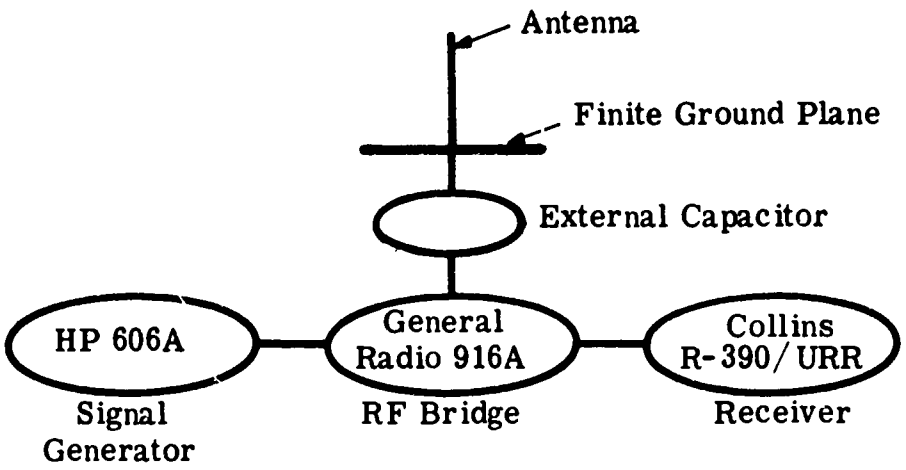

Fig. 2.2. Block diagram showing the impedance measurement set-up

Fig. 2.3. Antenna test site

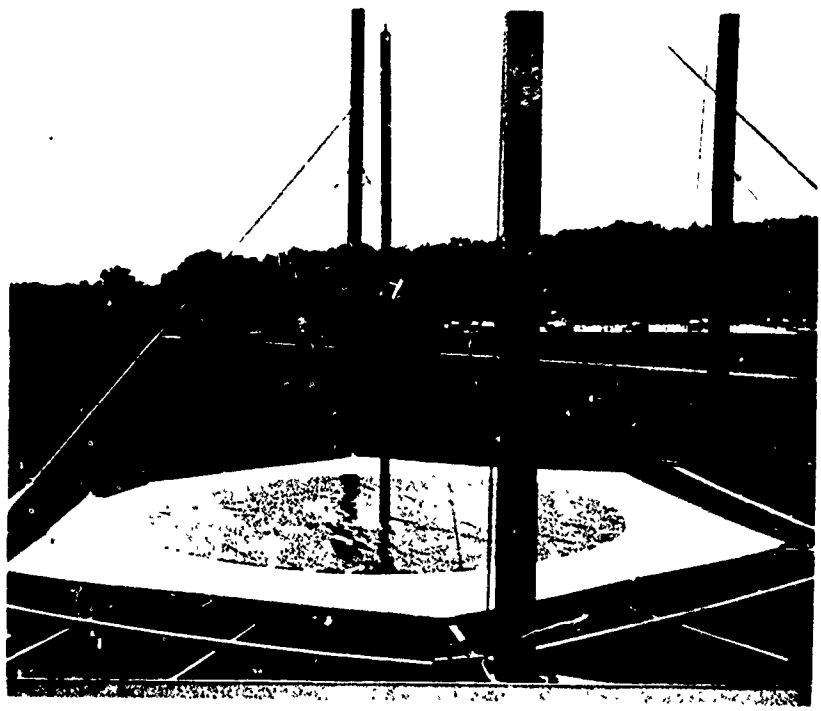

Fig. 2.4. A 2.5 meter monopole antenna on a 2.5 meter diameter ground plane supported by a styrofoam sheet

thick roll of aluminum sheeting is chosen for this purpose.

To support the flexible ground plane, a hexagonal structure was built and it was covered with 4 cm thick styrofoam sheet, which has a dielectric constant nearly equal to air.(Fig. 2.4). The ground plane was hoisted up to the proper height with ropes strung over rollers located at the top of the six supporting posts.

Initial measurements were carried out using a length of 50-ohm coaxial line to connect the base of the antenna to the impedance bridge. Readings taken with the bridge were referred to the antenna base by means of Smith charts. However, analysis shows appreciable inaccuracy to exist at low frequencies, where the antenna impedance Z_L is high. This inaccuracy was due to inaccuracies in the impedance transformation from the bridge terminals to the antenna base. In transmission line theory, an impedance Z_d at a point d meters away from the load impedance Z_L is

$$Z_d = Z_0 \frac{Z_L + j Z_0 \tan \frac{2\pi}{\lambda} d}{Z_0 + j Z_L \tan \frac{2\pi}{\lambda} d} \qquad (2.1)$$

where Z_0 is the characteristic impedance of the line and λ is the wavelength. If the load impedance is much greater than the characteristic impedance $Z_L >> Z_0$ at any frequency, then, this expression reduces to

$$Z_d = -jZ_0 \cot \frac{2\pi}{\lambda} d \qquad (2.2)$$

which is independent of the load impedance Z_L. Therefore, unless the characteristic impedance Z_0 is comparable in magnitude to Z_L, a small change in Z_L is difficult to detect for large load impedances. However, if d is chosen to be near zero then the changes in Z_L can be easily detected even if $Z_L >> Z_0$.

From equation 2.1

$$\Delta Z_d = Z_0 \frac{Z_0 + Z_0 \tan^2 \frac{2\pi}{\lambda} d}{(Z_0 + j Z_L \tan \frac{2\pi}{\lambda} d)^2} \Delta Z_L \qquad (2.3)$$

and therefore

$$\frac{\Delta Z_d}{Z_d} = \frac{\Delta Z_L}{Z_L} \frac{1}{\cos 2\theta + j\frac{1}{2}[\frac{Z_0}{Z_L} + \frac{Z_L}{Z_0}] \sin 2\theta} \qquad (2.4)$$

where

$$\theta = \frac{2\pi d}{\lambda}$$

In general,

$$\left| \frac{\Delta Z_d}{Z_d} \right| < \left| \frac{\Delta Z_L}{Z_L} \right| \qquad (2.5)$$

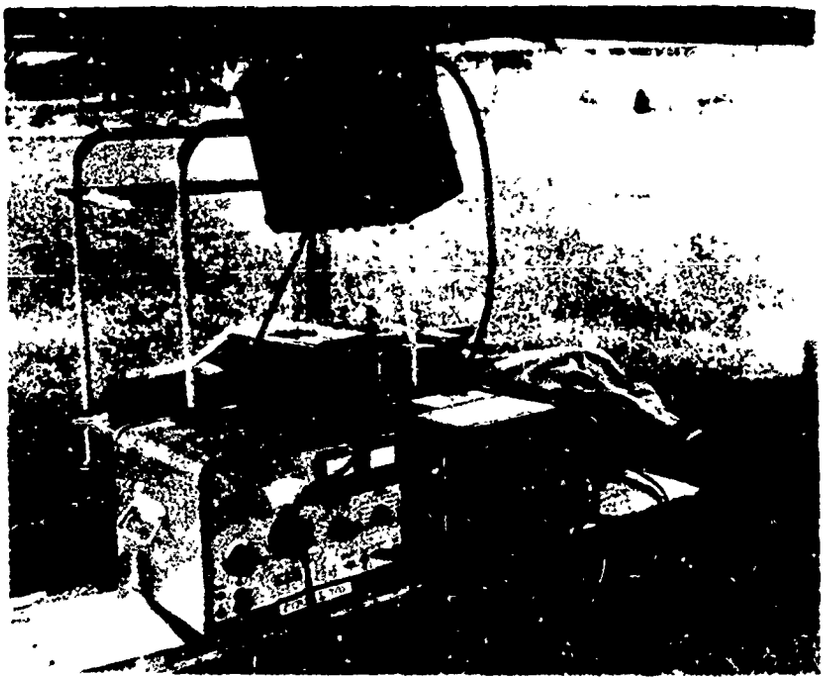

Fig. 2.5. Test equipment arrangement for the impedance measurement

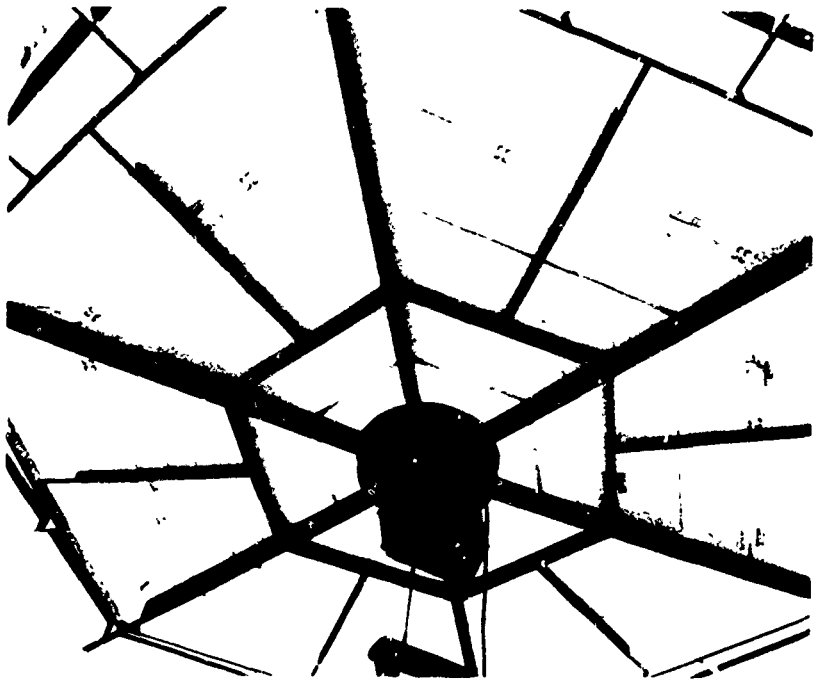

Fig. 2.6. Location of the impedance measurement bridge relative to the antenna base

whenever $Z_0 \approx Z_L$.

However, from the Eq. 2.3 when $\theta \approx 0$ or when $d \to 0$,

$$\frac{\Delta Z_d}{Z_d} \approx \frac{\Delta Z_L}{Z_L} \tag{2.6}$$

Equation 2.6 indicates that whenever the load impedance Z_L is much greater than the characteristic impedance of the line Z_0, the changes in Z_L can be detected much easier by choosing the line length $d = \frac{n\lambda}{2}$ where n is an integer.

The input impedance of a monopole above an infinite ground plane and that resonates at a certain frequency f_0 is capacitive at frequencies smaller than f_0. The magnitude of the capacitive reactance is a rapidly varying function of frequency.

Therefore, at the lower end of the frequency band, the technique of using a line extension to translate the impedance has a large error; and, for this reason, it was decided to modify the ground-plane support structure to accommodate the impedance bridge directly beneath the antenna base. This modification reduced the li length from the antenna to bridge to about 10 cm and thereby required a negligible impedance transformation. The set-up is shown in Figs. 2.5 and 2.6.

Measurements made using this set-up are hampered, however, by the limited range of the bridge. It is capable of recording only reactances of magnitude less than 5,000 ohms divided by the

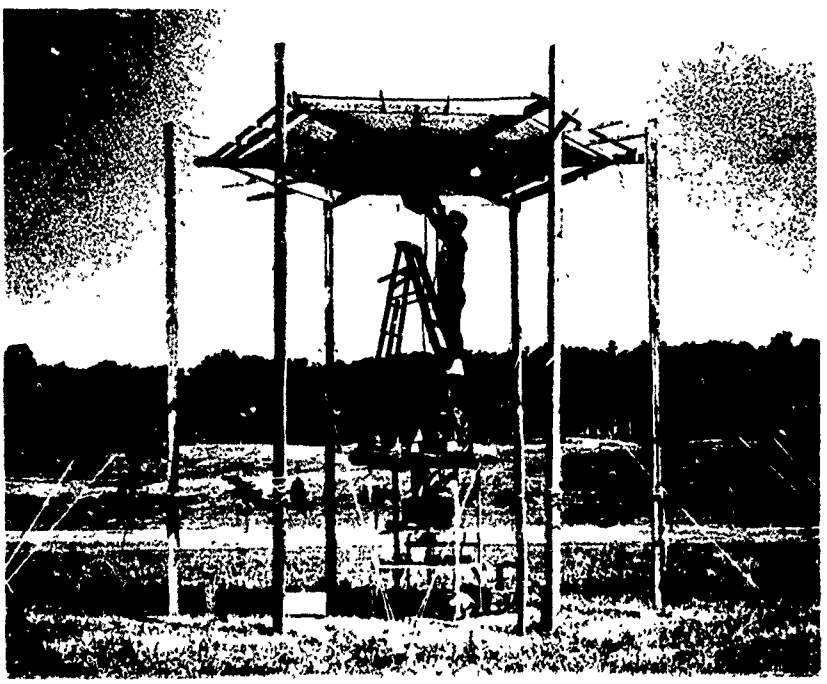

Fig. 2.7. Antenna located at 5 meters above the natural ground with 2.5 meter diameter ground plane

measurement frequency in megahertz. The antenna capacitive reactance at 5 MHz is greater than 1000 ohms. However, a high-Q capacitor of approximately 36 $\mu\mu$f placed in shunt with the antenna across its base terminals reduced the overall reactance to the range covered by the bridge, and was, therefore, used.

To obtain the input impedance of the antenna from the data obtained with the external shunt capacitor, the capacitor was itself carefully calibrated over the frequency range of 5 MHz to 30 MHz. Using this equipment, the capacitor impedance, with a nominal value of 36 $\mu\mu$f, was measured at every 2.5 MHz. The resistive component and the reactive component were carefully recorded at each frequency. These data were later used to obtain the actual input impedance of the antenna. The resistive component of the capacitor, over the frequency range of measurement, was always less than one-half of an ohm. In order to remove the errors of manual calculation, a computer program was written in which the calibration data for the external shunt capacitor and the measurement data of the experiment were fed in as raw data and the series resistive and reactive components of the input impedance were calculated on the IBM 7090 Computer.

The calibration of the capacitor was done periodically during the period of this experiment.

2.3 Scale Model Impedance Measurements

Since Maxwell's equations are linear ones, an electromagnetic structure that has certain properties at a given frequency

will have identical properties at another frequency nf, provided that all linear dimensions of the structure are scaled by the ratio 1/n. Therefore, an antenna design which operates over a certain range of frequencies can be made to operate over any other range of frequencies without additional re-design, if an exact scaling of dimensions is accomplished.

Aside from permitting one to transfer design relationships, it is convenient to use a practical size scale model for radiation pattern studies. Scaling is a relatively simple matter for most types of antennas. However, electromagnetic properties must also be scaled, as well as linear dimensions. The scaling factors are shown below.

Length	l	1/n
Frequency	f	nf
Permittivity	ϵ	same
Permeability	μ	same
Conductivity	σ	nσ

Table 2.1. Scale factors

Both the length and frequency can be scaled easily, the conductivity cannot. However, the conductivity scaling is important only through losses, and, since these are small for most antennas, the inability to scale the conductivity exactly is not a serious problem.

An exact scale model would retain the exact radiation pattern and input impedance of the full scale antenna. However, it is

not always possible to scale the model exactly, particularly since the transmission lines and screw fastenings, etc., cannot be scaled. Slight discrepancies in scaling will usually affect the impedance properties much more than they affect the radiation properties. The reason is that any discrepancies in scaling usually gives a rise in near-field effect which are attenuated out at far-field.

The model used for the antenna and ground plane studies here is intended, therefore, mainly for radiation pattern studies. The scale model is designed to be 1/40 of the original antenna system in linear dimensions. This scaling factor allows the new antenna and ground plane system to operate between 200 MHz and 1200 MHz, replacing the original 5 MHz to 30 MHz range.

As was pointed out previously, the principal difficulty in scaling lies with the conductivity. It is assumed here that the copper used for the scale model ground plane and the aluminum ground plane used for the full size antenna system both have infinitely large conductivity, so that the $n\sigma$ and σ are both infinitely large and therefore, that losses are negligible. Also, the large ground plane covered with aluminum foil to simulate the natural ground at the higher frequencies is assumed to influence the radiation pattern only to a minor extent.

Although the scale models are built mainly for radiation pattern studies, they will give qualitative information on the impedance as a function of frequency. The impedance measurements are, therefore, carried out in the laboratory on the scale model between 200

MHz and 1200 MHz using a HP 805A slotted line and a HP 415D VSWR meter for frequencies above 500 MHz, and a HP 803A VHF impedance bridge with a HP 417A VHF detector for the frequencies below 500 MHz. A difficulty of measuring an impedance Z_L of an unknown load when Z_L is much greater than the characteristic impedance of a transmission line Z_0 was pointed out in Section 2.2. As one way to eliminate this difficulty, the line length d from the position of the load Z_L to the measuring point Z_d was shortened. However, on the scale model simulating an infinitely large natural ground, the measurement equipment could not be mounted right at the input terminal of the antenna, thereby reducing d to zero.

A 50-ohm solid copper outer conductor coaxial line of approximately 20 centimeters was used to connect the antenna to the measuring equipment. Figure 2.8 shows a schematic diagram of the experimental arrangement. Each measurement was performed first with a short at the position of the load and then with the load connected. This technique accounts for the length of line used between the measurement equipment and the load, when a Smith chart is used to obtain the actual input impedance of an antenna. The measurement performed in this manner is reliable at higher frequencies where $Z_L \cong Z_0$ than it is at the lower frequencies where $Z_L >> Z_0$. The results are shown in Figs. 2.15 and 2.16.

In a further study, another set of scale models were built using hemispherical ground planes, instead of flat circular

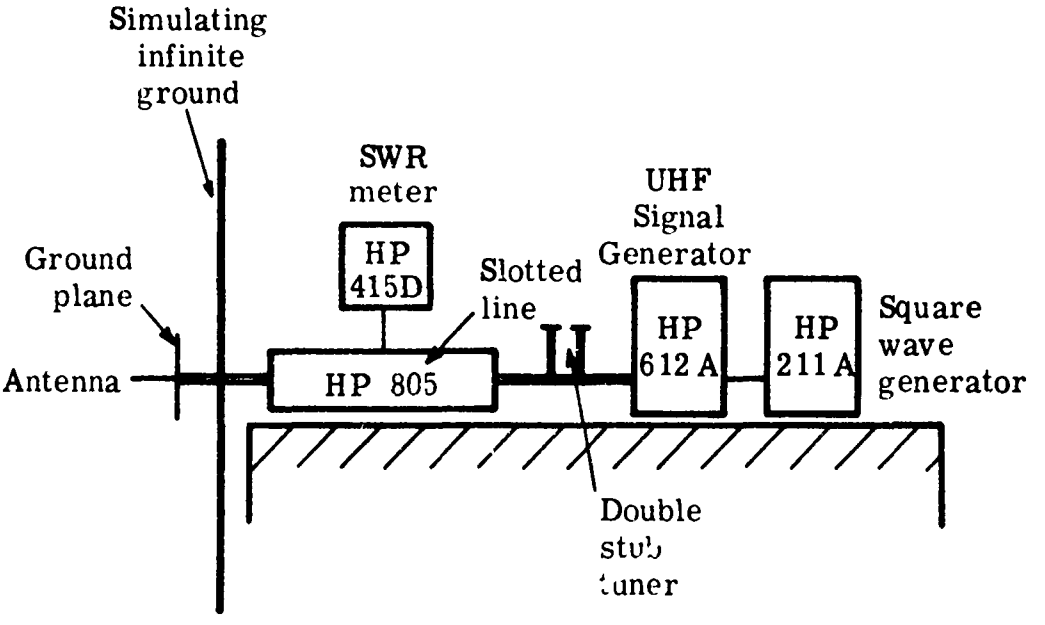

Fig. 2.8. Block diagram showing an impedance measurement set-up for a scale model antenna system

ground planes, to examine any similarities in the radiation patterns of the two systems. The frequencies selected were such that the diameter of the hemispnerical ground planes was less than a wavelength at 1476 MHz. This is, in effect, a 49.2:1 scale model for simulating operation between 5 MHz and 30 MHz. Impedance measurements were also made on this model, as well as the radiation pattern studies reported in Section 4.4.

In studying the impedance of the scale models, the flat circular disc ground planes were placed at heights a_1 and a_2 above the simulated natural ground. The displacement a_1 is the radius of the semi-spherical ground plane. The displacement a_2 is the radius of the flat disc equal in surface area to that of the spherical ground plane.

Figure 2.9 shows, in detail, the experimental arrangements of scale models. In the first case, Fig. 2.9(a), the displacement of a finite ground plane above an infinite ground is the same as the radius of a hemispherical ground plane a. In the second case, Fig. 2.9(b), the displacement, a , of a finite ground plane above an infinite ground is chosen to be equal to 0.707 times the radius of a circular disc. With this value, the surface area of the hemisphere, $2\pi a^2$, is equal to the surface area of the circular disc. That is, in the first case, displacements above an infinite ground plane are equal, and in the second case the surface areas of the small ground equal. The object of this study was to determine the relative

impedance characteristics of the two antenna systems and to determine the dependence of the system upon ground plane surface area and upon its location with respect to the larger ground plane. The results of the laboratory impedance measurement on both scale models are shown in Figs. 2.15 and 2.16.

2.4 Results of Measurement

Antenna input impedance measurements taken with 5, 2.5, 1.25, and 0.625 meter diameter ground plane at heights .5, 2.5, 1.25, and 0.625 meter above natural ground are shown as a function of frequency in Figs. 2.11 to 2.14. The data are arranged to show the effect of ground plane sizes with their location fixed at constant level and the effect of ground plane locations with the size fixed.

The capacitive reactance components are, in general, less dependent upon the ground plane height than upon its diameter. However, the resistive component varies with the height markedly and shows a peak at particular frequencies. The input impedance of a monopole antenna that is located over an infinite ground plane is shown in Figs. 2.10(a) and 2.10(b). These curves are derived from Brown and Woodward's (Ref. 2) experimental data where the length to diameter ratio of approximately 400 is used. Comparison between results of infinite ground planes and finite ground planes above natural ground shows the two are similiar in reactance but not in resistance.

The results from measurements using actual size of antenna show that, for a fixed diameter disc ground plane, a resistive

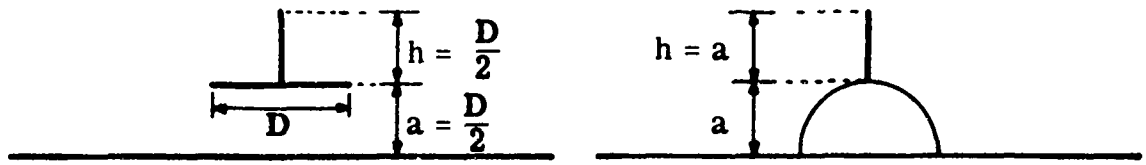

(a)

Semi-spherical surface area $A_S = 2\pi a^2$

Circular disc surface area $A_D = 2\pi a^2 = A_S$

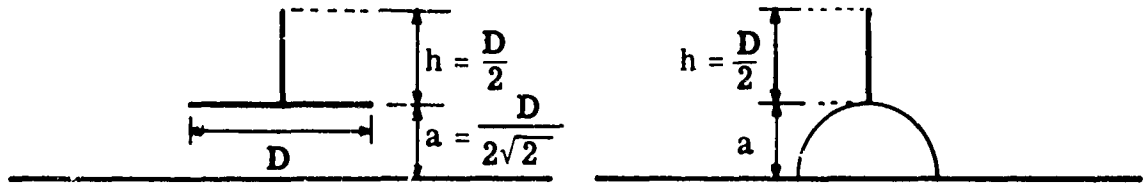

(b)

Fig. 2.9. Scale models used for impedance measurements

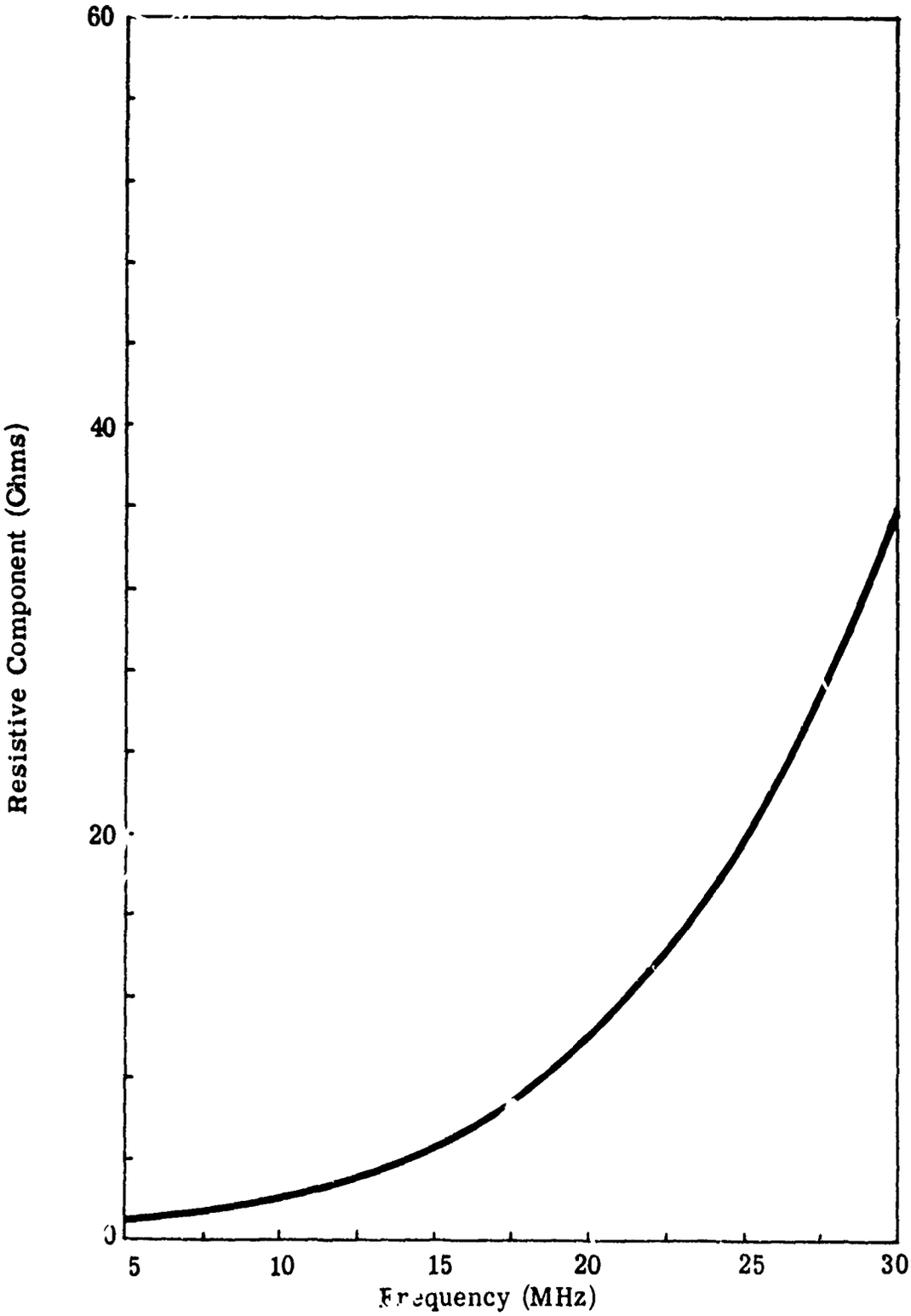

Fig. 2. 10(a).Input resistance as a function of frequency
for a quarter wavelength monopole at 30 MHz
on an infinite ground plane

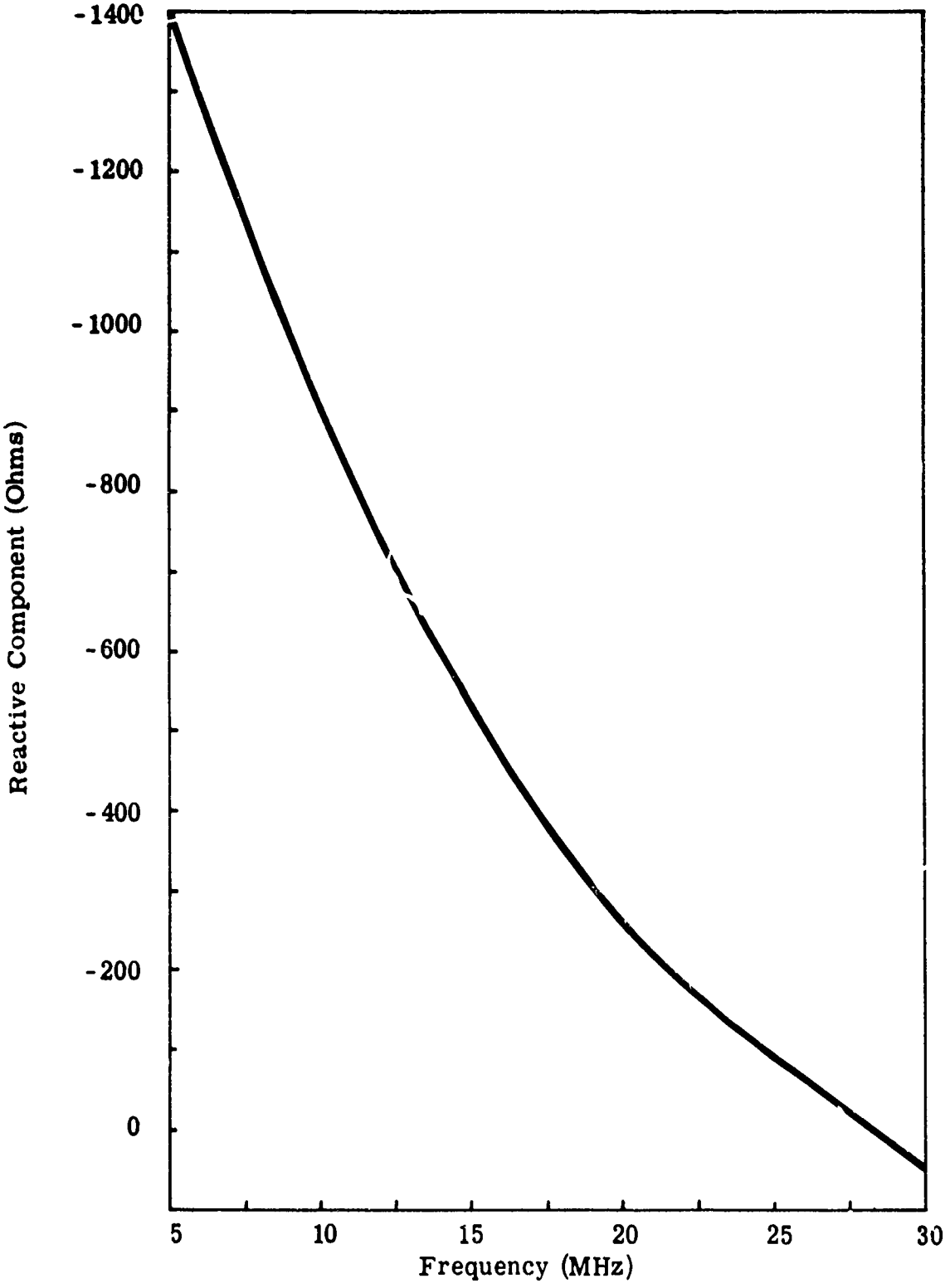

Fig. 2. 10 (b). Input reactance as a function of frequency for a quarter wavelength monopole at 30 MHz on an infinite ground plane.

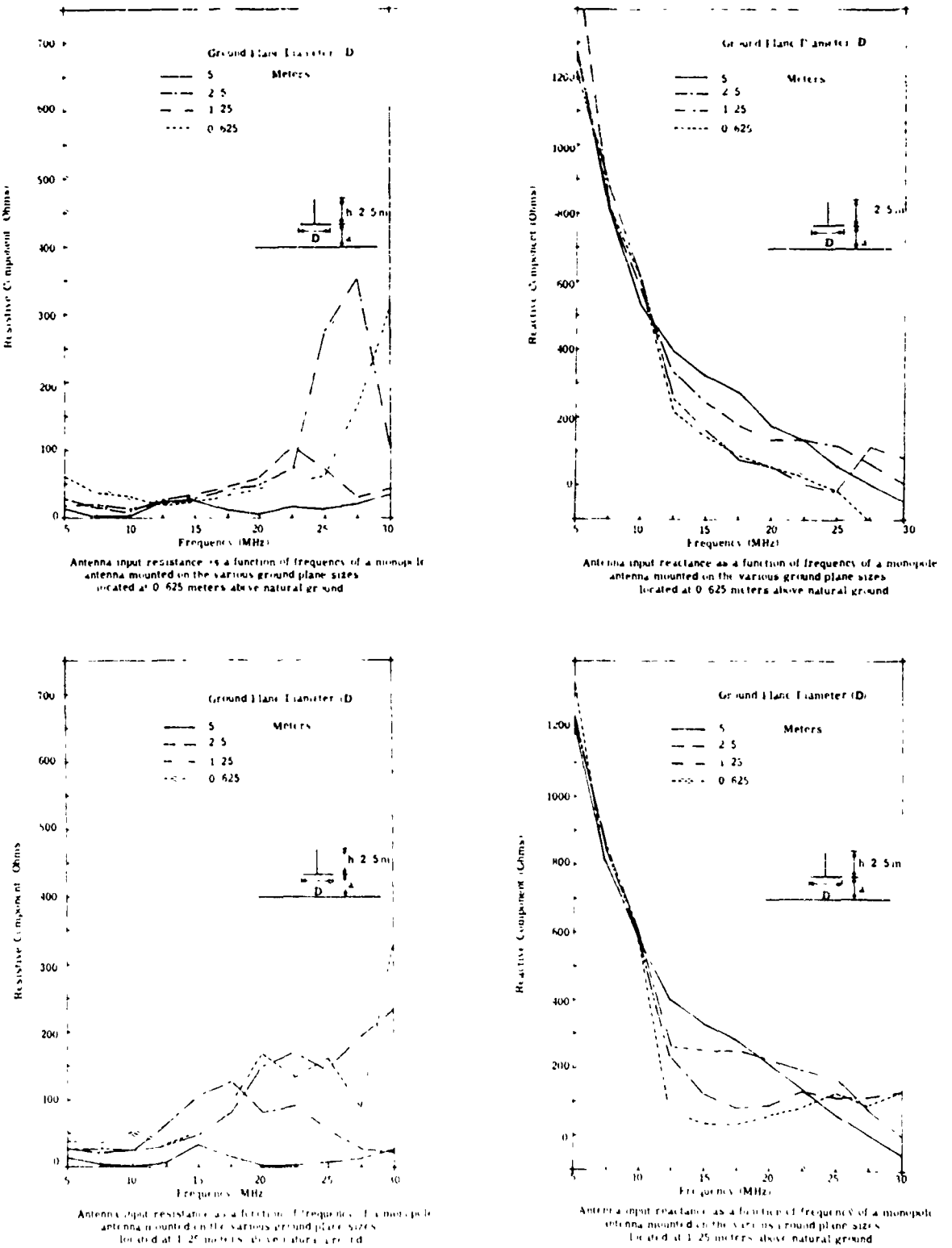

Antenna input resistance as a function of frequency of a monopole antenna mounted on the various ground plane sizes located at 0 625 meters above natural ground

Antenna input reactance as a function of frequency of a monopole antenna mounted on the various ground plane sizes located at 0 625 meters above natural ground

Antenna input resistance as a function of frequency of a monopole antenna mounted on the various ground plane sizes located at 1 25 meters above natural ground

Antenna input reactance as a function of frequency of a monopole antenna mounted on the various ground plane sizes located at 1 25 meters above natural ground

Fig. 2.11..Input impedance versus frequency

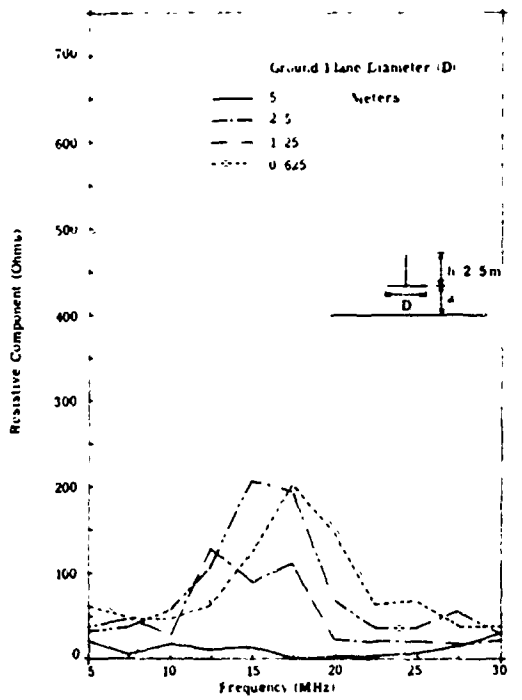

Antenna input resistance as a function of frequency of a monopole antenna mounted on the various ground plane sizes located at 2 5 meters above natural ground

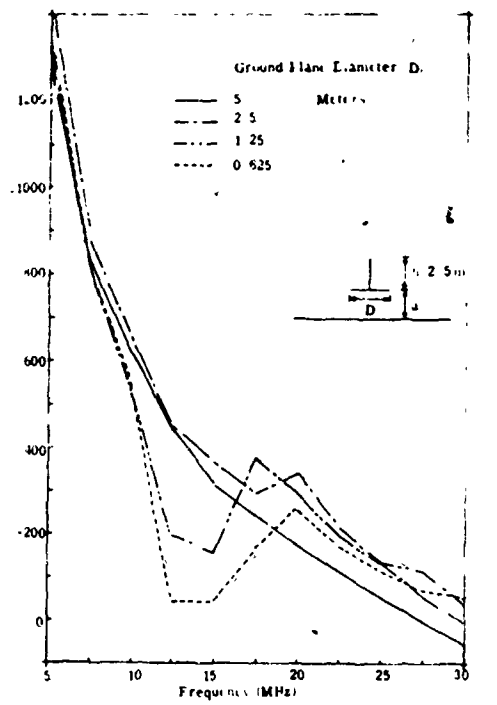

Antenna input reactance as a function of frequency of a monopole antenna mounted on the various ground plane sizes located at 2 5 meters above natural ground

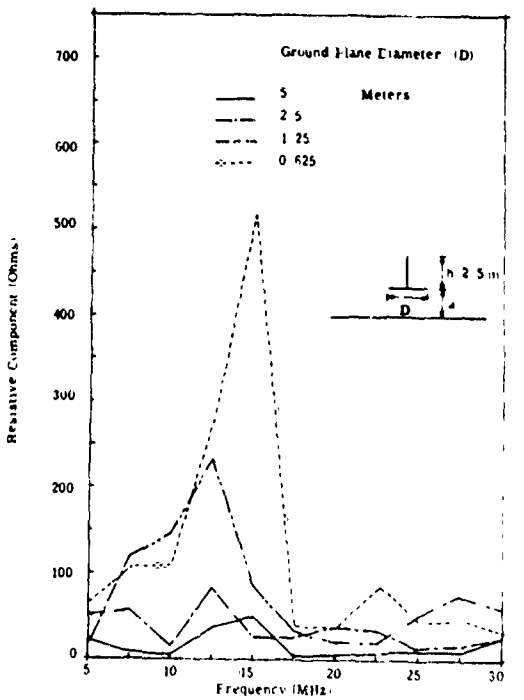

Antenna input resistance as a function of frequency of a monopole antenna mounted on the various ground plane sizes located at 5 meters above natural ground

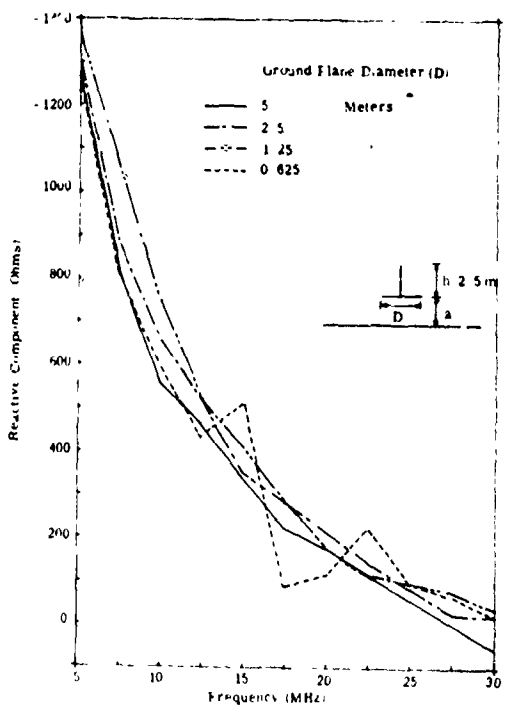

Antenna input reactance as a function of frequency of a monopole antenna mounted on the various ground plane sizes located at 5 meters above natural ground

Fig. 2.12. Input impedance versus frequency

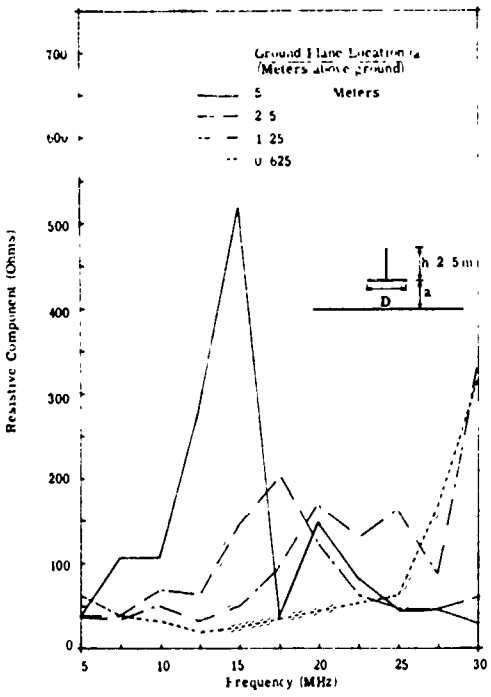

Antenna input resistance as a function of frequency for a monopole antenna mounted on a 0 625 meter diameter ground plane at various locations above natural ground

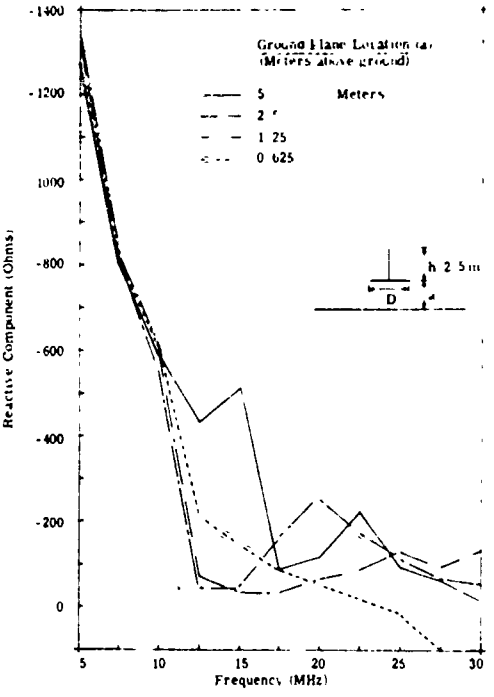

Antenna input reactance as a function of frequency for a monopole antenna mounted on a 0 625 meter diameter ground plane at various locations above natural ground

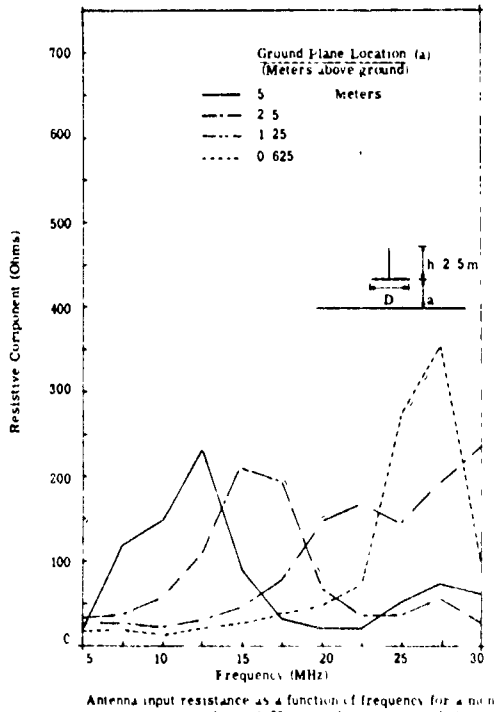

Antenna input resistance as a function of frequency for a monopole antenna mounted on a 1 25 meter diameter ground plane at various locations above natural ground

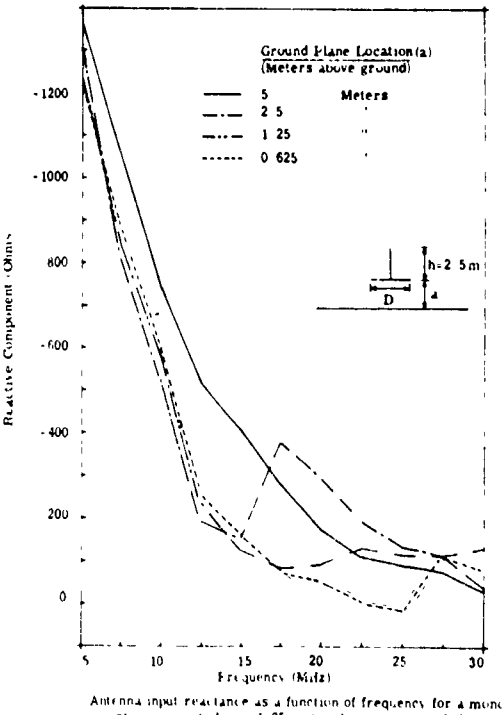

Antenna input reactance as a function of frequency for a monopole antenna mounted on a 1 25 meter diameter ground plane at various locations above natural ground

Fig. 2.13. Input impedance versus frequency

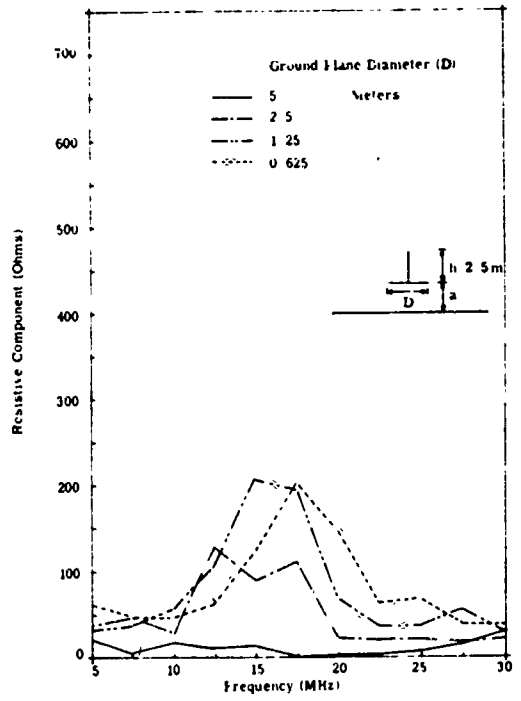

Antenna input resistance as a function of frequency of a monopole antenna mounted on the various ground plane sizes located at 2 5 meters above natural ground

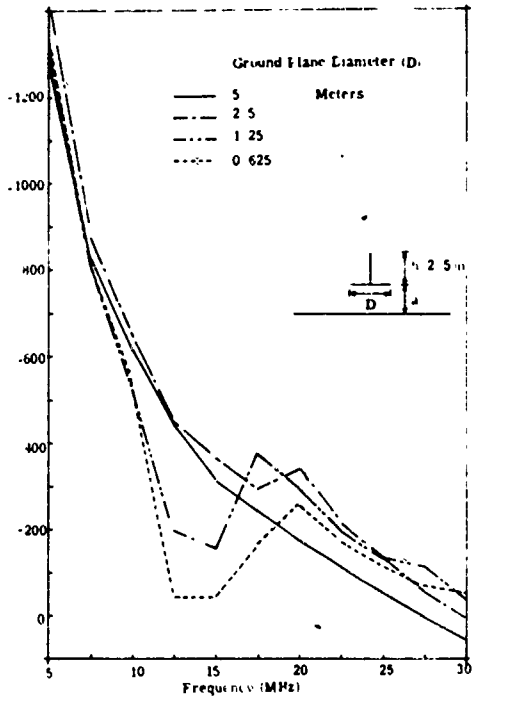

Antenna input reactance as a function of frequency of a monopole antenna mounted on the various ground plane sizes located at 2 5 meters above natural ground

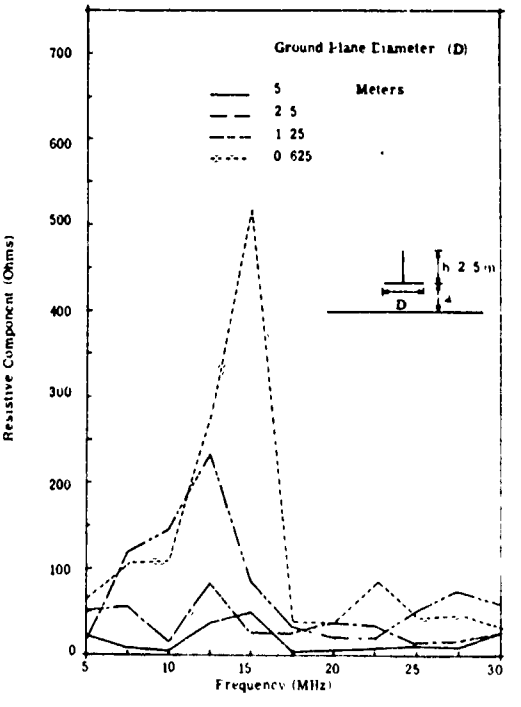

Antenna input resistance as a function of frequency of a monopole antenna mounted on the various ground plane sizes located at 5 meters above natural ground

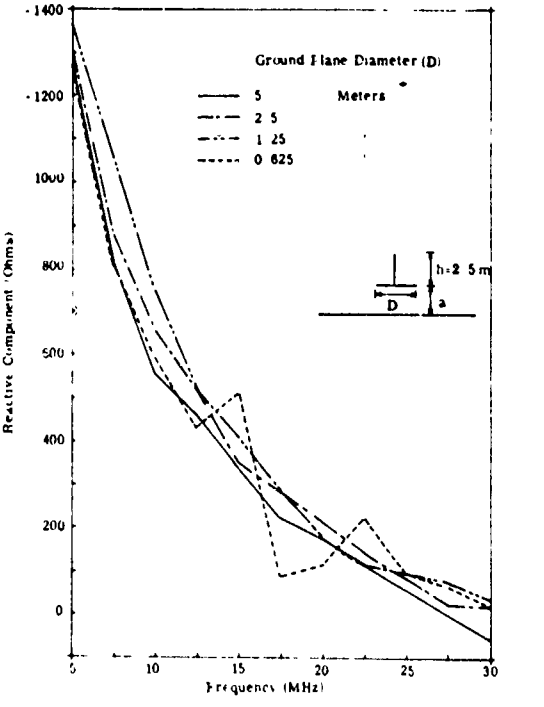

Antenna input reactance as a function of frequency of a monopole antenna mounted on the various ground plane sizes located at 5 meters above natural ground

Fig. 2.12. Input impedance versus frequency

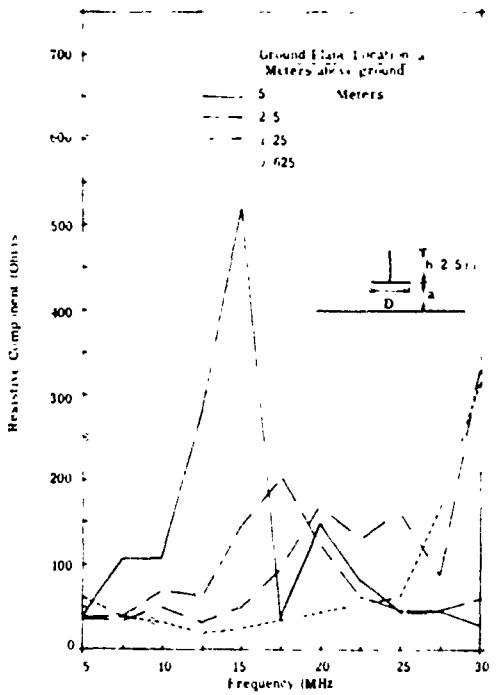

Antenna input resistance as a function of frequency for a monopole antenna mounted on a 0 625 meter diameter ground plane at various locations above natural ground

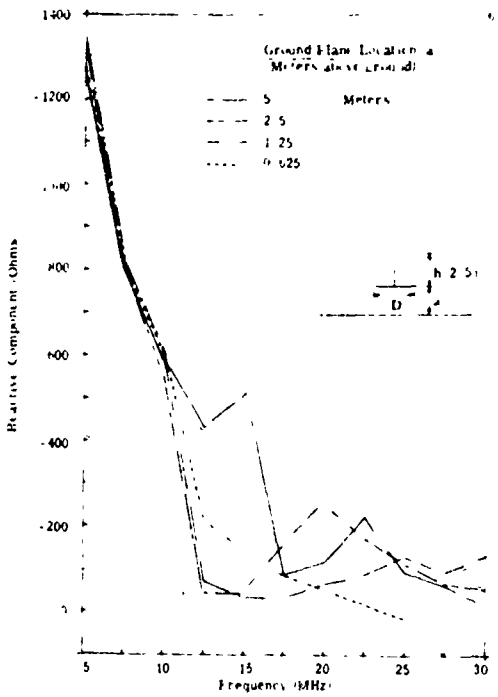

Antenna input reactance as a function of frequency for a monopole antenna mounted on a 0 625 meter diameter ground plane at various locations above natural ground

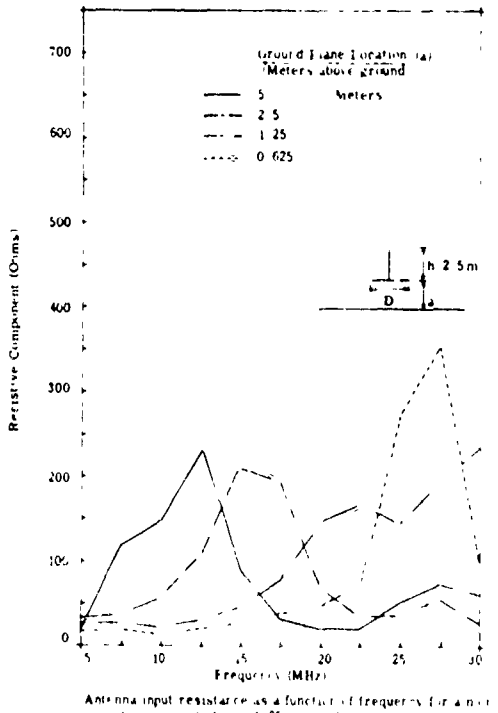

Antenna input resistance as a function of frequency for a monopole antenna mounted on a 1 25 meter diameter ground plane at various locations above natural ground

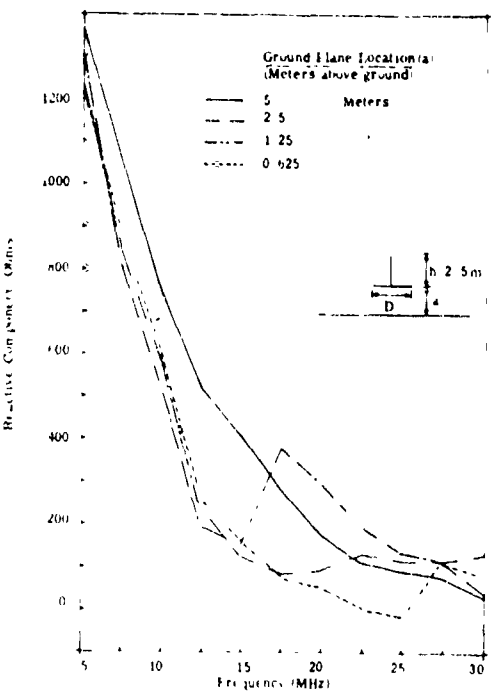

Antenna input reactance as a function of frequency for a monopole antenna mounted on a 1 25 meter diameter ground plane at various locations above natural ground

Fig. 2.13. Input impedance versus frequency

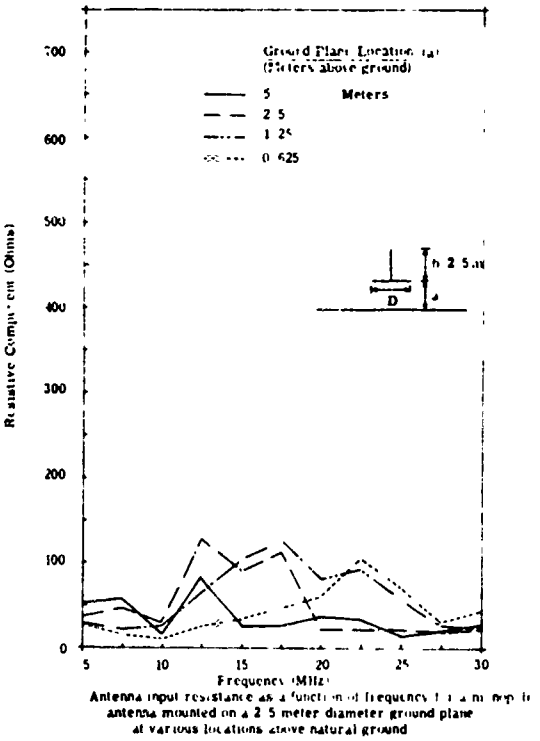

Antenna input resistance as a function of frequency for a monopole antenna mounted on a 2 5 meter diameter ground plane at various locations above natural ground

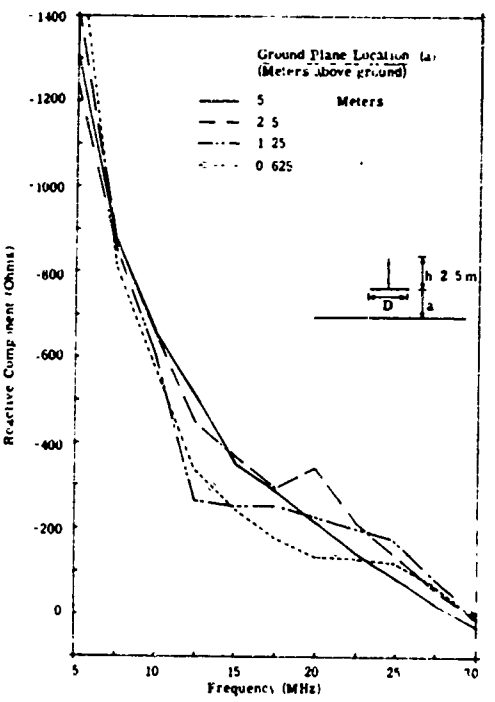

Antenna input reactance as a function of frequency for a monopole antenna mounted on a 2 5 meter diameter ground plane at various locations above natural ground

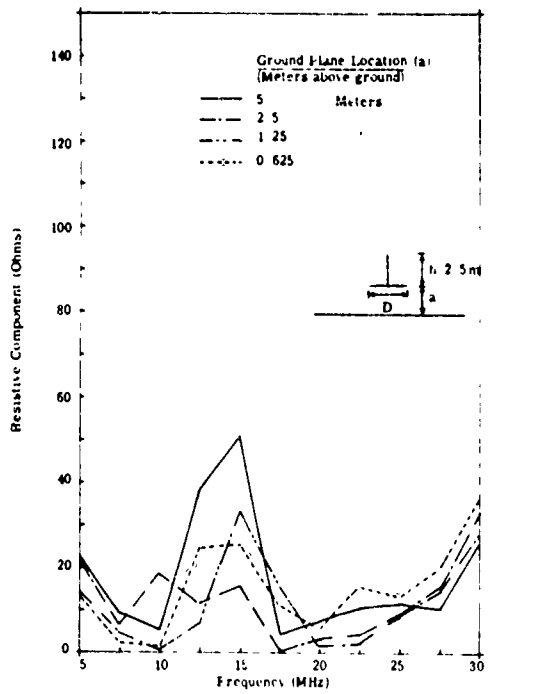

Antenna input resistance as a function of frequency for a monopole antenna mounted on a 5 meter diameter ground plane at various locations above natural ground

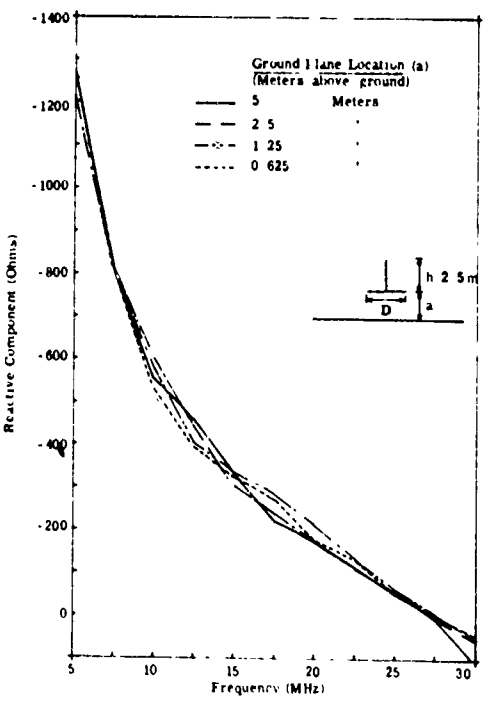

Antenna input reactance as a function of frequency for a monopole antenna mounted on a 5 meter diameter ground plane at various locations above natural ground

Fig. 2. 14. Input impedance versus frequency

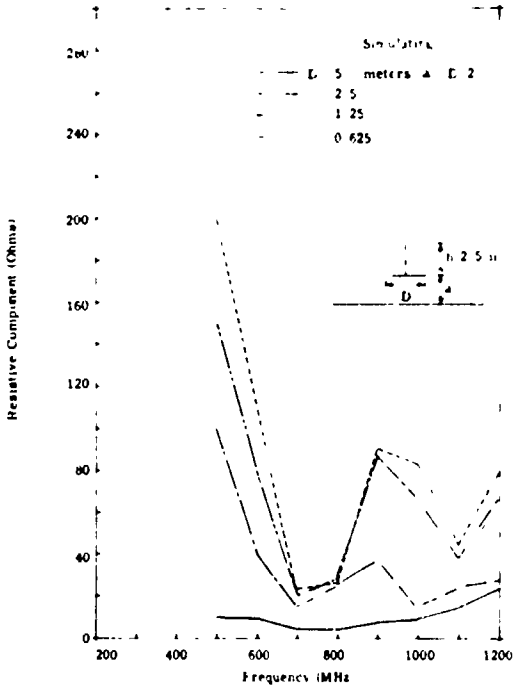

Antenna input resistance as a function of frequency of a 40 1 scale model monopole antenna mounted on the various ground planes with diameter D located at a above natural ground

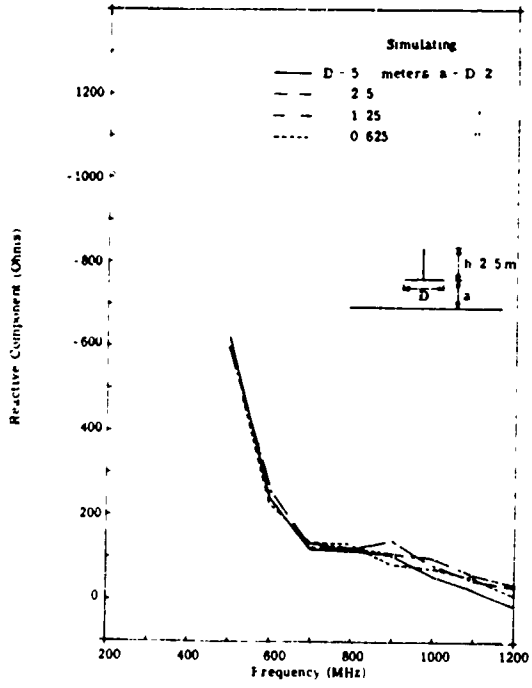

Antenna input reactance as a function of frequency of a 40 1 scale model monopole antenna mounted on the various ground planes with diameter D located at a above natural ground

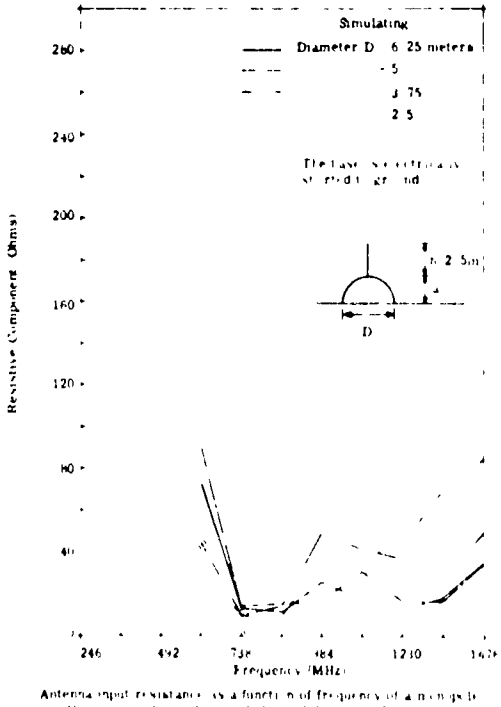

Antenna input resistance as a function of frequency of a monopole with a semi spherical ground plane of diameter D

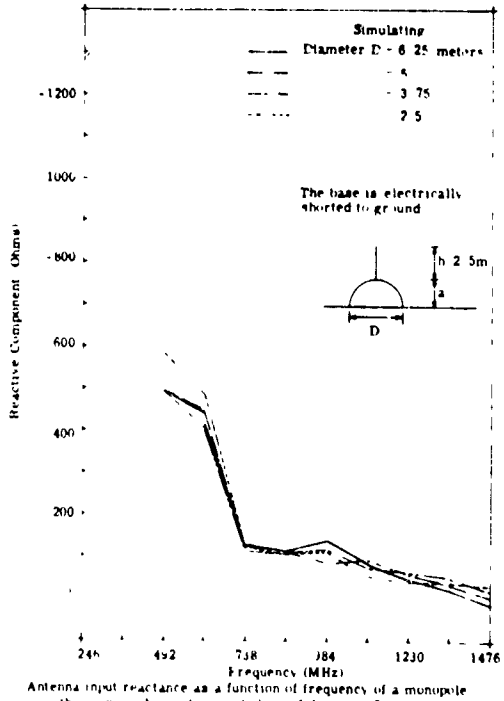

Antenna input reactance as a function of frequency of a monopole with a semi spherical ground plane of diameter D

Fig. 2. 15. Input impedance versus frequency

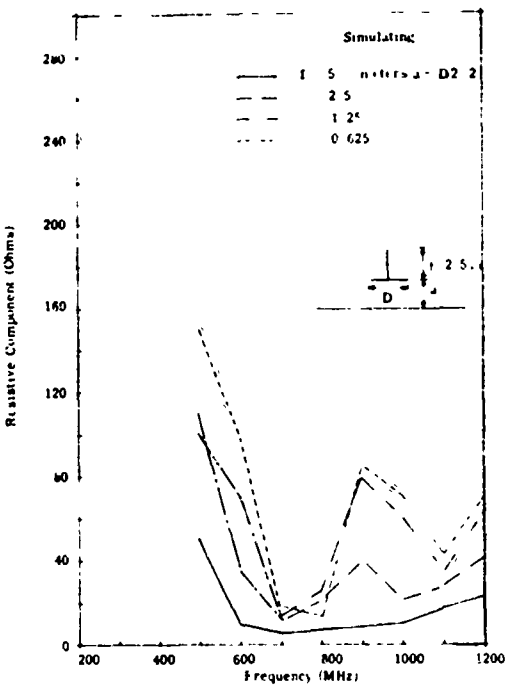

Antenna input resistance as a function of frequency of a 40 1 scale model monopole antenna mounted on the various ground planes with diameter D located at a above natural ground

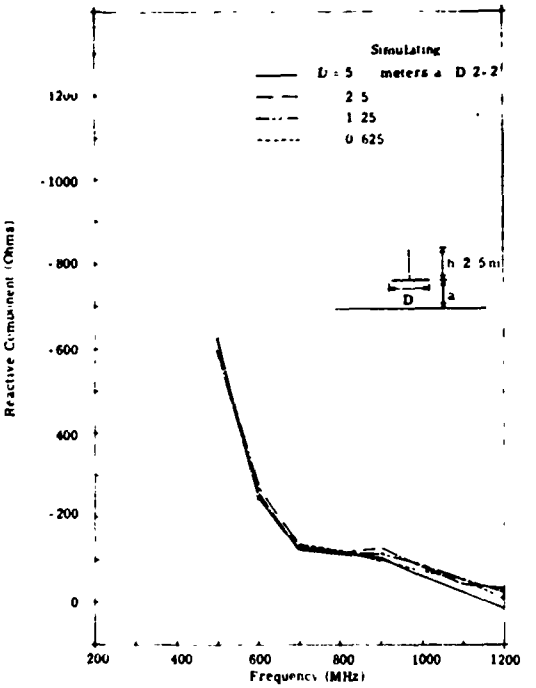

Antenna input reactance as a function of frequency of a 40 1 scale model monopole antenna mounted on the various ground planes with diameter L located at a above natural ground.

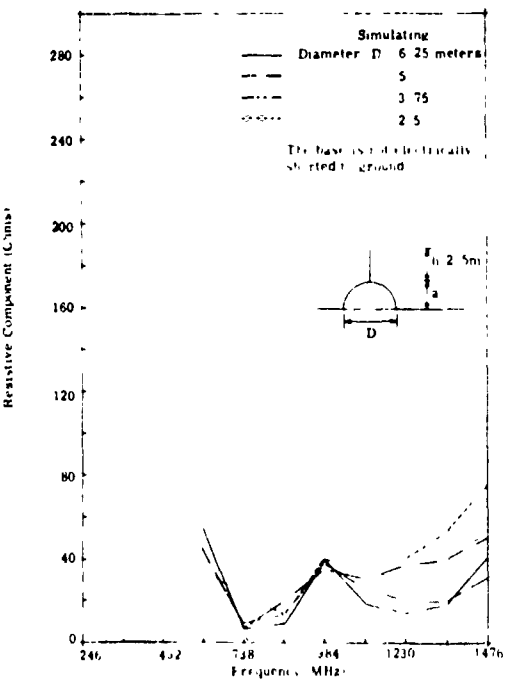

Antenna input resistance as a function of frequency of a monopole with a semi spherical ground plane of diameter D

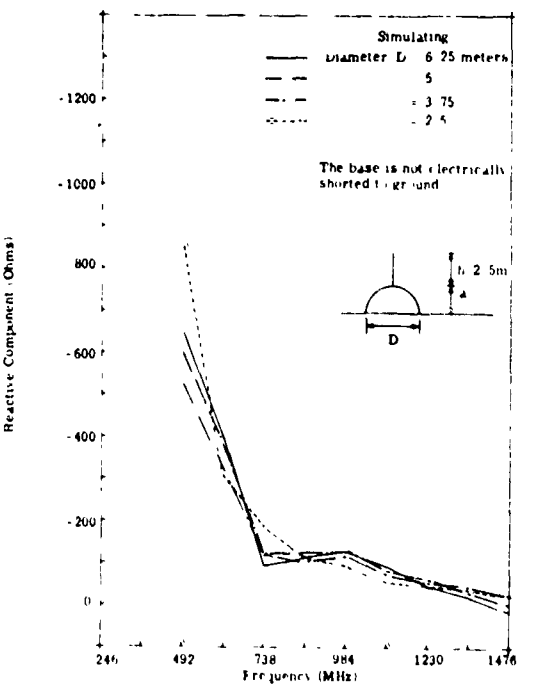

Antenna input reactance as a function of frequency of a monopole with a semi spherical ground plane of diameter D

Fig. 2. 16. Input impedance versus frequency

peak occurs at higher frequencies as the location of this ground plane gets higher with respect to an infinite ground. Also, the peak values of the resistive components are decreasing as the fixed diameter size is increased. A general conclusion which can be drawn from these results is that the resonant peak occurs at a frequency where $k(\frac{D}{2} + a)$ is constant. Therefore, as a diameter of the ground plane and a displacement above infinite ground plane gets larger, a peaking occurs at lower frequencies. As for the reactive components of the impedance, the reactance versus frequency curve is similar to that of a monopole above an infinite ground plane when the diameter of a disc is 5 meters. The displacement above an infinite ground does not seem to affect the reactive component as much as the diameter of a finite ground plane. However, even for $D = 5$ meters, reactance values are lower than that of a monopole antenna with the same length to diameter ratio on an infinite ground.

A limited number of impedance measurements has been conducted using a scale model which is mainly constructed to take a far-zone radiation pattern of the antenna and ground plane system. The input terminals as well as infinite natural ground simulations have not been able to scale ideally. These discrepancies usually affect impedance measurements more than radiation patterns obtained at far-zone area. Under these circumstances, only a qualitative comparison of the impedance has been possible.

First, the actual model and the scale model antenna and ground plane system at a ground plane diameter equal to a half wave-

length at 30 MHz compared favorably in both real part and imaginary part.

Secondly, the scale model antenna with a disc ground plane and a hemispherical ground plane comparison shows that neither the diameter of the two types of ground planes or the area of the ground planes has a basis of similarity in impedances. However, it is deduced qualitatively from the limited number of experimental data that the distance between the base of the antenna to the natural ground and the conductivity along this path has a greater bearing upon the resonance phenomena observed in the impedance measurements. In other words, $k(a + \frac{D}{2})$ = const for a disc ground plane and ka = const for a semi-spherical ground plane will determine the resonance conditions. These constants seem different in general for different ratio of a to D.

In addition to these observations, the determination of whether resonance peak observed in input resistance measurement is largely due to increase in radiation resistance or not will be shown in the rest of this chapter and in Chapter 5.

In studying impedance measurement data, it is also observed that both real and imaginary part of the impedance behave, in most cases, such as in Fig. 2.17(c). Frequencies where peaking effect occurs are, of course, a function of a and D. Figure 2.17(a) shows an input impedance as a function of frequency for a monopole on an infinite conducting ground plane and its equivalent circuit.

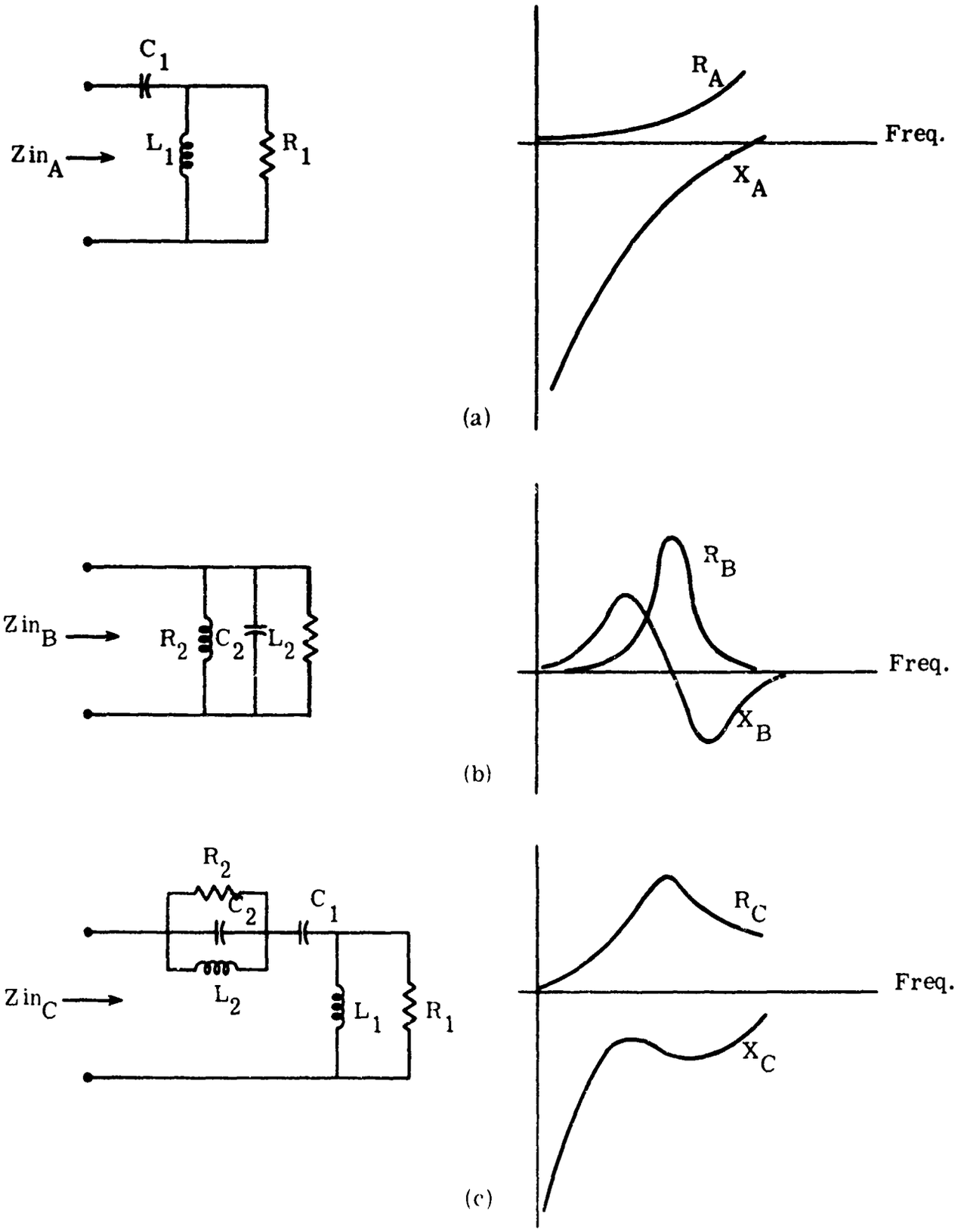

Fig. 2.17. An equivalent circuit of a monopole on a finite disc ground plane above an infinite ground

Figure 2. 17(b) shows a parallel resonance circuit whose impedance characteristics add up with Fig. 2.17(a) to give an impedance characteristic which is observed in the measurements.

Therefore, it is possible to synthesize an equivalent circuit of a type shown in Fig. 2. 17(c) to further study the effect of a finite ground plane upon an equivalent circuit. In this way, a correlation may be obtained between a, D and the circuit parameters.

2. 5 Copper Losses Due to the Antenna and the Ground Plane

The real part of the antenna input impedance contains a part

$$R_r = \frac{1}{|I|^2} \oint\!\!\oint \frac{1}{2} \operatorname{Re} (\bar{E} \times \bar{H}^*) \cdot d\bar{S} \qquad (2.9)$$

that is directly proportional to the radiated power of an antenna, for a constant input current. Consequently, it is important to separate the resistive component of the input impedance measurement data into the resistive loss, which is due to several causes, as explained in the following section, and the radiation resistance. This permits determination of whether the unusual variation of the input resistance as a function of frequency, which has been found in the input impedance measurements, is due to an increase in loss or to an increase in the radiation resistances at particular frequencies.

The total antenna resistance is the sum of the several separate components

(1) Radiation resistance R_r

(2) Ground terminal resistance R_g

(3) Resistance of tuning units R_t

(4) Resistance of equivalent insulation loss R_i

(5) Resistance of equivalent conductor losses R_ω

(6) Transmission line loss R_m.

Among the six separate contributions, R_t and R_i are not present in this case because there are no tuning units attached when the measurements are taken and, as a low potential receiving antenna, no appreciable insulation losses are involved.

The loss due to the transmission line (R_m) was evaded by measuring the impedance at the base directly below the ground plane, for the actual size and by taking a short circuit measurement with the short placed at the input terminal of the scale model. The loss in the line was subtracted from the measured data.

In the out-door measurement with the natural ground below the finite aluminum ground plane R_g cannot be exactly calculated without precise information of the conductivity and other parameters of the dirt ground. The impedance measurement on the scale model when the natural ground is simulated by the aluminum foil enables both R_g and R_ω to be computed.

The following analysis is to permit the calculation of R_ω for both the actual model and the scale model and R_g of the scale model.

2.5.1 The Internal Impedance of the Plane Conductor.

The current density resulting from the movement of charges in a conductor is given by Ohm's law:

$$\bar{J} = \sigma \bar{E} \tag{2.8}$$

The constant σ is the conductivity of the conductor, and the Maxwell's equation is

$$\nabla \times \bar{H} = \sigma \bar{E} + \frac{\partial \bar{D}}{\partial t} \tag{2.9}$$

For a harmonically oscillating field with $e^{j\omega t}$ time dependence

$$\nabla \times \bar{H} = (\sigma + j\omega\epsilon)\bar{E} \tag{2.10}$$

In the absence of free charges ρ, $\nabla \cdot \bar{D} = 0$. Also, for most conductors, the displacement current $\partial \bar{D} / \partial t$ is negligibly small compared to the conduction current.

Then,

$$\nabla \times \nabla \times \bar{E} = \nabla(\nabla \cdot \bar{E}) - \nabla^2 \bar{E} = \nabla \times (\frac{-\partial \bar{B}}{\partial t}) = \frac{\partial}{\partial t} \mu \nabla \times \bar{H}$$

$$\therefore \quad \nabla^2 \bar{E} = \mu\sigma \frac{\partial \bar{E}}{\partial t} = j\omega \mu\sigma \bar{E} \tag{2.11}$$

Similarly, using $\bar{J} = \sigma \bar{E}$

$$\nabla^2 \bar{J} = j\omega\mu\sigma \bar{J} \tag{2.12}$$

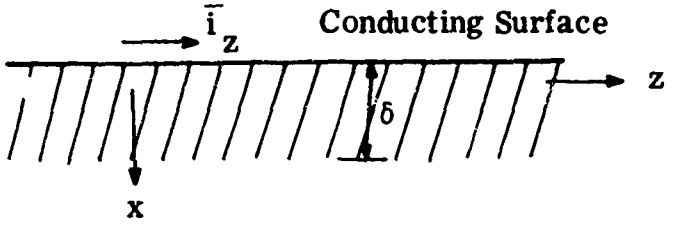

Fig. 2.18. Plane solid conductor

For a plane conductor of infinite depth, with no field variations along the length or width as shown in Fig. 2.18.

$$\frac{d^2 i_z}{dx^2} = j\omega\mu\sigma i_z = \tau^2 i_z \qquad (2.13)$$

where

$$\tau^2 = j\omega\mu\sigma$$

Since

$$\sqrt{j} = \frac{(1+j)}{\sqrt{2}}$$

and

$$\tau = (1+j)\sqrt{\pi f\mu\sigma} \qquad (2.14)$$

where by definition $\delta = \dfrac{1}{\sqrt{\pi f\mu\sigma}}$, is called depth of penetration of the field, or the skin depth.

The solution of differential equation 2.13 is then given as

$$i_z = i_0 e^{\frac{-(1+j)}{\delta}x} \tag{2.15}$$

The total current flowing in the plane conductor is found by integrating the current density i_z from the surface to the infinite depth. For a unit width,

$$J_z = \int_0^\infty i_z \, dx = \int_0^\infty i_0 e^{-\frac{(1+j)}{\delta}x} \, dx = \frac{i_0 \delta}{1+j} \tag{2.16}$$

The electric field at the surface is $E_{zo} = \frac{i_0}{\sigma}$. Therefore, the internal impedance per unit length and unit width is

$$Z_s = \frac{E_{zo}}{J_z} = \frac{1+j}{\sigma\delta} \tag{2.17}$$

If Z_s is defined as $Z_s = R_s + j\omega L_i$, then

$$R_s = \frac{1}{\sigma\delta} = \sqrt{\frac{\pi f \mu}{\sigma}} \tag{2.18}$$

R_s is the resistance of the plane conductor for a unit length and unit width. For a finite area of conductor, the resistance is obtained by multiplying R_s by length, and dividing by the width.

For a circular ground plane with radial current distribution, the total surface resistance is obtained by multiplying R_s by the radius and dividing by the mean circumference of the plate.

For an aluminum ground plane which has material constants of:

$$\sigma = 3.72 \times 10^{7} \text{ mhos/meter}$$

$$\mu = 4\pi \times 10^{-7} \text{ henries/meter}$$

$$\delta = \frac{0.0826}{\sqrt{f}} \text{ meters}$$

f = frequency in Hertz

the surface resistivity is computed to be

$$R_s = 3.26 \times 10^{-7} \sqrt{f} \qquad (2.19)$$

which becomes

at f = 30 MHz $\quad R_s = 3.26 \times 10^{-7} \sqrt{3 \times 10^{7}} = 1.79 \times 10^{-3}$ ohms/square

= 5 MHz $\quad = 3.26 \times 10^{-7} \sqrt{5 \times 10^{6}} = 7.3 \times 10^{-4}$ "

When the aluminum ground plane has a diameter equal to a quarter-wavelength at 30 MHz, the radius r is 2.5 meters and the mean circumference is πr. The total surface resistance is, therefore,

$$R_\omega = R_s \cdot \frac{r}{\pi r} = \frac{R_s}{\pi} \qquad (2.20)$$

The numerical values computed at 5 MHz and 30 MHz become

$$R_\omega = \frac{1.79 \times 10^{-3}}{3.14} \text{ ohms} = 5.7 \times 10^{-4} \text{ ohms at 30 MHz}$$

$$= \frac{7.3 \times 10^{-4}}{3.14} \text{ ohms} = 2.32 \times 10^{-4} \text{ ohms at 5 MHz .}$$

The contribution of the ground plane surface resistance toward the input resistance is, therefore, negligible.

2.5.2 Internal Impedance of a Conductor with a Circular Cross Section

2.5.2.1 Current in a Wire of a Circular Cross Section.

Let the current flowing on the antenna of a circular cross section, 1/4 inch in diameter be assumed to flow mainly on the axial direction; $\vec{i} = i_z \hat{z}$. Also, no axial or circumferential variation is assumed.

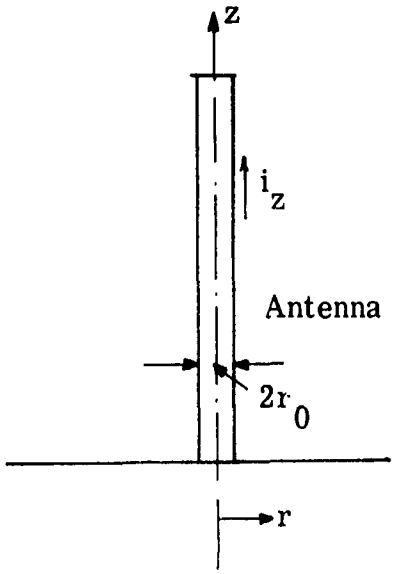

Fig. 2.19. Current in a cylindrical wire

Then $\nabla^2 \vec{i} = j\omega\mu\sigma\vec{i}$ becomes in the cylindrical coordinate system,

$$\frac{d^2 i_z}{dr^2} + \frac{1}{r}\frac{di_z}{dr} = j\omega\mu\sigma i_z \tag{2.21}$$

If we let $T^2 = -j\omega\mu\sigma$

$$\frac{d^2 i_z}{d_z^2} + \frac{1}{r}\frac{di_z}{dr} + T^2 i_z = 0 \tag{2.22}$$

For a solid wire, the solution must be finite at $r = 0$. Therefore, it takes the form of

$$i_z = AJ_0(Tr) \tag{2.23}$$

Let

$$i_z = i_0 \text{ at } r = r_0 \tag{2.24}$$

then

$$A = \frac{i_0}{J_0(Tr_0)} \tag{2.25}$$

$$\therefore \; i_z = i_0 \frac{J_0(Tr)}{J_0(Tr_0)} \tag{2.26}$$

Since

$$T^2 = -j\omega\mu\sigma$$

$$T = \sqrt{-j\omega\mu\sigma} = \sqrt{\frac{\omega\mu\sigma}{j}} = \sqrt{\frac{\omega\mu\sigma}{2}}\,(1 - j) \tag{2.27}$$

Since

$$J_0\left(\frac{v}{\sqrt{j}}\right) = \text{Ber}\,(v) + j\,\text{Bei}\,(v) \tag{2.28}$$

Where

$$\text{Ber}\,(v) \equiv \text{Real part of } J_0\left(\frac{v}{\sqrt{j}}\right)$$

$$\text{Bei}(v) \equiv \text{Imaginary part of } J_0\left(\frac{v}{\sqrt{j}}\right)$$

The current density in the axial direction can be written as now

$$i_z = i_0 \frac{\text{Ber}\left(\frac{\sqrt{2}r}{\delta}\right) + j\,\text{Bei}\left(\frac{\sqrt{2}r}{\delta}\right)}{\text{Ber}\left(\frac{\sqrt{2}r_0}{\delta}\right) + j\,\text{Bei}\left(\frac{\sqrt{2}r_0}{\delta}\right)} \tag{2.29}$$

If the ratio of r_0/δ is large, the $\left|i_z/i_0\right|$ plot will agree closely with the plane conductor derivation of

$$\left|\frac{i_z}{i_0}\right| = e^{-(r_0-r)/\delta} \tag{2.30}$$

where $r_0 - r$ replaced x for the case of a plane conductor.

Also,

$$\oint \overline{H} \cdot d\bar{\ell} = I \quad \text{and} \quad 2\pi r_0 H_\phi \Big|_{r=r_0} = I \tag{2.31}$$

From the Maxwell's equations,

$$\nabla \times \overline{E} = -j\omega\mu\overline{H} \tag{2.32}$$

and for the round wire

$$H_\phi = \frac{1}{j\omega\mu} \frac{dE_z}{dr} \tag{2.33}$$

Since

$$E_z = \frac{i_z}{\sigma} = \frac{i_0}{\sigma} \frac{J_0(Tr)}{J_0(Tr_0)} \tag{2.34}$$

$$\therefore \quad H\phi = - \frac{i_0}{T} \frac{J_0'(Tr)}{J_0(Tr_0)} \tag{2.35}$$

Consequently,

$$I = - \frac{2\pi r_0}{T} i_0 \frac{J_0'(Tr)}{J_0(Tr_0)} \tag{2.36}$$

2.5.2.2. The Internal Impedance of a Round Wire.

The internal impedance Z_i is defined as

$$Z_i \equiv \frac{E_z\Big|_{r=r_0}}{I} = \frac{T\, J_0(Tr_0)}{2\pi r_0 \sigma J_0'(Tr_0)} \tag{2.37}$$

Using the formula that

$$\text{Ber}\,(v) + j\,\text{Bei}\,(v) = J_0\left(\frac{v}{\sqrt{j}}\right)$$

and

$$\text{Ber}'(v) + j\,\text{Bei}'(v) = \frac{d}{dv}\left[\text{Ber}\,(v) + j\,\text{Bei}\,(v)\right] = \frac{J_0'\left(\frac{v}{\sqrt{j}}\right)}{\sqrt{j}} \tag{2.38}$$

The internal impedance becomes

$$Z_i = R + j\omega L_i = \frac{jR_s}{\sqrt{2\pi r_0}} \left[\frac{\text{Ber } q + j \text{ Bei } q}{\text{Ber' } q + j \text{ Bei' } q}\right] \qquad (2.39)$$

where

$$R_s = \frac{1}{\sigma \delta} = \sqrt{\pi f \mu \sigma} \qquad (2.40)$$

and

$$q = \frac{\sqrt{2} r_0}{\sigma} \qquad (2.41)$$

or

$$R = \frac{R_s}{\sqrt{2\pi r_0}} \left[\frac{\text{Ber } q \text{ Bei' } q - \text{Bei } q \text{ Ber' } q}{(\text{Ber' } q)^2 + (\text{Bei } q)^2}\right] \text{ ohms/meter} \qquad (2.42)$$

$$\omega L_i = \frac{R_s}{\sqrt{2\pi r_0}} \left[\frac{\text{Ber } q \text{ Ber' } q + \text{Bei } q \text{ Bei' } q}{(\text{Ber' } q)^2 + (\text{Bei } q)^2}\right] \text{ ohms/meter}$$

Using the same analysis except that the wall thickness is small enough with respect to the radius of the tube to be able to consider the tublar conductor as a flat conductor of finite thickness, the internal impedance can be found to be

$$Z = (1 + j) R_s \frac{\text{Cosh } \tau d}{\text{Sinh } \tau d} \qquad (2.43)$$

where

$$\tau = \frac{(1 + j)}{\sigma}$$

d = thickness of the tubular wall

$$R_s = \frac{\sqrt{\pi f \mu}}{\sigma}$$

Ther

$$\frac{R}{R_s} = \frac{\text{Sinh}\left(2d/\delta\right) + \text{Sin}\left(2d/\delta\right)}{\text{Cosh}\left(2d/\delta\right) - \text{Cos}\left(2d/\delta\right)} \quad \text{ohm/unit length} \qquad (2.44)$$

The impedance per unit length is, then,

$$\omega L_i = \frac{R_s}{2\pi r_0}\left[\frac{\text{Sinh}\left(2d/\delta\right) - \text{Sin}\left(2d/\delta\right)}{\text{Cosh}\left(2d/\delta\right) - \text{Cos}\left(2d/\delta\right)}\right] \text{ohm/unit length}$$

(2.45)

$$R = \frac{R_s}{2\pi r_0}\left[\frac{\text{Sinh}\left(2d/\delta\right) + \text{Sin}\left(2d/\delta\right)}{\text{Cosh}\left(2d/\delta\right) - \text{Cos}\left(2d/\delta\right)}\right] \text{ohm/unit length}$$

The tubular antenna used for impedance measurement has the following dimensions:

radius = 3.17×10^{-3} meters

wall thickness = 6.35×10^{-4} meters

length of antenna = 2.5 meters

The skin depth δ computed for the copper at both ends of the frequency band are

$$\delta = 1.1 \times 10^{-5} \text{ meters at 30 MHz}$$

$$= 3 \times 10^{-5} \text{ meters at 5 MHz}$$

Therefore, the ratio $2d/\delta$ for equation 2.45 becomes

$$2d/\delta = 11.4 \text{ at 30 MHz}$$

$$= 42.4 \text{ at 5 MHz}$$

For large values of x, both sinh x and cosh x approach $(1/2)e^{x}$ and sinh x $\rightarrow$ sin x and cosh x $\rightarrow$ cos x. Equation 2.45 then simplifies to

$$R_{\omega} \simeq \frac{R_s}{2\pi r_0} \simeq \omega L_i \quad \text{when} \quad 2d/\delta > 1 \qquad (2.46)$$

For the copper tubular antenna 2.5 meters long the real part of the internal impedance becomes

$$R_{\omega} \doteq 0.189 \text{ ohms at 30 MHz}$$

$$\doteq 0.063 \text{ ohms at 5 MHz}$$

The contribution of the copper loss, as shown above, toward the antenna input impedance is also negligible.

In this section, a numerical calculation of ground terminal resistance R_g and conductor loss resistance R_ω was made. In the actual antenna and ground plane system, the conductivity of the infinite ground below the finite ground must be known. However, calculations performed here did not take the natural ground into account. The only ground considered is an aluminum ground plane used as a finite ground below the antenna. Contributions from the tubular antenna of 2.5 meters in length, used for a monopole, to R_ω were also considered. In the frequency range of 5 to 30 MHz, where the experiment was carried out, the ground loss from the largest ground plane (D = 5 meters) used was computed to be less than 5.7×10^{-4} ohms. The loss from the tubular antenna conductor itself was less than 0.2 ohms.

In the scale model, the ground plane used to simulate an infinite natural ground was a 4-foot diameter aluminum circular ground plane. The conductivity data and skin-depth data available for aluminum, both large and small ground plane loss were calculated.

Also, a conduction loss from an AWG No. 28 wire of 6.25 cm in length used to simulate a monopole antenna was calculated. The overall loss due to R_g and R_ω for the scale model was well below 1 ohm and there was no obvious peaking effect due to R_g and R_ω as frequency was varied from 200 MHz to 1200 MHz.

Therefore, it seems that the resonant peak observed in the real part of the antenna input impedance in the experiment originate from sources other than R_g and R_ω.

CHAPTER III

CURRENT MEASUREMENTS

3. 1 Introduction

In this chapter, an extensive study of the current distribution on a monopole antenna one quarter wavelength long at 30 MHz is reported as functions of a ground plane size and its location. King and Harrison (Ref. 9) computed analytically the current distribution of a symmetrically center-driven antenna. For this dipole, the current distribution was found to be extremely close to the sinusoidal distribution that is normally assumed, so long as the antenna length to diameter ratio is very large. However, the effect of a small ground plane whose diameter is less than a half wavelength upon the antenna current when the system is placed above an infinite ground has not been reported.

The particular emphasis here is to show the differences between the current distribution on an antenna over an infinite ground plane and the same size of antenna over a finite ground displaced less than a wavelength above an infinite ground plane.

3. 2 Theory of Current Probe

In order to detect the current densities on the antenna, a rectangular loop antenna whose dimensions are much smaller than a wavelength was used as a probe. The theory of operation of this loop as a probe has been studied by King and Whiteside (Ref. 10). The

CHAPTER III

CURRENT MEASUREMENTS

3. 1 Introduction

In this chapter, an extensive study of the current distribution on a monopole antenna one quarter wavelength long at 30 MHz is reported as functions of a ground plane size and its location. King and Harrison (Ref. 9) computed analytically the current distribution of a symmetrically center-driven antenna. For this dipole, the current distribution was found to be extremely close to the sinusoidal distribution that is normally assumed, so long as the antenna length to diameter ratio is very large. However, the effect of a small ground plane whose diameter is less than a half wavelength upon the antenna current when the system is placed above an infinite ground has not been reported.

The particular emphasis here is to show the differences between the current distribution on an antenna over an infinite ground plane and the same size of antenna over a finite ground displaced less than a wavelength above an infinite ground plane.

3. 2 Theory of Current Probe

In order to detect the current densities on the antenna, a rectangular loop antenna whose dimensions are much smaller than a wavelength was used as a probe. The theory of operation of this loop as a probe has been studied by King and Whiteside (Ref. 10). The

components are also present, even though small, which are proportional to the average electric field in the plane of the loop.

When electro-magnetic fields are incident upon a loop, there are re-radiated fields in addition to the incident field. The total field, therefore, is

$$\overline{B} = \overline{B}^{i} + \overline{B}^{r} \tag{3.1}$$

where $\overline{B}$ is the total field, $\overline{B}^{i}$ the incident field, and $\overline{B}^{r}$ the re-radiated field. From Maxwell's curl equation,

$$\nabla \times \overline{E} = - \frac{\partial \overline{B}}{\partial t} \tag{3.2}$$

Assuming that the incoming signal has $e^{j\omega t}$ time dependence, the curl equation becomes

$$\nabla \times \overline{E} = -j\omega \overline{B} = -jk\,c\,\overline{B} \tag{3.3}$$

where

$$k = \frac{2\pi}{\lambda} = \frac{\omega}{c}$$

Integrating both sides over loop, this becomes

$$\iint \nabla \times \overline{E} \cdot d\overline{S} = -jk \iint c\,\overline{B} \cdot d\overline{S} \tag{3.4}$$

$$\oint \overline{E} \cdot d\overline{\ell} = -jkc \iint \overline{B} \cdot d\overline{S} \tag{3.5}$$

If the loop area is very small, then the magnetic field in the loop is uniform with magnitude $\bar{B}^{i}_{0}$. The integral is

$$e = -jkc \iint \bar{B} \cdot d\bar{S} = -jkc\, B_0\, A \tag{3.6}$$

Where e is the induced emf; and where A is the area of a loop. Defining an effective height of a loop antenna as

$$h_b = -jkA \tag{3.7}$$

the low frequency input admittance of a loop with a constant current (Ref. 12) is

$$Y_0 = \left[\oint Z_i\, d\ell + \frac{j\omega\mu}{4\pi} \oint\oint \frac{e^{-jkR}}{R}\, d\bar{\ell}' \cdot d\bar{\ell}\right]^{-1} \tag{3.8}$$

An unloaded magnetic sensitivity K_B is defined as

$$K_B = Y_0 h_b / \lambda \quad \text{(Ref. 10)} \tag{3.9}$$

Now

$$e = I_0 / Y_0 = -jkA\, cB_0 \tag{3.10}$$

$$I_0 = (-jkA)\, Y_0\, cB_0 = h_b\, Y_0\, cB_0 = \lambda K_B (cB_0) \tag{3.11}$$

I_0, therefore, is a measure of the normal component of the magnetic field at the center of the loop, independently of the electric field. The loop sensitivity for the electric field, K_E, is a function of the size of the loop.

Let the current in the loop due to the incident fields consist of the zero and the first phase-sequence currents, i.e.,

$$I(s) = I^{0}(s) + I^{(1)}(s)$$

$$I(s + \ell/2) = I^{0}(s) - I^{(1)}(s) \qquad (3.12)$$

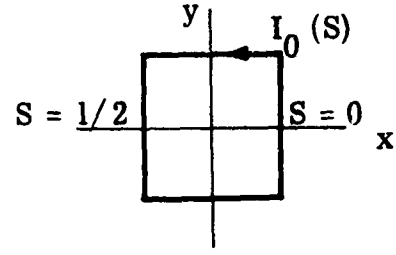

Fig. 3.1 Rectangular current loop

The first phase current $I^{(1)}(s)$ depends directly upon the electric field (Ref. 10). Let the loop lie on the x-y plane and the center of the loop at the origin, then $I^{(1)}(s)$ can be further broken up into

$$I^{(1)} = I_x^{(1)} + I_y^{(1)} \qquad (3.13)$$

corresponding to $E_{x_0}^{(1)}$ and $E_{y_0}^{(i)}$. Therefore, the current at s = 0 is

$$I_y^{(1)}(0) = h_e Y_i E_{y_0}^{i} \qquad (4)$$

For a short dipole, $h_e = \ell/2$ where ℓ is the length of the antenna.

Then,

$$I_y^{(1)}(0) = \lambda K_E E_{y_0}^{(i)} \tag{3.15}$$

where

$$K_E = Y_I h_{eI} / \lambda \tag{3.16}$$

For a magnetic loop with a diameter D, the effective height h_b becomes:

$$h_b = -jk\pi D^2/4 \tag{3.17}$$

and the magnetic sensitivity defined in Eq. 3.9 becomes

$$K_B = \frac{-\pi D}{\lambda \eta_0 \left(\Omega - 3.52 + 13.0 \frac{D^2}{\lambda^2}\right)} \tag{3.18}$$

where

$$\Omega = 2 \ln \frac{2D}{a}$$

a = radius of wire loop

The current induced on the portion of the loop parallel to the incident field is from the electric sensitivity.

$$I(\phi) = E_{y_0}^{i} \frac{D}{j\eta a_1} \cos \phi \tag{3.19}$$

where η is the characteristic impedance of the medium, and a_1 is an expansion coefficient given by Storer (Ref. 13). For $D \leq 0.1\lambda$, the electric sensitivity reduces to

$$K_E = (j\,2\pi^2 D^2/\lambda^2)/\eta_0\,(\Omega - 3.52)(1 - 9.8\,D^2/\lambda^2) \quad (3.20)$$

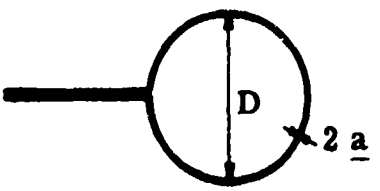

Fig. 3.2. Circular loop probe

Also, it can be shown that for a loop with a diameter $D << 0.03\,\lambda$

$$K_E \propto \frac{D}{\lambda^2}$$
$$K_B \propto \frac{D}{\lambda} \quad (3.21)$$

From the dependences of electric and magnetic sensitivities upon the loop size, and since the loop current is directly proportional to the sensitivities K_E and K_B, the loop diameter should be as small as possible to minimize the effect of electric field upon the total current measured. The lower limit, however, is dictated by the fabrication technique and the receiver sensitivity.

3. 3 Experimental Procedures

The current measurement on the antenna was obtained by detecting the magnetic field locally along the antenna with a circular probe that is sensitive to magnetic fields. Initially, the experiment was carried out on a model at a frequency range between 5 MHz through 30 MHz. The antenna used for the impedance measurement was 2. 5 meters long, which represents a quarter wavelength at 30 MHz. A one-quarter-inch copper tubing was used an an antenna, and the current along the antenna was detected with a traveling probe moved along an axial slit cut in the antenna. This technique was first developed by King et al. for measurement of antenna current distributions.

Since the object of this study was to examine the effects of the size and location of a finite-size ground plane, a systematic variation of ground plane diameters and their locations above the natural ground, up to a half wavelength at the highest frequency, was planned. In the frequency band chosen, this size represented a ground plane diameter and its location up to 5 meters. Due to the bulky physical size of the full scale system, a smaller scale model was adopted.

The scale models used were the same ones used in the radiation pattern studies. For current distribution measurements, the entire system was put into an anechoic chamber that is designed to operate above 100 MHz. The detecting probe for the local magnetic field along the antenna has a loop diameter much smaller than a wavelength, even at the higher frequency of 200 MHz through 1200 MHz.

The probe was suspended from the top of the anechoic chamber to the current element and its movement was synchronized using a Scientific-Atlanta recorder. The detected signal was then fed into a recorder and the result recorded.

The probe, the anechoic chamber, and the equipment used for this measurement are shown in Fig. 3. 3 through 3. 5. The block diagram showing the current measurement set-up is shown in Fig. 3. 6.

Detection of a current along a current element with an external probe, as shown in our experiment, was accepted fully by many people. Since the near field may be disturbed by the presence of the probe, and its lead, a probe traveling inside an antenna with only that part of the probe which is used for detecting the local magnetic field exposed through a slit was the optimum choice. However, if the probe is very small, compared with a wavelength, and if the lead from the probe to the recorder is well shielded from any stray pick-up, the effect of the external probe upon the antenna current was minimal. The lead from the probe to the recorder was a solid copper outer-conductor coaxial line (Micro Coax cable) with an outer diameter of 0. 5 mm. The probe lead was oriented perpendicular to the antenna current element, to minimize the disturbance of the near-zone electric field parallel to the current element.

To test the accuracy of this type of current measurement, a quarter-wavelength monopole was mounted over a ground plane, that simulated natural, infinite ground. The ground plane was a 5 wavelength

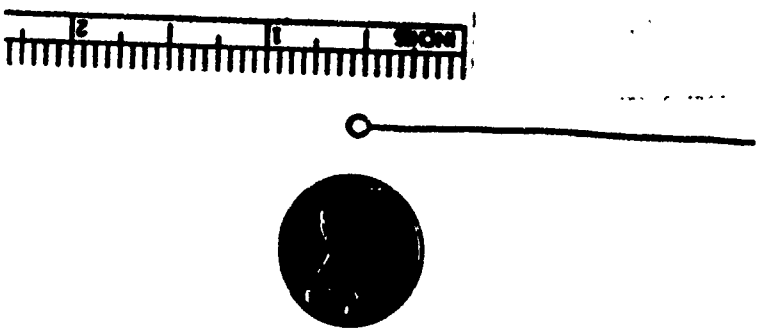

Fig. 3. 3. Current probe

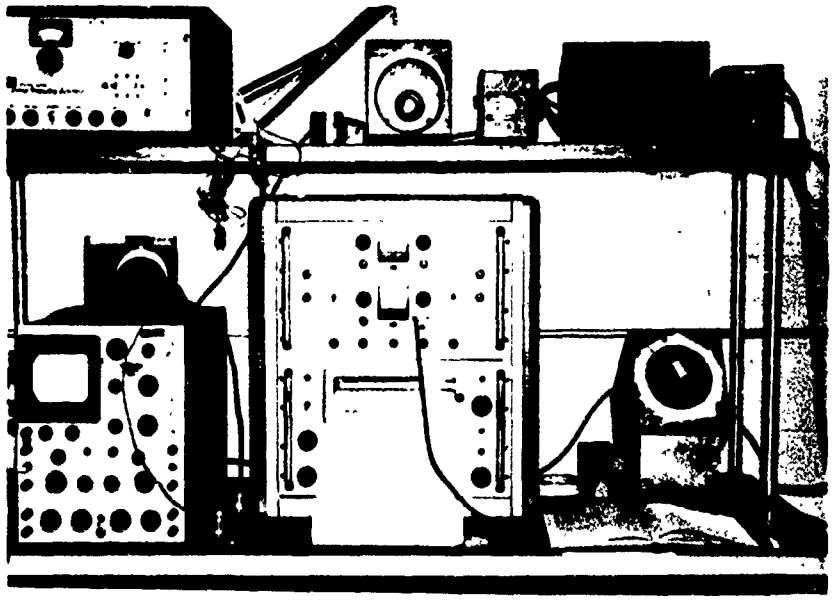

Fig. 3. 4. Current measurement set up

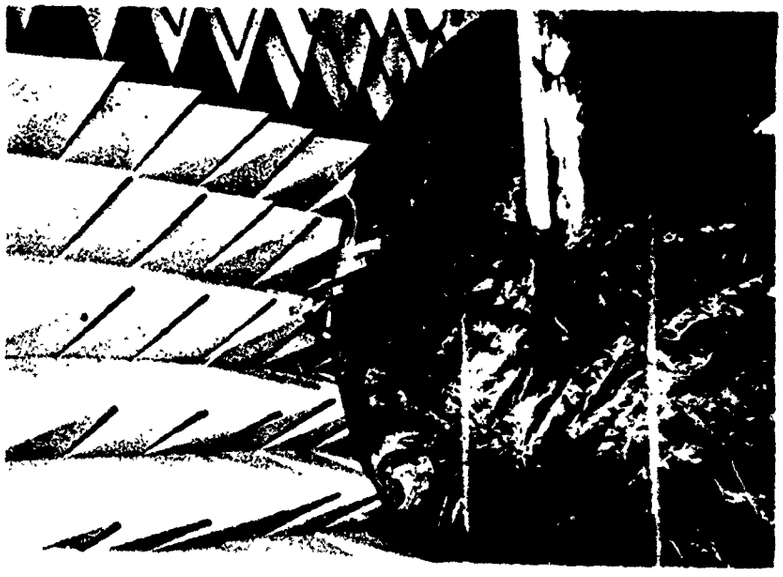

Fig. 3.5. Anechoic chamber

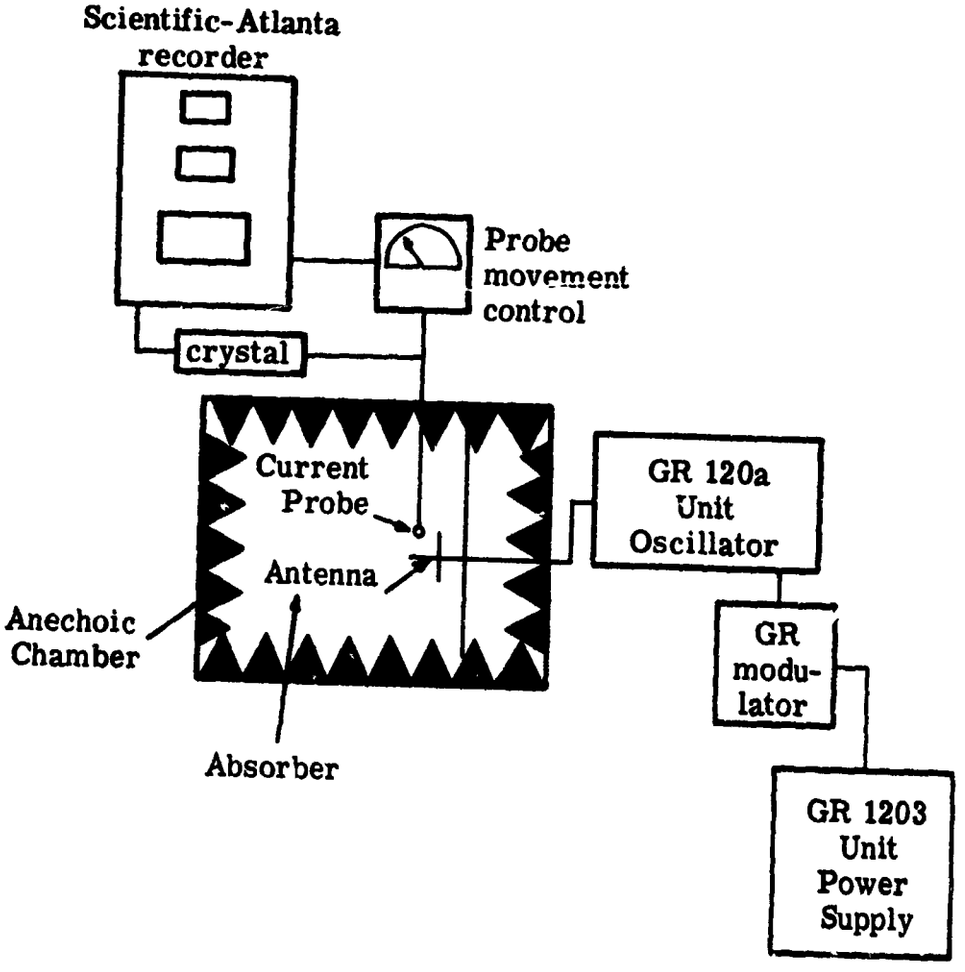

Fig. 3.6. Block diagram for current measurement set-up

in diameter aluminum ground plane. The test frequency was 1200 MHz, where 6.25 cm is a quarter-wavelength. The measured current distribution at this frequency was plotted against an exact sinusoidal distribution in Fig. 3.7. This measurement agrees very closely with the King measurement of a current on a cylindrical antenna with a probe traveling inside the cylindrical antenna with a slit cut along the axial direction.

3.4 Measurement Results

The variables for the current measurements were the same as those for the radiation pattern measurement. In Fig. 3.8, a plot of the theoretical current distribution of a monopole over an infinitely large conducting ground is made for 6 different frequencies. The antenna was a quarter-wavelength at the upper end of the frequency, namely 30 MHz, and as frequency was reduced to 5 MHz in 4 steps, the resulting antenna current distribution was plotted in order to compare these currents with those on the same length of antenna over a finite ground plane located various distances away from the large ground. In Figs. 3.9 through 3.14 at each frequency the diameter of a small ground plane was fixed at a given fraction of wavelength and locations of this ground plane were varied in four steps. Figures 3.15 through 3.20 show the effect of ground plane diameter when located at a fixed distance away from the large ground.

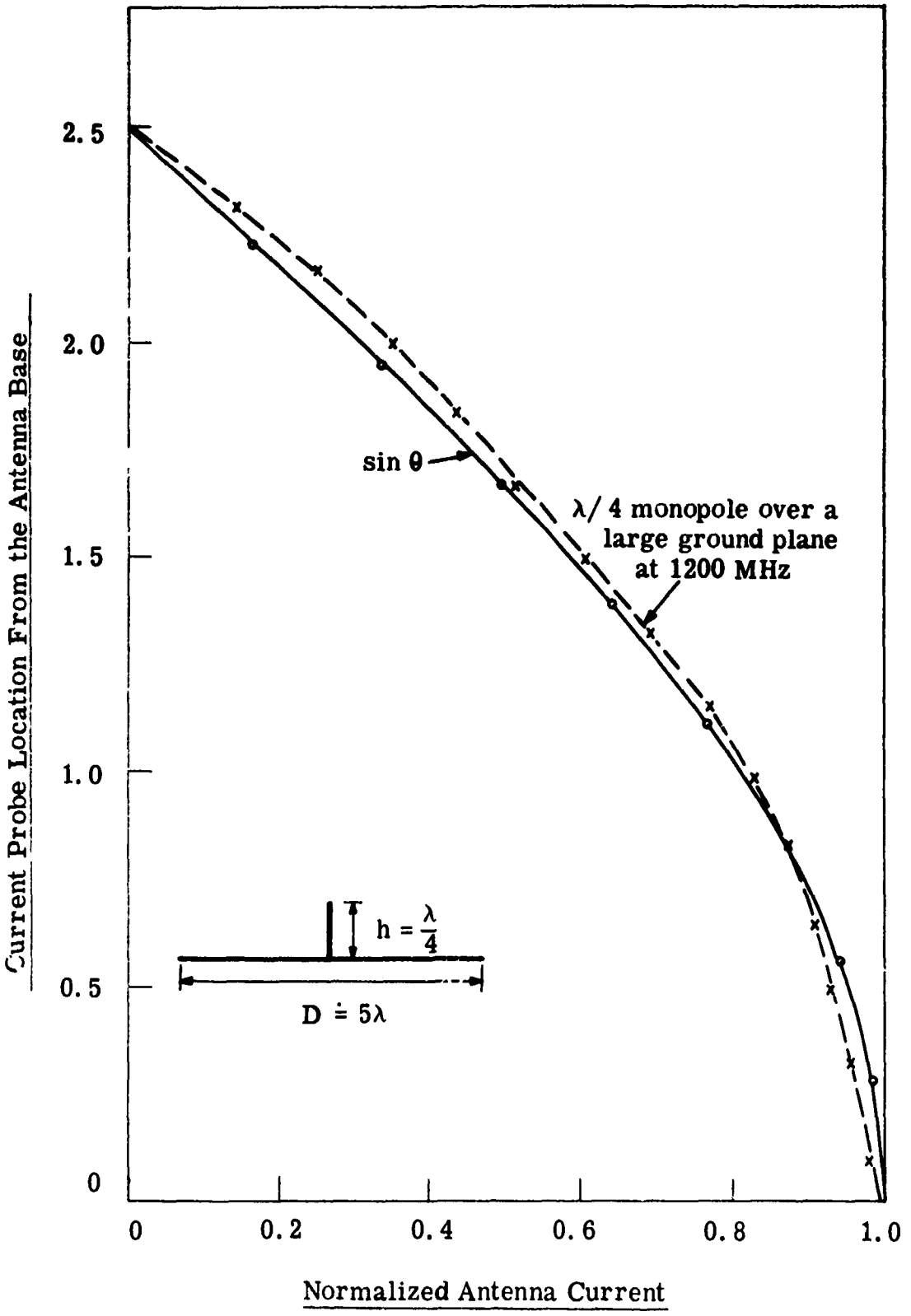

Fig. 3.7. Comparison of a sine curve with a current distribution of a monopole over a large ground plane

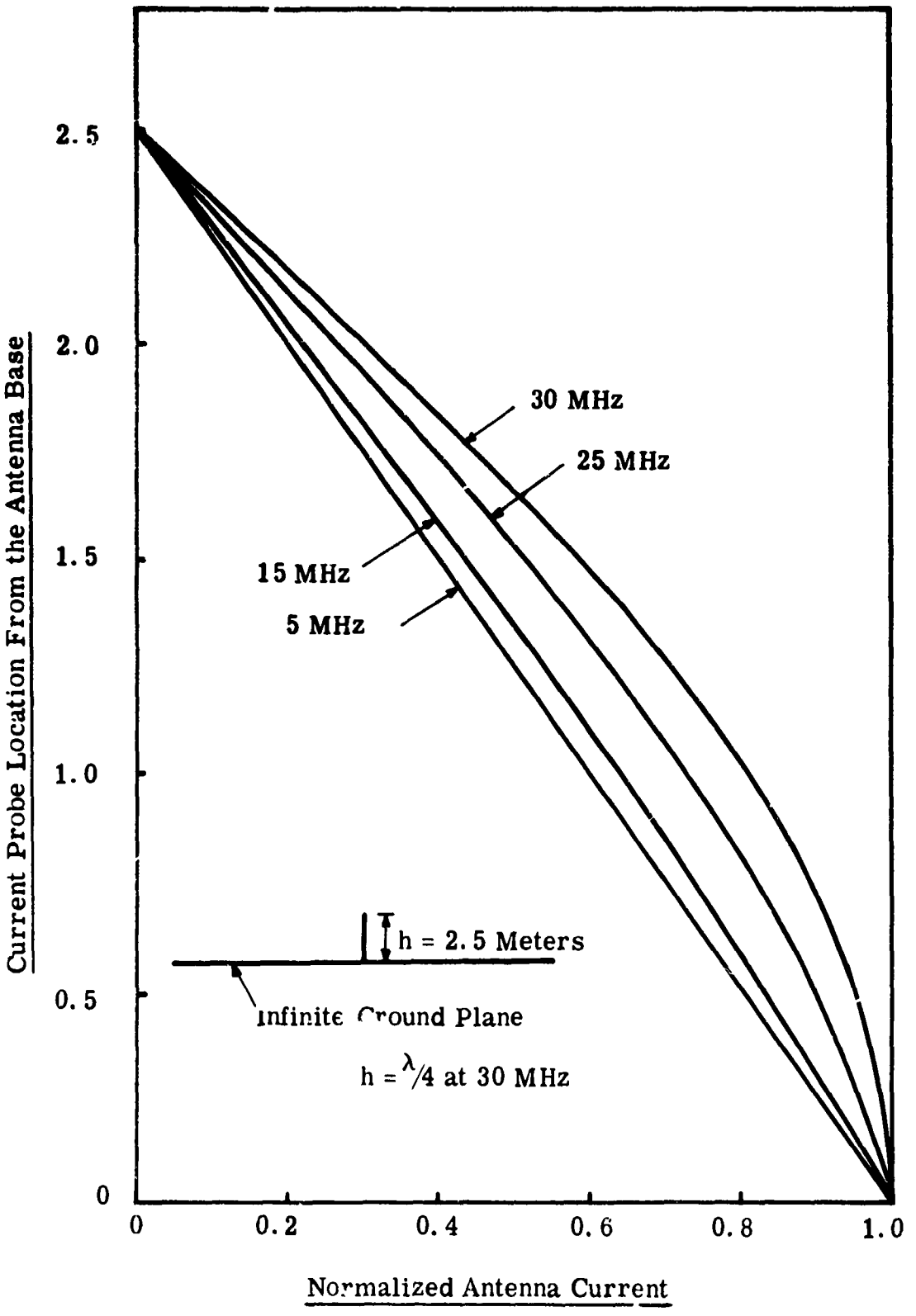

Fig. 3.8. Theoretical current distribution of a monopole on an infinite ground plane.

The same measurement was performed with a hemispherical ground plane, in order to study the validity of a sinusoidal current assumed on the antenna for a theoretical study which was carried out in Chapter 5. These measurement results are plotted in Figs. 3.21 through 3.22.

Only amplitudes of the current on the antenna have been measured, and the maximum amplitude for each set of measurements was normalized to 1.

The theory developed in Chapter 5 for an antenna on a hemispherical ground plane began with an assumption that the current distribution on the antenna is in the sinusoidal form. It was further assumed that the antenna current was independent of the induced current on the ground plane surface. Accuracy of the theoretical results largely depend upon the accuracy of this assumption. From the measurement results shown in Fig. 3.21 through 3.22, it can be seen that at frequencies where the antenna is near a quarter-wavelength long, the assumption of a sinusoidal current distribution was fairly accurate. However, at frequencies below 20 MHz, the currents on the antenna were modified appreciably due to interaction between the antenna current and the ground plane current. At 5 MHz, in particular, the current distribution on the antenna was almost constant in magnitude, similar to the current distribution normally assumed for a Hertzian dipole. Original assumption of a sinusoidal current distribution should, on the other hand, provide a form close to a triangular distribution at 5 MHz

for an antenna resonating at 30 MHz. This type of distribution is similar to the current distribution of so-called Abraham dipole. Assuming that the physical length of these two antennas were the same, their effective heights differ by a factor of 2. Therefore, a constant current distribution gives a radiation resistance as large as 4 times that of a triangular current distribution provided that the amplitude of the triangular currents are the same.

A monopole with a finite disc antenna shows a better agreement between the assumed sinusoidal current distribution and the experimentally measured distribution at both the high and low ends of frequency band. However, at the midband, the current distributions show lower amplitudes compared with a sinusoidal distribution. Also noticed was that for a given size of disc diameters, the changes in the location of the ground plane height (a) affects the current distribution more than the changing ground plane diameters at a fixed position. It was also noticed that when the ground plane diameter was less than 1.25 meters, the current distribution was such that the amplitudes were bigger than those of sinusoidal distribution.

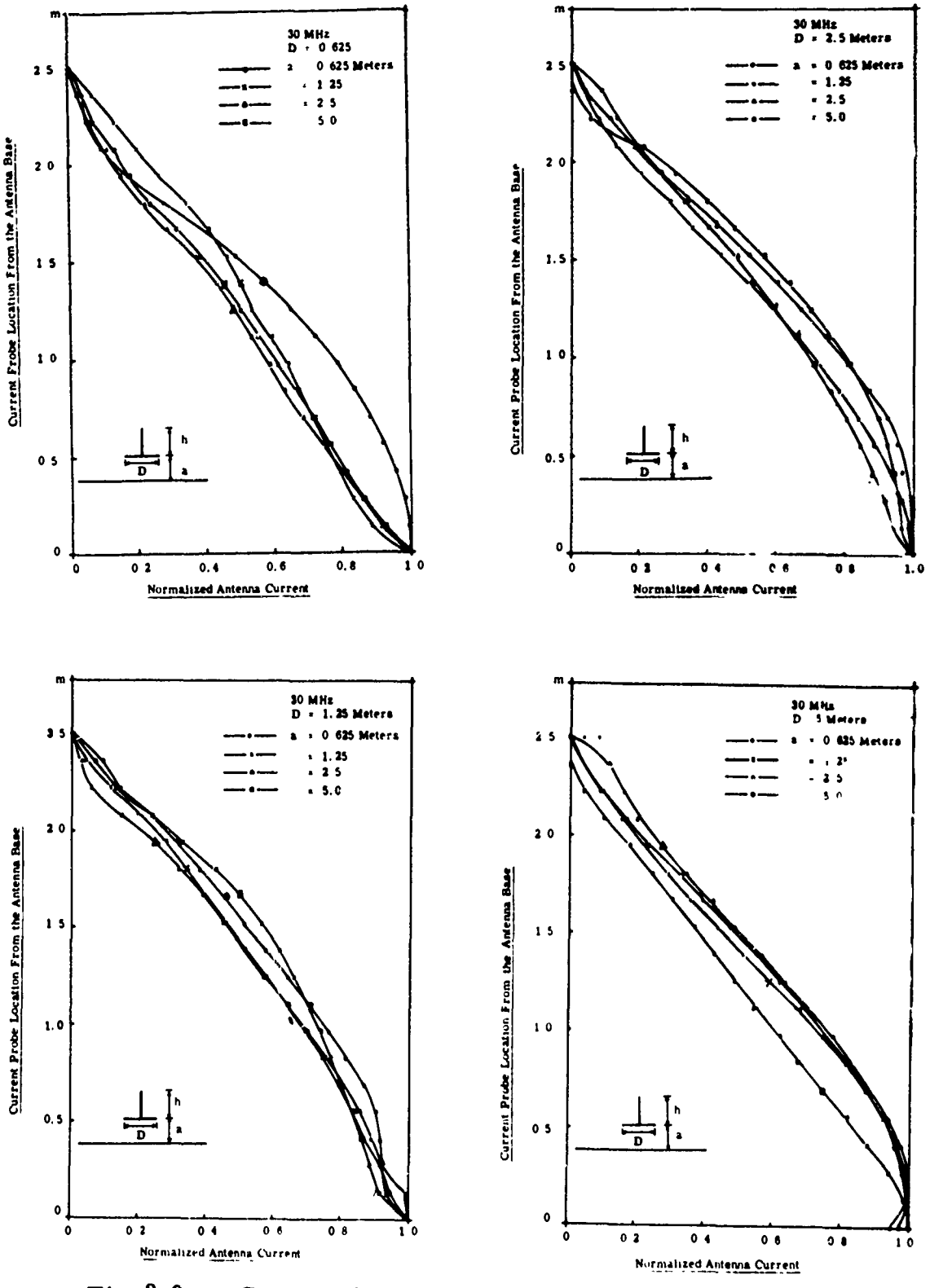

Fig. 3.9. Current distribution on a monopole antenna with a finite ground plane at various locations with respect to an infinite ground at 30 MHz

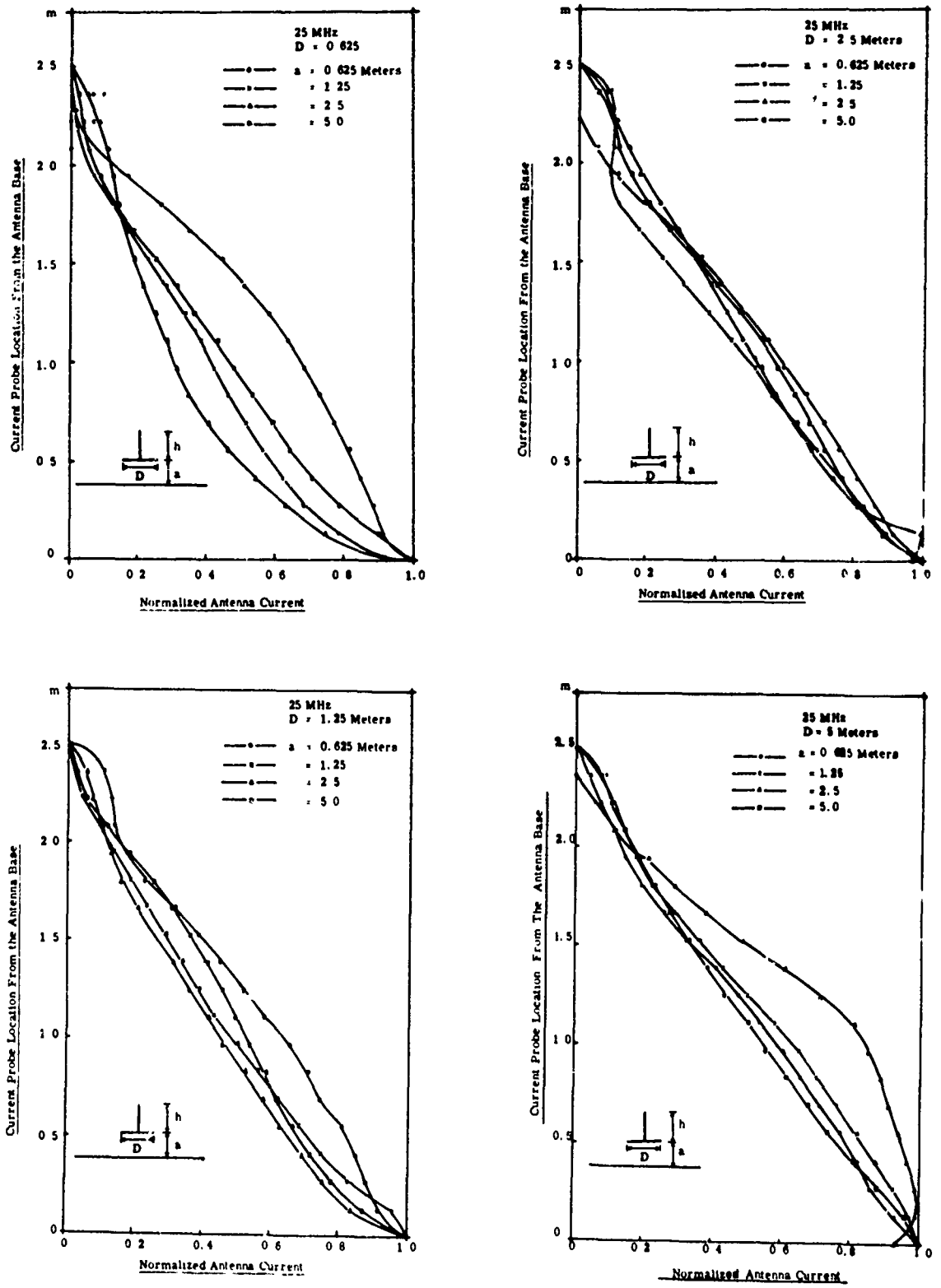

Fig. 3. 10. Current distribution on a monopole antenna with a finite ground plane at various locations with respect to an infinite ground at 25 MHz

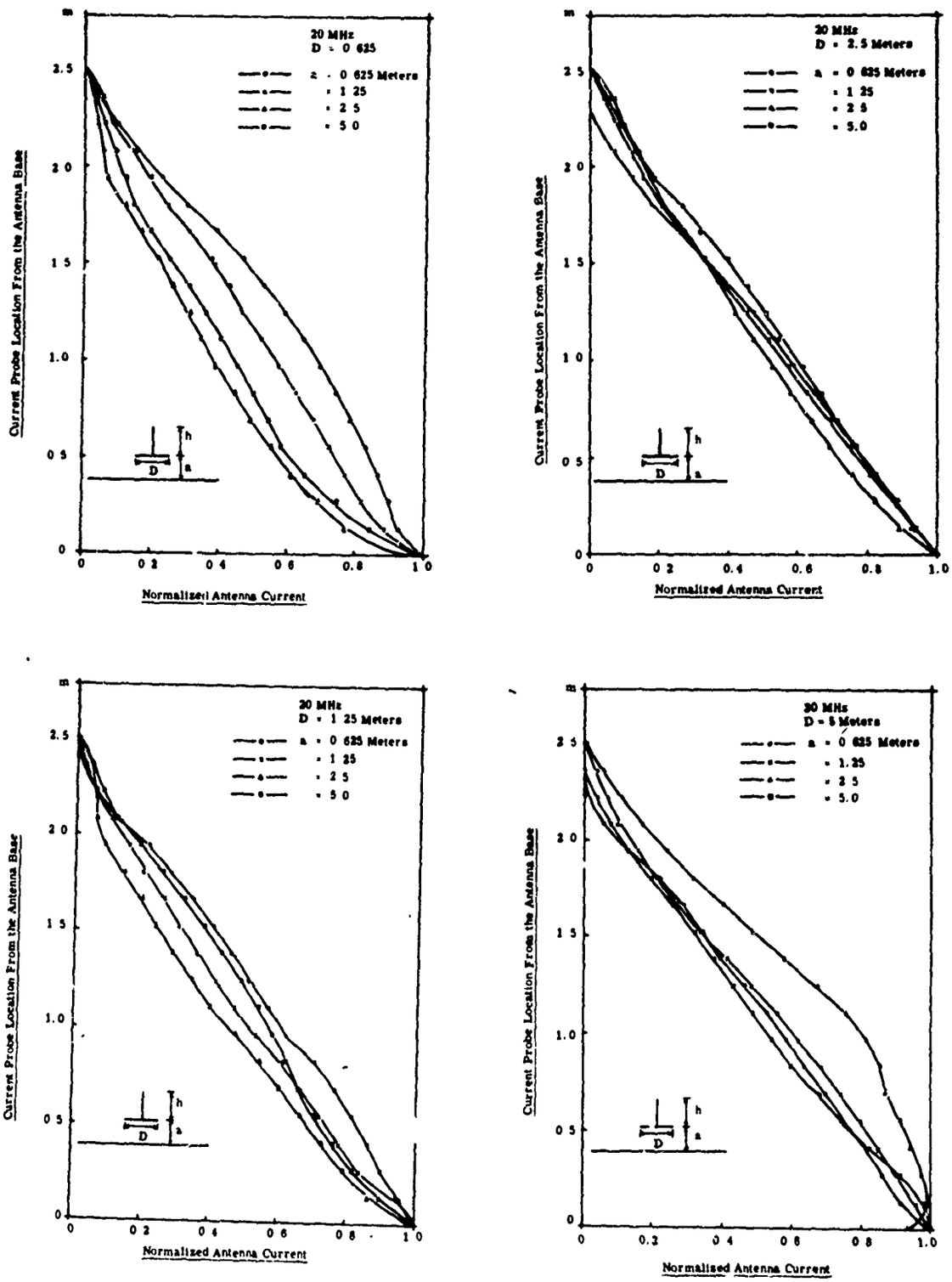

Fig. 3. 11. Current distribution on a monopole antenna with a finite ground plane at various locations with respect to an infinite ground at 20 MHz

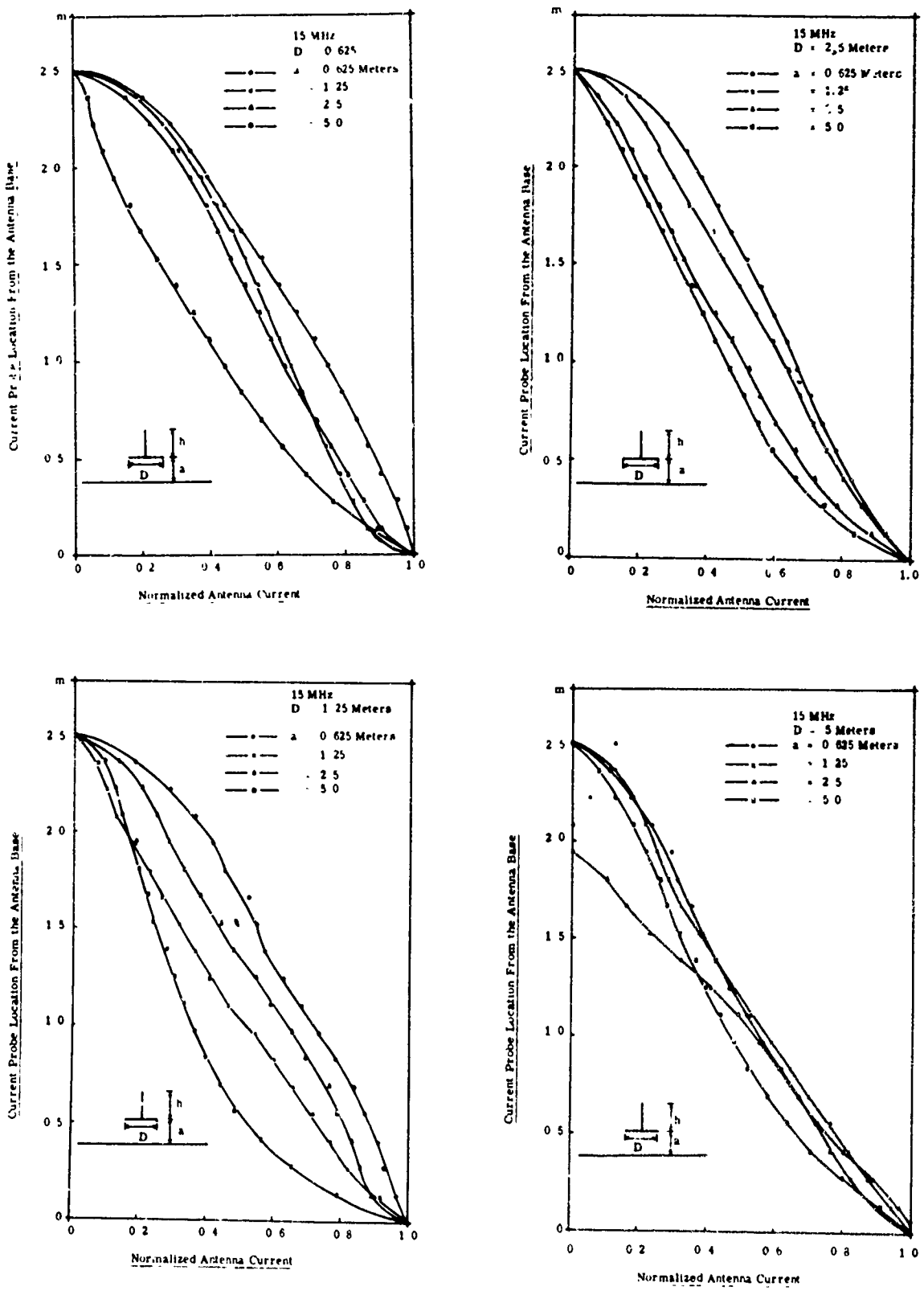

Fig. 3. 12. Current distribution on a monopole antenna with a finite ground plane at various locations with respect to an infinite ground at 15 MHz

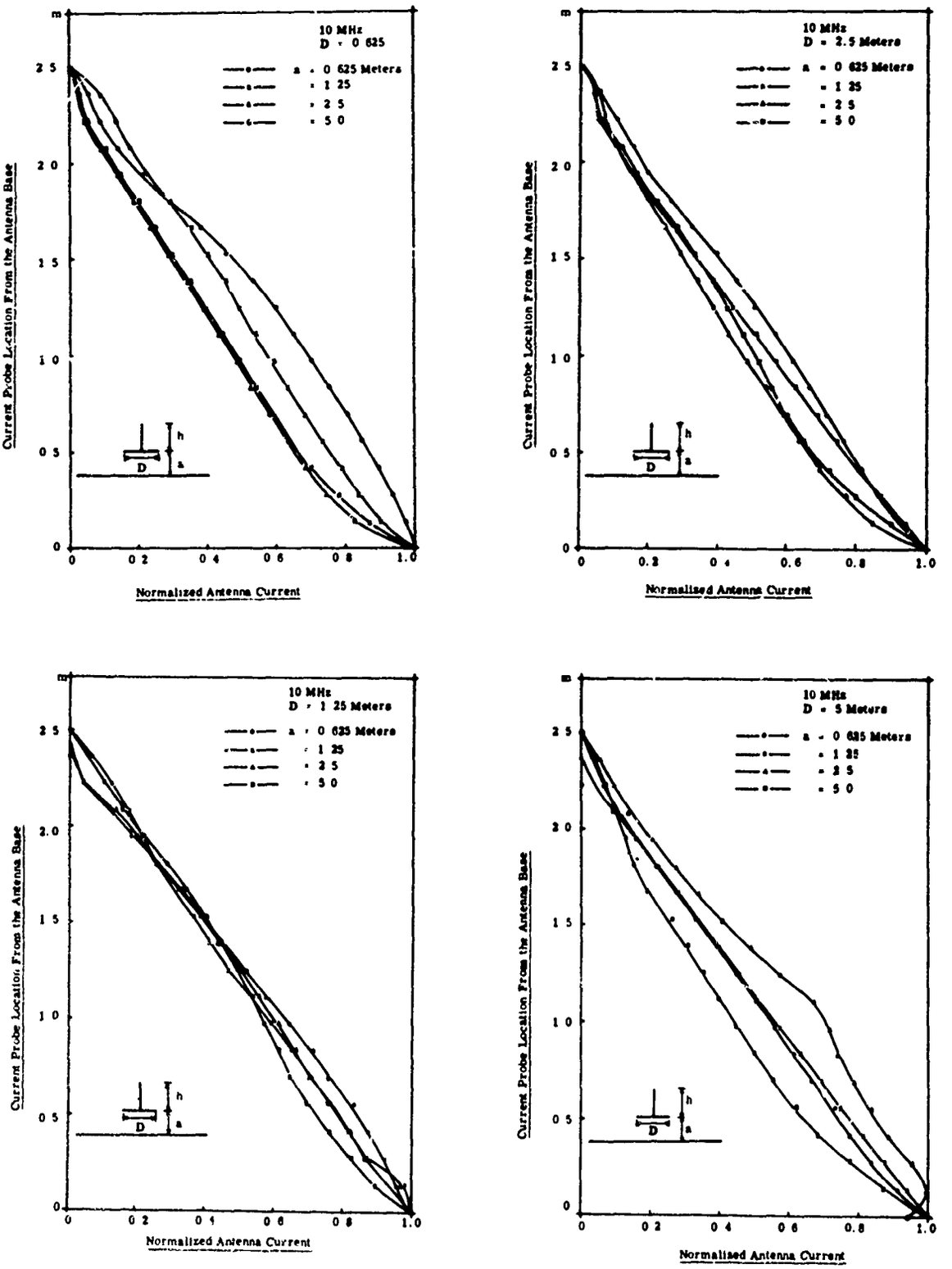

Fig. 3. 13. Current distribution on a monopole antenna with a finite ground plane at various locations with respect to an infinite ground at 10 MHz

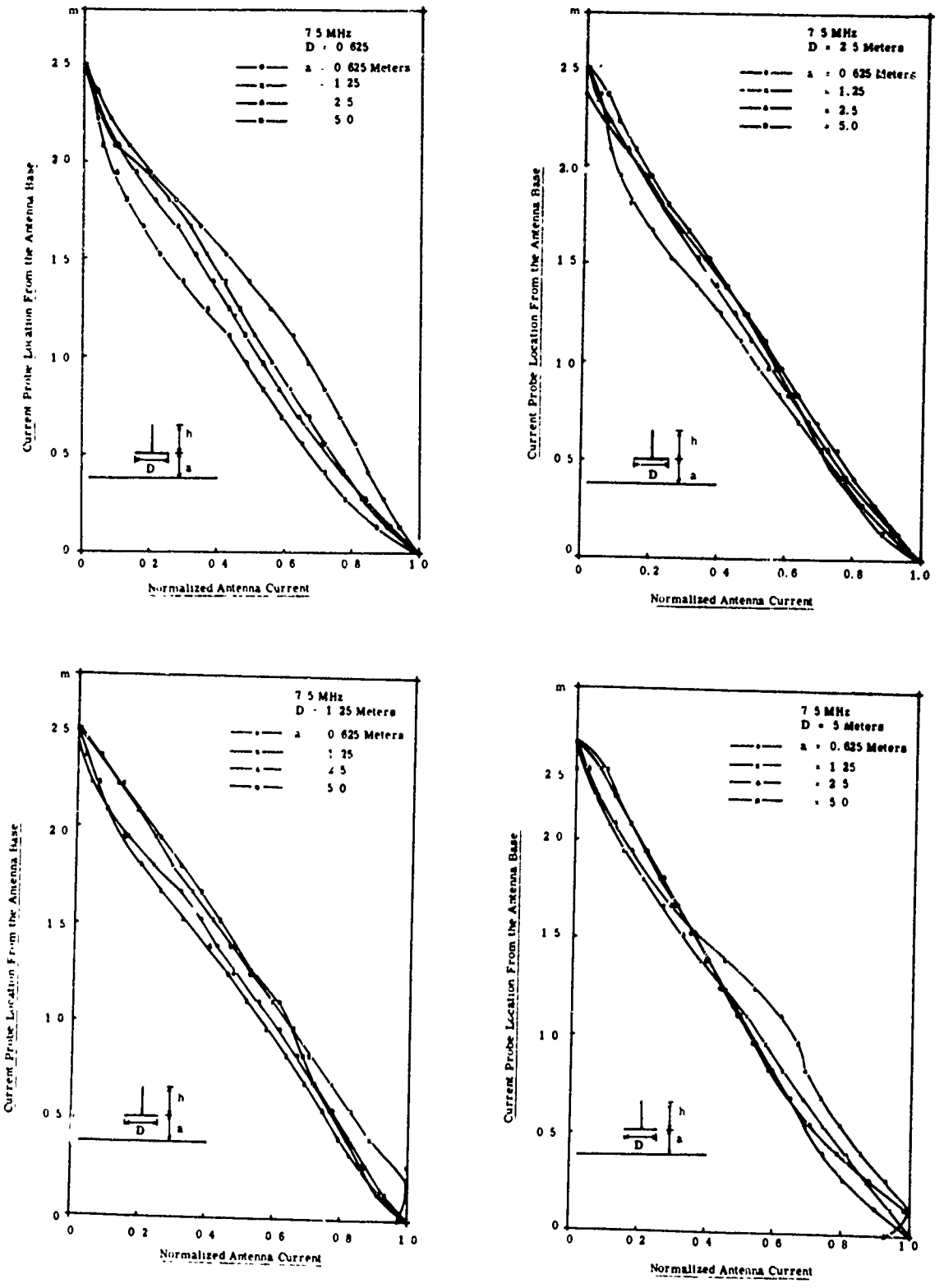

Fig. 3.14. Current distribution on a monopole antenna with a finite ground plane at various locations with respect to an infinite ground at 7.5 MHz

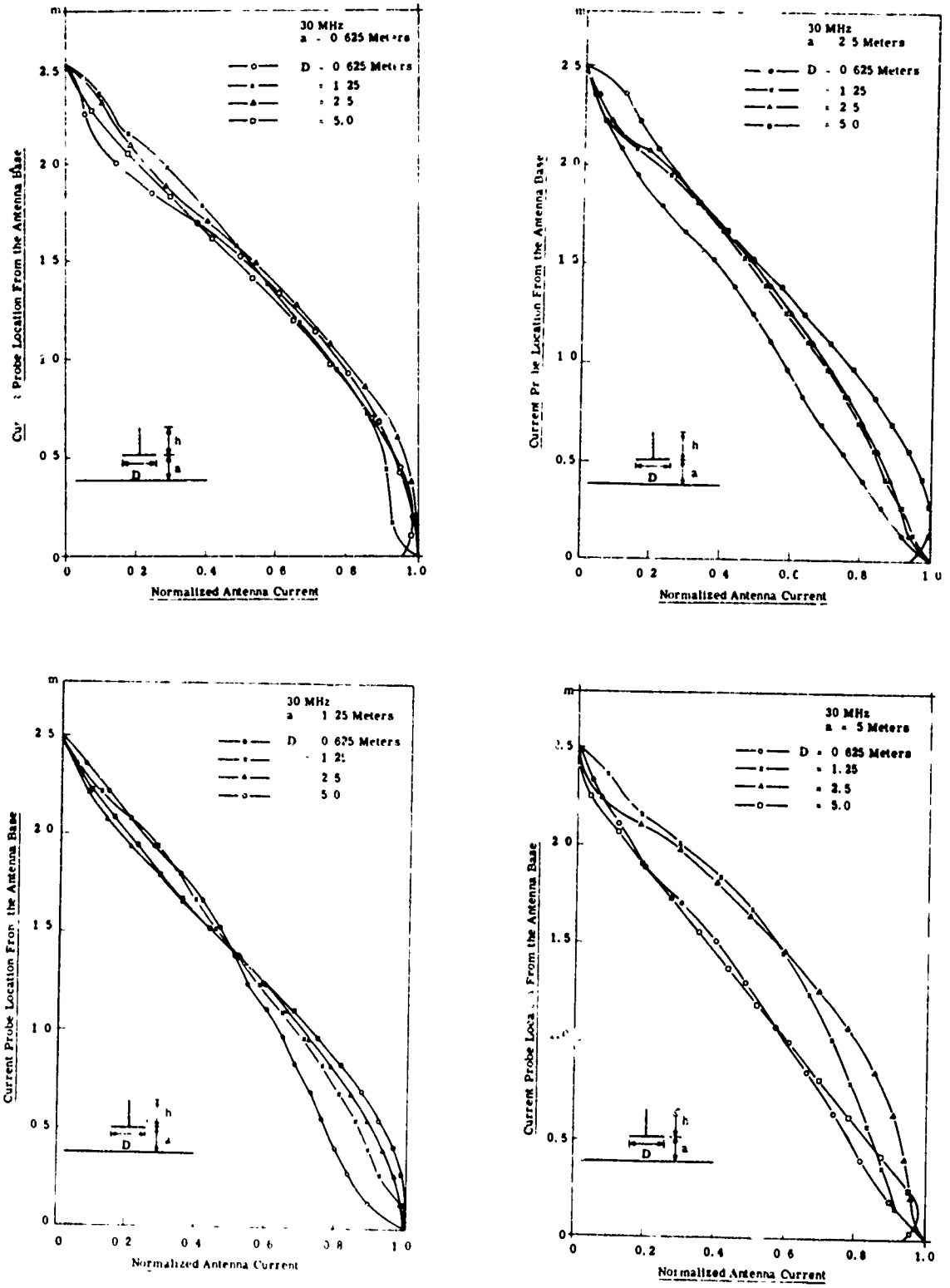

Fig. 3. 15. Current distribution on a monopole antenna with a ground plane of various diameters at a given location with respect to an infinite ground at 30 MHz

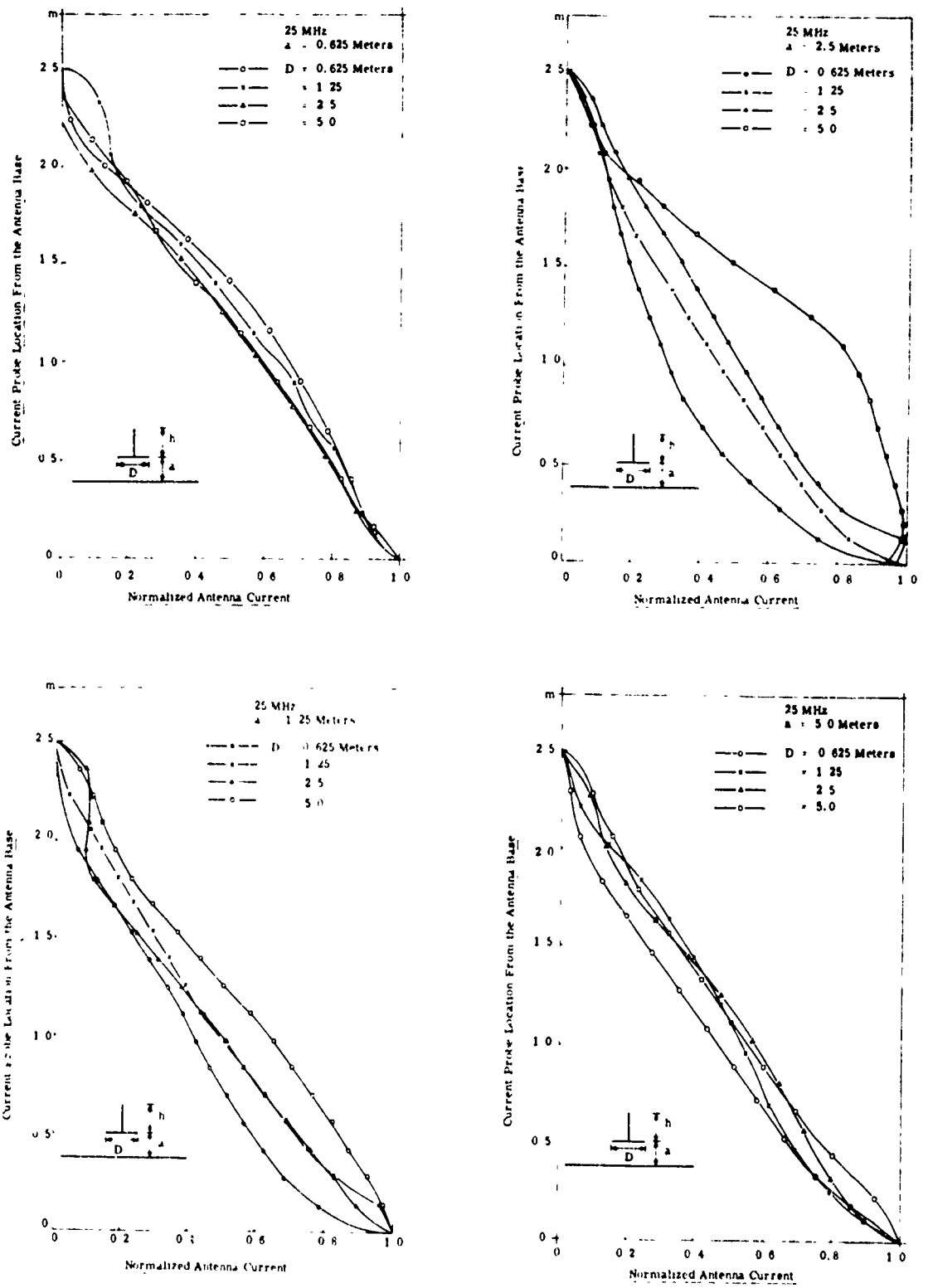

Fig. 3. 16. Current distribution on a monopole antenna with a ground plane of various diameters at a given location with respect to an infinite ground at 25 MHz

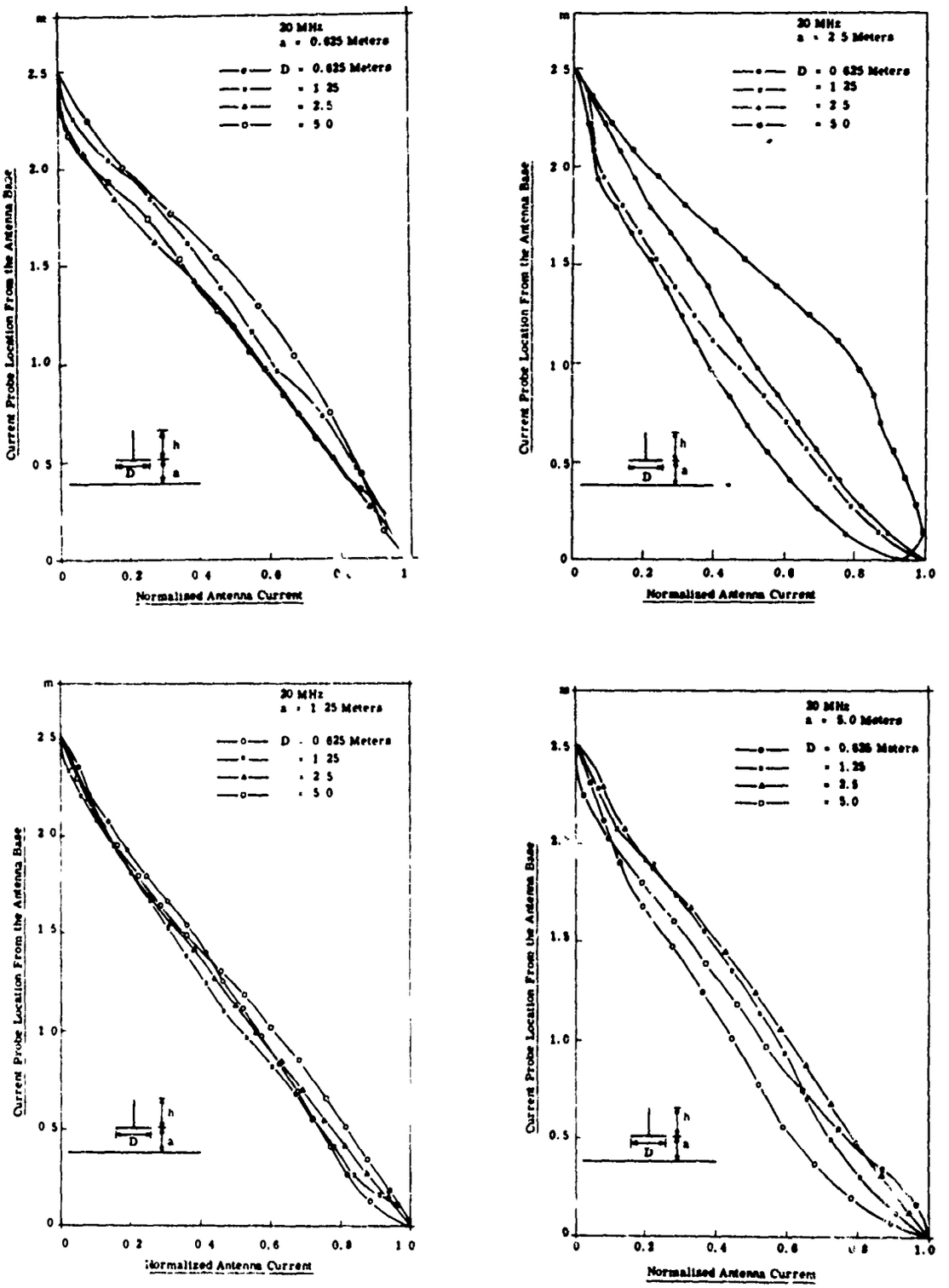

Fig. 3.17. Current distribution on a monopole antenna with a ground plane of various diameters at a given location with respect to an infinite ground at 20 MHz

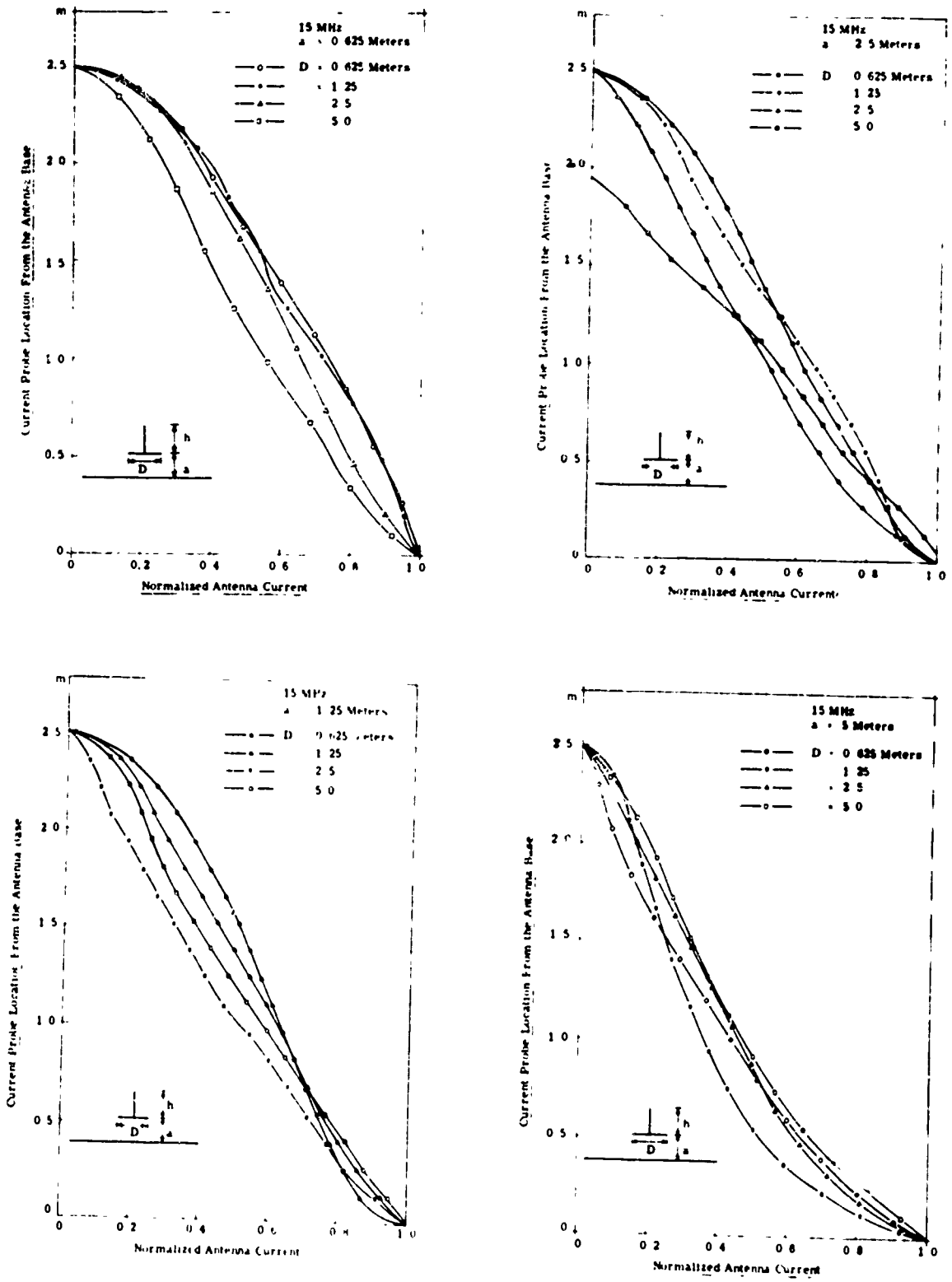

Fig. 3. 18. Current distribution on a monopole antenna with a ground plane of various diameters at a given location with respect to an infinite ground at 15 MHz

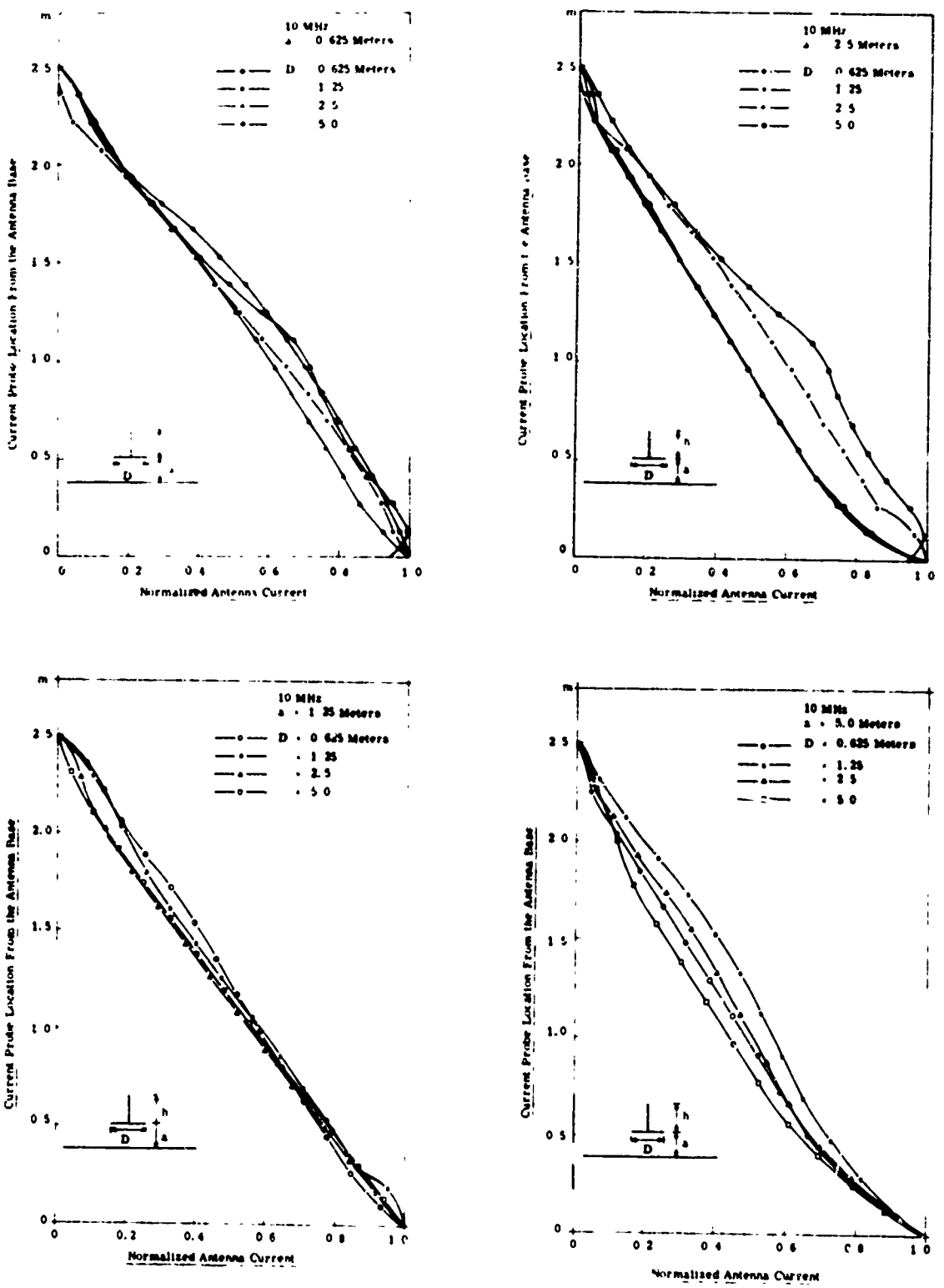

Fig. 3.19. Current distribution on a monopole antenna with a ground plane of various diameters at a given location with respect to an infinite ground at 10 MHz

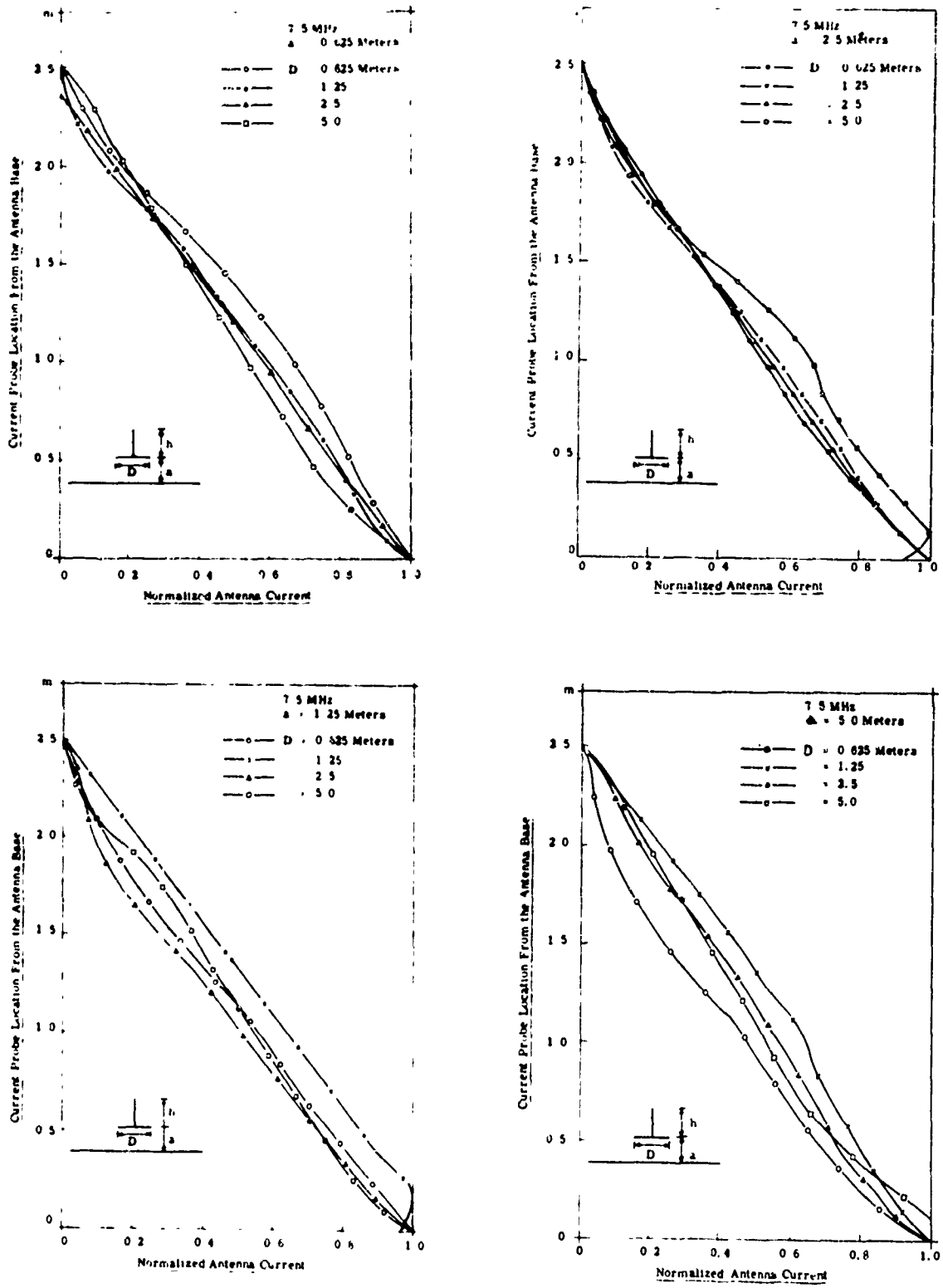

Fig. 3.20. Current distribution on a monopole antenna with a ground plane of various diameters at a given location with respect to an infinite ground at 7.5 MHz

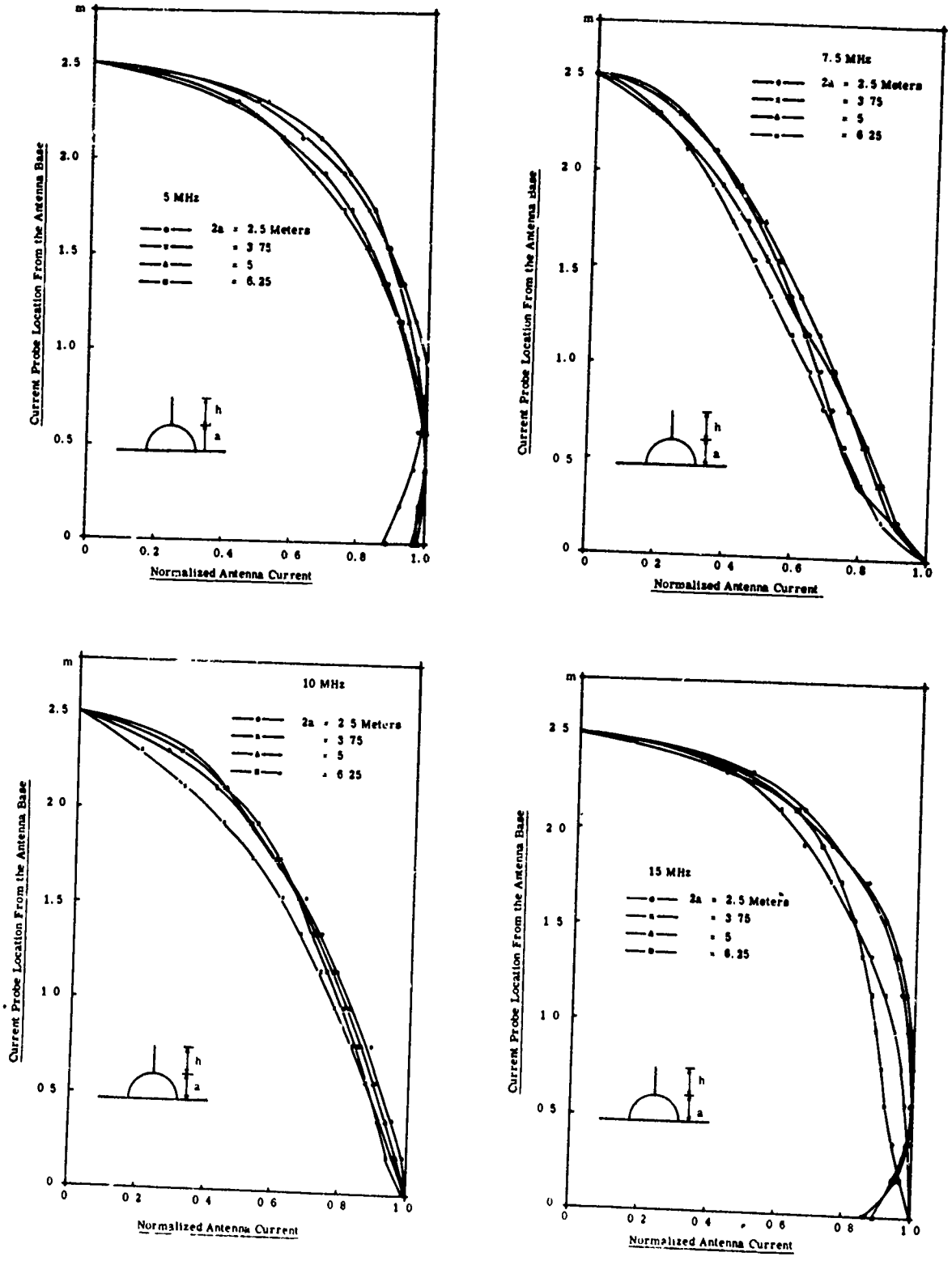

Fig. 3. 21. Current distribution on a monopole antenna with a hemispherical ground plane of various sizes

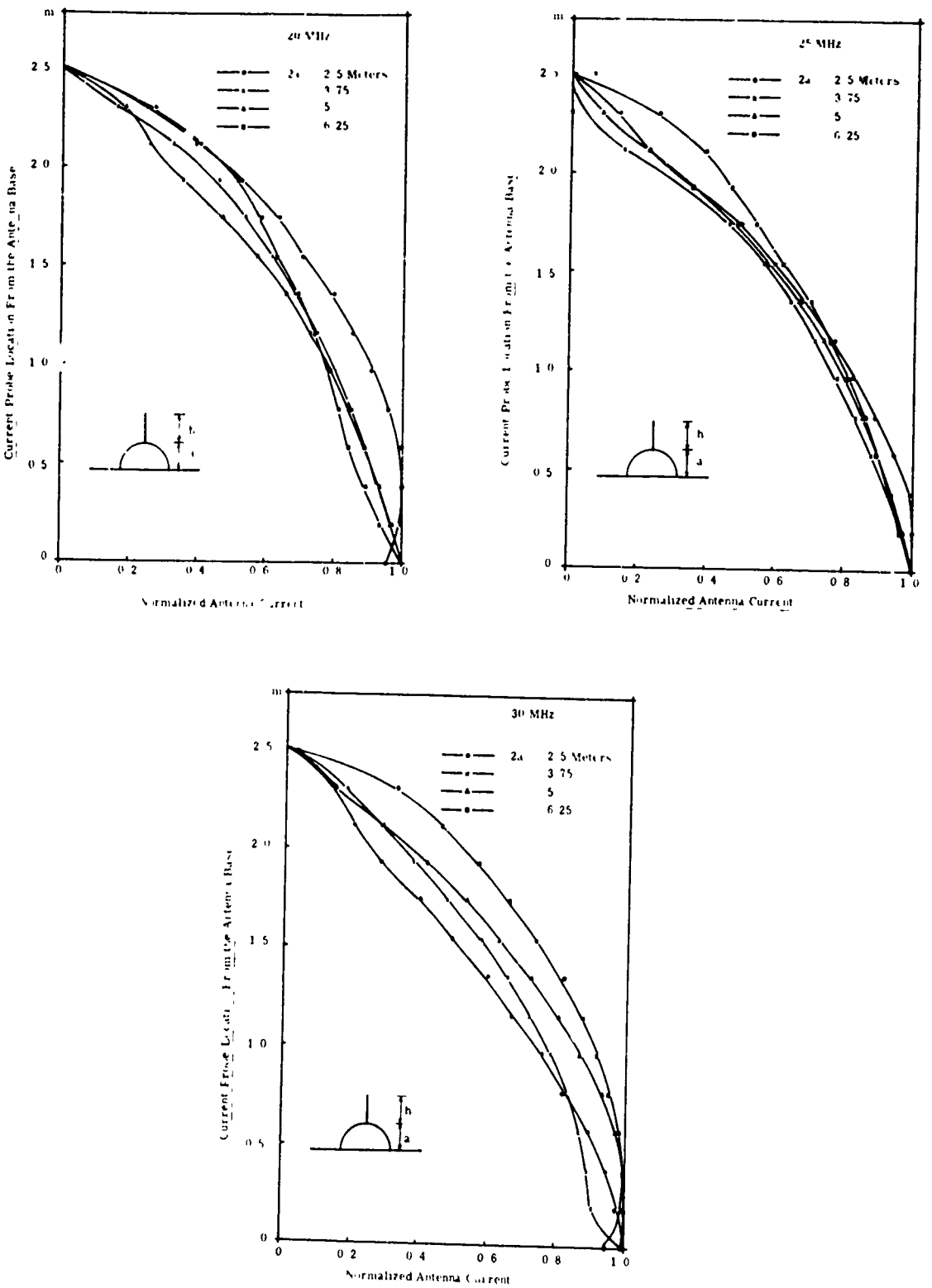

Fig. 3. 22. Current distribution on a monopole antenna with a hemispherical ground plane of various sizes

CHAPTER IV

RADIATION PATTERN MEASUREMENTS

4.1 Introduction

The important parameters of any antenna are its radiation patterns and its input impedance. In this chapter, the experimental results of the radiation pattern measurements are given. The arrangement of the experimental results is intended to show the effect of the ground plane size and its location with respect to the infinitely large natural ground upon the radiation properties of the antenna system. Certain approximations and assumptions had to be made because of the practical limitations that confront this type of experiment, and they are discussed.

4.2 Measurement Problems

The input impedance measurements discussed in Chapter II were performed with a monopole a quarter wavelength long at 30 MHz and a ground plane whose diameter varied from 0.625 meter up to 5 meters. The experiment was conducted in the frequency band of 5 MHz through 30 MHz. In performing the radiation pattern measurements, several assumptions and approximations were made. The antenna test range was originally designed for high frequency operation, mainly because the required physical size and distance between the transmitting and receiving antenna were more practically realizable in the higher

frequency ranges. The linear dimensions of the original antenna and ground plane were reduced by a factor of 40 so that the operating test frequency was between 200 MHz to 1200 MHz. The electromagnetic scaling and conditions under which this is valid have been discussed in detail in Chapter 2.

In the original antenna and ground plane measurement, the infinite ground below a finite ground plane was the natural ground with a certain electrical conductivity (σ). One of the conditions for scaling the electromagnetic system is increasing the conductivity of the scale model by a scale factor. In this case, the large ground plane simulating the infinite natural ground must have a conductivity of 40 σ . Also, the antenna and the ground plane for the scaled model should have been fabricated with a material whose conductivity was 40 times higher than the copper and aluminum used for the monopole and ground plane, respectively.

For practical reasons, copper was used for both the antenna and for the finite ground plane. Copper mesh screen was used for simulating the infinite natural ground of the reduced model. The copper mesh screen used was in the form of a rectangular screen 5 feet by 5 feet in size. This represents 6 wavelengths on one side at the upper end of the frequency band and 1 wavelength long for each side at the lower end of the band.

Due to the finite size of this simulated infinite-ground-plane, the radiation patterns, in general, tend to have their maximum

radiation intensity off the horizontal axis, where ordinary polar angle (θ) in the spherical coordinate system is 90 degrees.

A quarter wavelength monopole on an infinite conducting ground plane has a radiation pattern in the form of $\sin\theta$, which gives the maximum intensity of the radiation field in the direction of $\theta = 90^{o}$. Leitner and Spence (Ref. 3) have showed, theoretically, the dependence of this pattern on ground plane size. For a circular ground plane of radius a, the far-field radiation patterns were plotted for ka = 3, 4, 5 and 6.5. They all have maximum intensity off the horizontal axis where $\theta = 90^{o}$.

Therefore, the results obtained from this experiment are expected to differ somewhat from the theoretical results where the ground plane was assumed to be infinite

4.3 Experimental Technique

The radiation patterns obtained in this experiment are taken in an x-z plane as a function of polar angle θ, as shown in Fig. 4.1. When the antenna and the ground plane are oriented in this way, the axis of the monopole coincides with the $\hat{z}$ axis of a rectangular coordinate system, the antenna is vertically polarized. This pattern is sometimes called the "E plane" pattern where E_{θ}, with ϕ constant as a function of θ, is the quantity actually measured.

The antenna range must satisfy a number of important conditions before it can be used for antenna radiation pattern measurements.

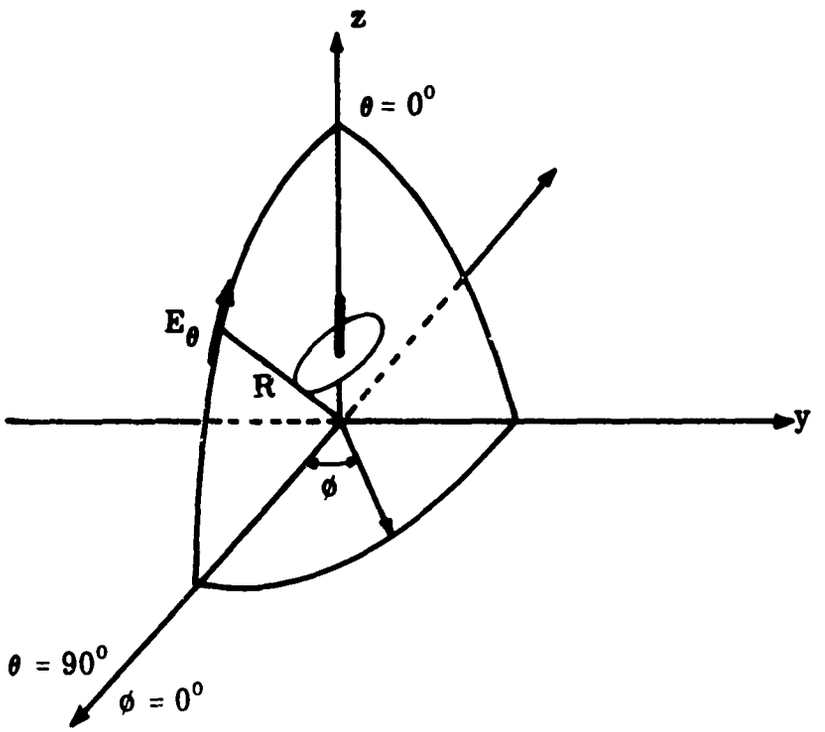

Fig. 4. 1. Radiation patterns in the vertical plane

The distance between the transmitting antenna and the test antenna must be sufficiently large to assure an accurate far-field radiation pattern. For an accurate far-field measurement, the antenna under test must be illuminated with a plane wave front. Since perfect plane wave is only possible at an infinite distance, some practical limits must be

established as a guide to an acceptable distance between the transmitting and receiving test antenna. A common criteria is that the phase difference between the center and the edge of the antenna under test be no greater than $\lambda/16$ (Ref. 11). Then the minimum acceptable distance between the antennas is given by the equation

$$R \geq \frac{4a^2}{\lambda} \tag{4.1}$$

where

$$\delta << R \quad \text{and} \quad \delta << a \ . \tag{4.2}$$

The distance requirement is shown in Fig. 4.2.

$$R^2 + a^2 = (R+\delta)^2 \tag{4.3}$$

$$\delta \doteq \frac{a^2}{2R} \tag{4.4}$$

The range used for this experiment was constructed with $R \approx 20$ meters. Since the radius of the finite ground plane, a, is as large as $\lambda/4$

$$\frac{4a^2}{\lambda} \leq \frac{\lambda}{4} \tag{4.5}$$

where λ varies from 1.5 meters to 0.25 meter from 200 MHz to 1200 MHz, the distance R is more than enough to satisfy the condition (4.1).

Another possible source of error in the radiation pattern measurement is due to ground reflection, when both the transmitting

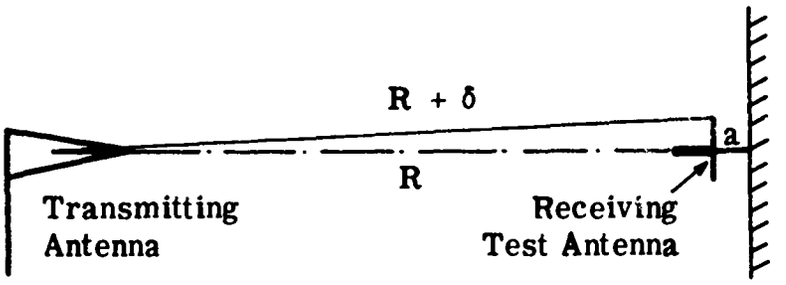

Fig. 4.2. Phase difference between center and edge of the test antenna

and receiving antennas are located close to the ground level. One way to avoid this problem is to utilize a narrow beam transmitting antenna. Another possibility is, of course, locating both antennas far above the ground level.

The transmitting and receiving antennas for this experiment were located approximately 10 meters above the roof level of a three-story building. The transmitting antenna used was a wide-band, frequency independent, log-periodic sheet triangular-tooth structure designed to operate above 150 MHz. It was linearly polarized and had a beam width of approximately 60^{o}.

The test setup used for the experiment is shown in Fig. 4.3.

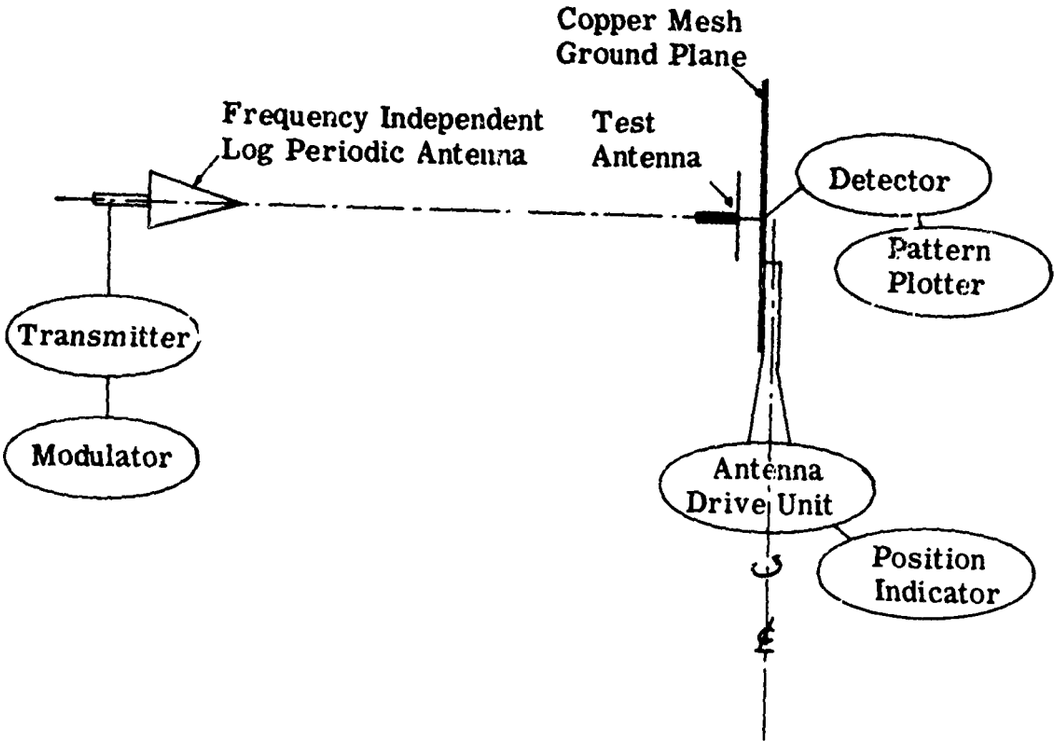

Fig. 4.3 Radiation pattern measurement set-up, block diagram

4.4 Measurement Results

The experiment performed here was designed to observe the effect of a finite ground plane upon the radiation characteristics of a monopole displaced a certain distance above an infinite conducting ground. The geometrical arrangement of each component of this antenna system is shown in Fig. 4.4.

The values used for a, h, and ℓ in the experiments were as follows. The physical length of h for Fig. 4.4 was fixed so that it is one quarter wavelength at the upper end of the test frequencies, which ranged from 200 MHz through 1200 MHz for a flat disc ground plane. The spherical ground plane shown in Fig. 4.4(b) also had a fixed length of antenna which was one quarter wavelength at the upper end of the frequency band ranging from 246 MHz through 1475 MHz.

The frequencies chosen for the spherical ground plane were based mainly on the available size of copper half spheres. A quarter wavelength at 1475 MHz is 2 inches or 5.08 cm. A set of half-spheres available was 2 inches, 3 inches, 4 inches and 5 inches in diameter, and at the frequency of 1475 MHz, they correspond to $\lambda/4$, $3\lambda/8$, $\lambda/2$, and $5\lambda/8$ in diameter. The radiation patterns are later studied as a function of ground plane size in terms of wavelength λ.

The experimental results are arranged first in Fig. 4.6 to see the effect of a ground plane size when it is located at a given height (a) above the infinite ground plane. The ground plane diameters were changed from 0.0156 meter to 0.125 meter which simulates the

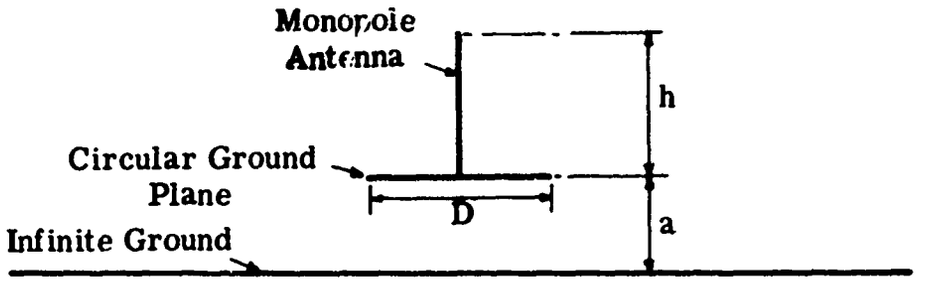

(a)

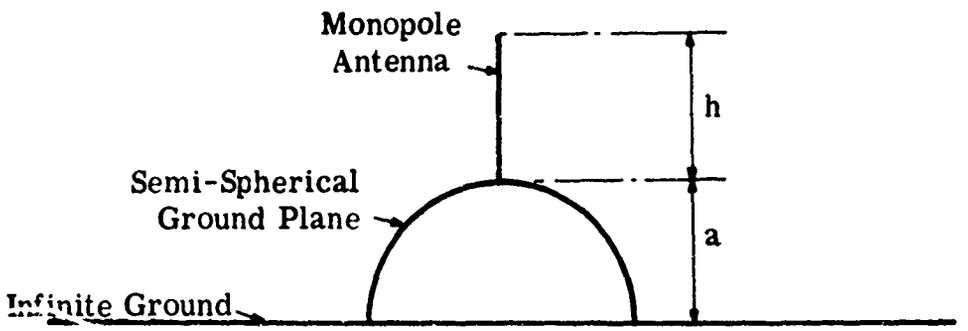

(b)

Fig. 4.4 Geometrical arrangement of an antenna and ground plane

diameters of 0.625 meter to 5 meters of the original antenna system. These diameters correspond to $\lambda/16$ through $\lambda/2$ at 1200 MHz and 30 MHz. The changes in the diameter were made in four steps, with the size of the ground plane doubling its diameter each time. Thus, the diameters of the flat disc used for the experiment were $\lambda/16$, $\lambda/8$, $\lambda/4$ and $\lambda/2$.

Second, in Fig. 4.10, the location (a) of the ground plane was changed for the given size of a ground plane diameter. The steps taken for different a were the same as discussed above for the variable size of ground plane, namely, $a = \lambda/16$, $\lambda/8$, $\lambda/4$, and $\lambda/2$.

In Fig. 4.5, a monopole above a semi-spherical ground plane of various size has been tested for its radiation patterns. When the ground plane size becomes larger with respect to wavelengths, side lobes become noticeable. When $ka \approx 2$, the side lobe level shows over 60 percent of the major lobe level. However, for smaller values of ka, side lobe effect is negligible. Typical experimentally observed beam widths measured between 3db points range from approximately 30 degrees to 70 degrees. These patterns are later compared with the theoretical results obtained in Chapter 5.

Figures 4.6 through 4.13 show that when displacement between the disc ground plane and a simulated infinite ground plane is less than $\lambda/2$, major lobes are directed considerably off from the horizontal

position with a small side lobe along horizontal direction. This type of phenomena can be also observed for a center fed dipole of 1.5λ in length (Ref. 14). This indicates that by using a monopole with a finite ground plane displaced a certain distance away from an infinite ground plane, the system behaves like a longer dipole antenna. A finite ground plane and a gap between the finite and infinite ground plane simulates an extension of an antenna length. It is also noticed that the radiation patterns generally are more sensitive to the gap distance a than the ground plane diameter D. In particular, when the gap distance $a = \lambda/4$, the pattern shows a considerable difference from other patterns.

In summing up the results of radiation pattern studies, it can be concluded that the finite ground plane used in conjunction with an infinite ground below causes radiation patterns mainly to be directed off from the horizontal direction due to an equivalent antenna arm created by the finite ground plane and the distance to the infinite ground. Although minor lobes are present in most cases, their relative levels, compared with major lobes, are insignificant. Also, it shows that the distance a is more significant for the radiation patterns than the diameter of a finite ground plane D. Finally, there seems to be some similarities in radiation patterns between the monopole with hemispherical ground plane and the sleeve dipole (Ref. 15). However, a detailed comparison is not possible because very few corresponding dimensions between two antennas are available.

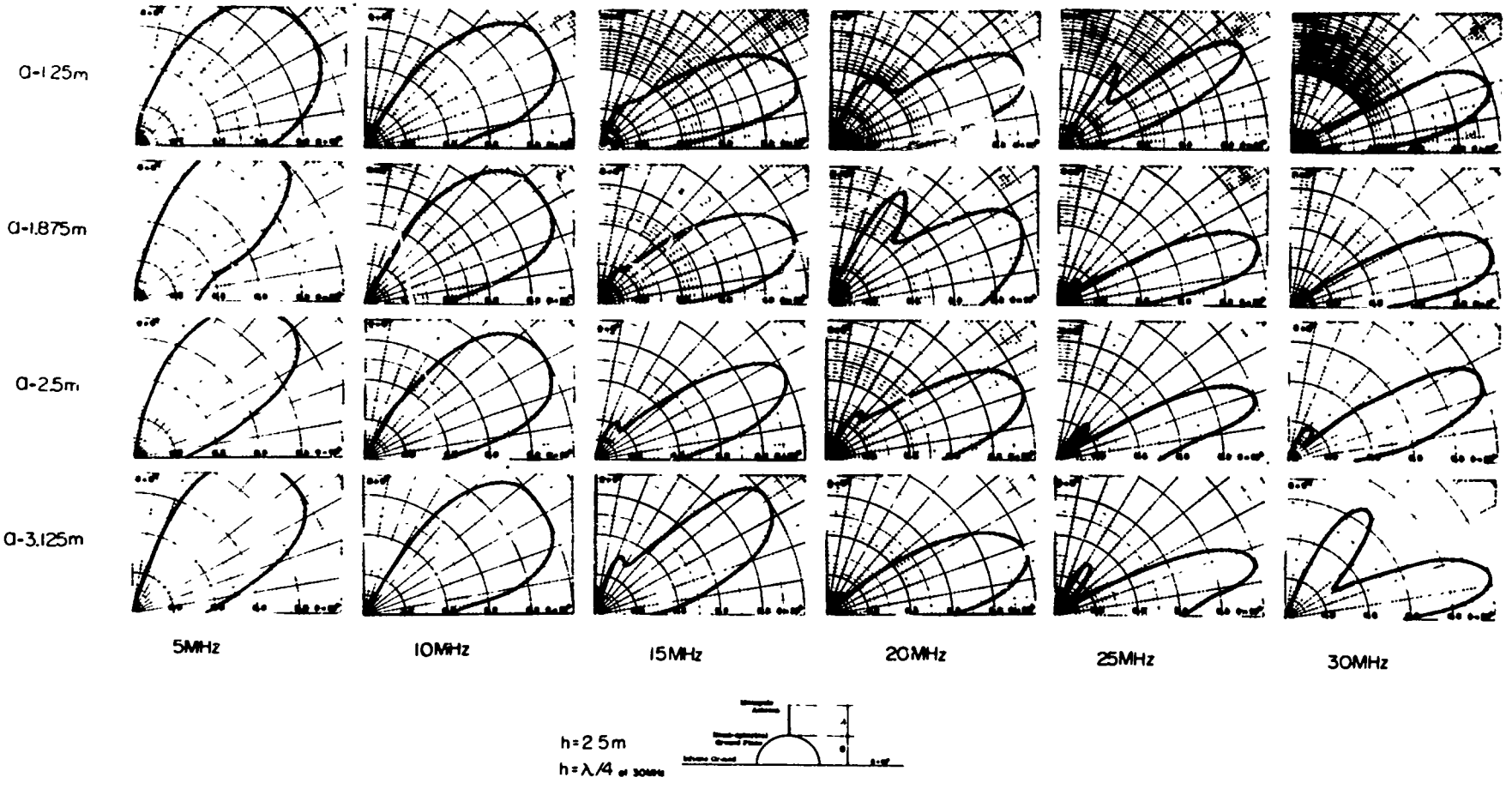

Fig. 4.5. Radiation patterns $|E_\theta|^2$ for a monopole with a hemispherical ground plane of various diameters

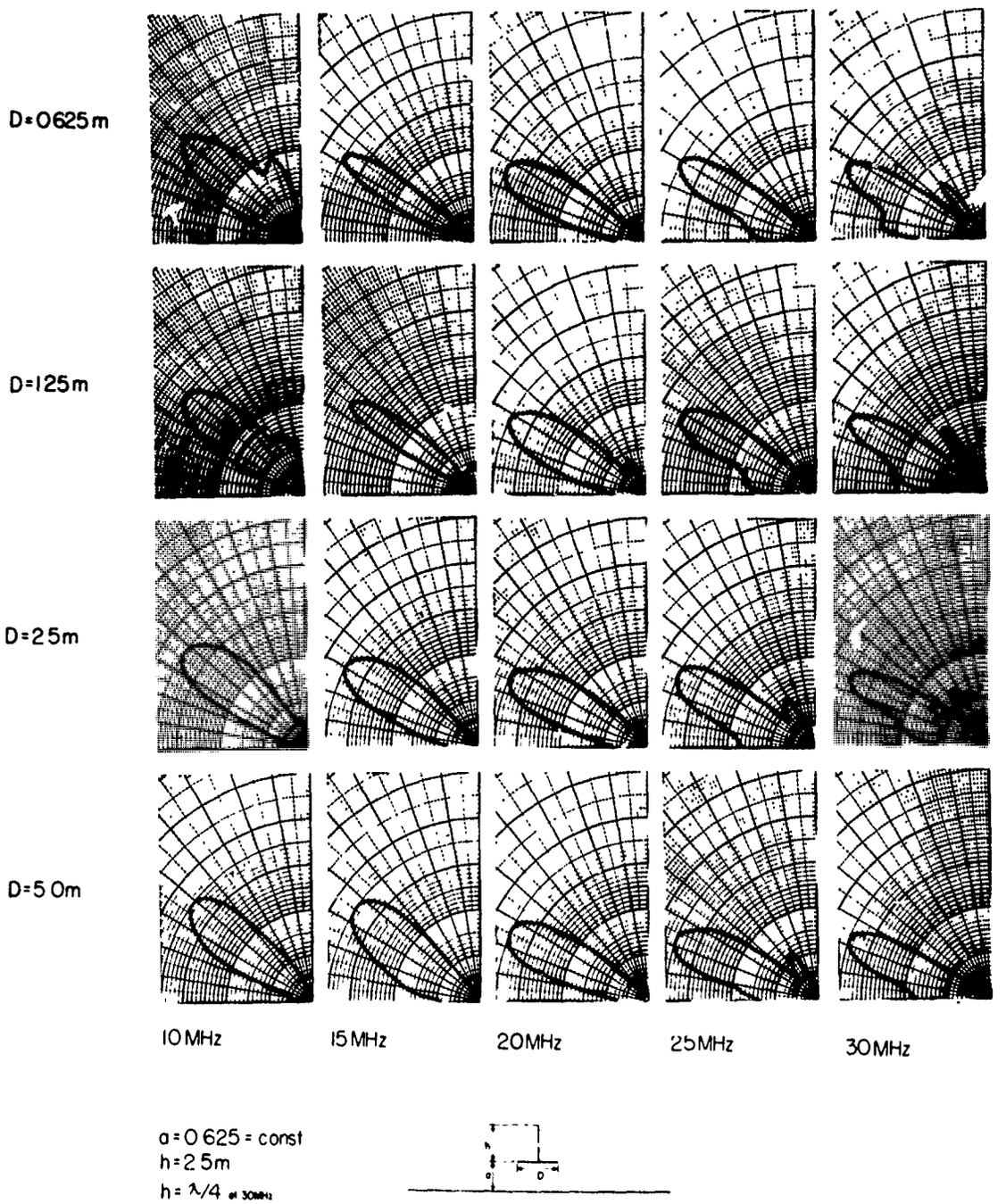

Fig. 4.6. Radiation patterns $|E_\theta|^2$ for various ground plane diameters (D) with a = 0.625m

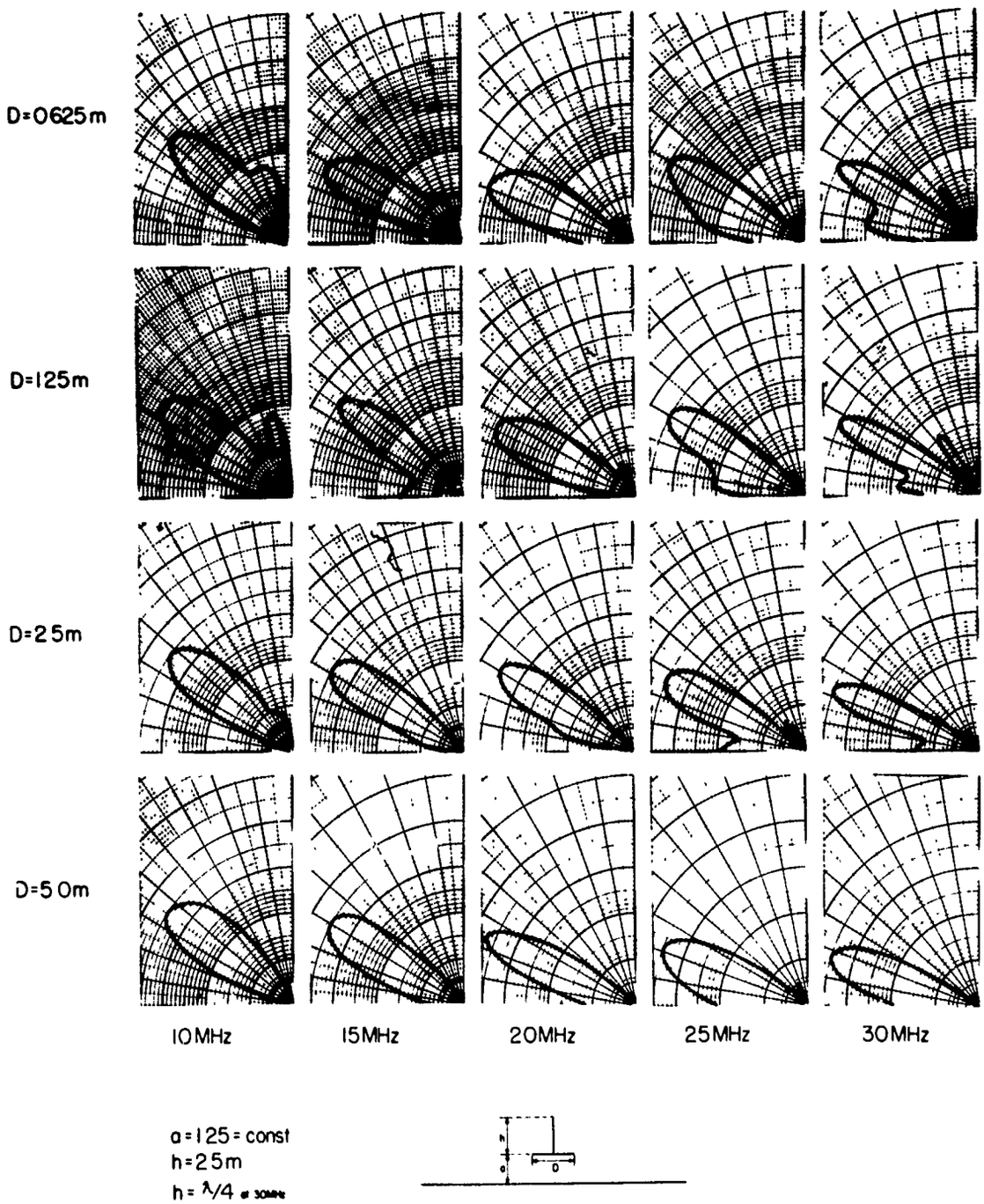

Fig. 4.7. Radiation patterns $|E_\theta|^2$ for various ground plane diameters (D) with a = 1.25m

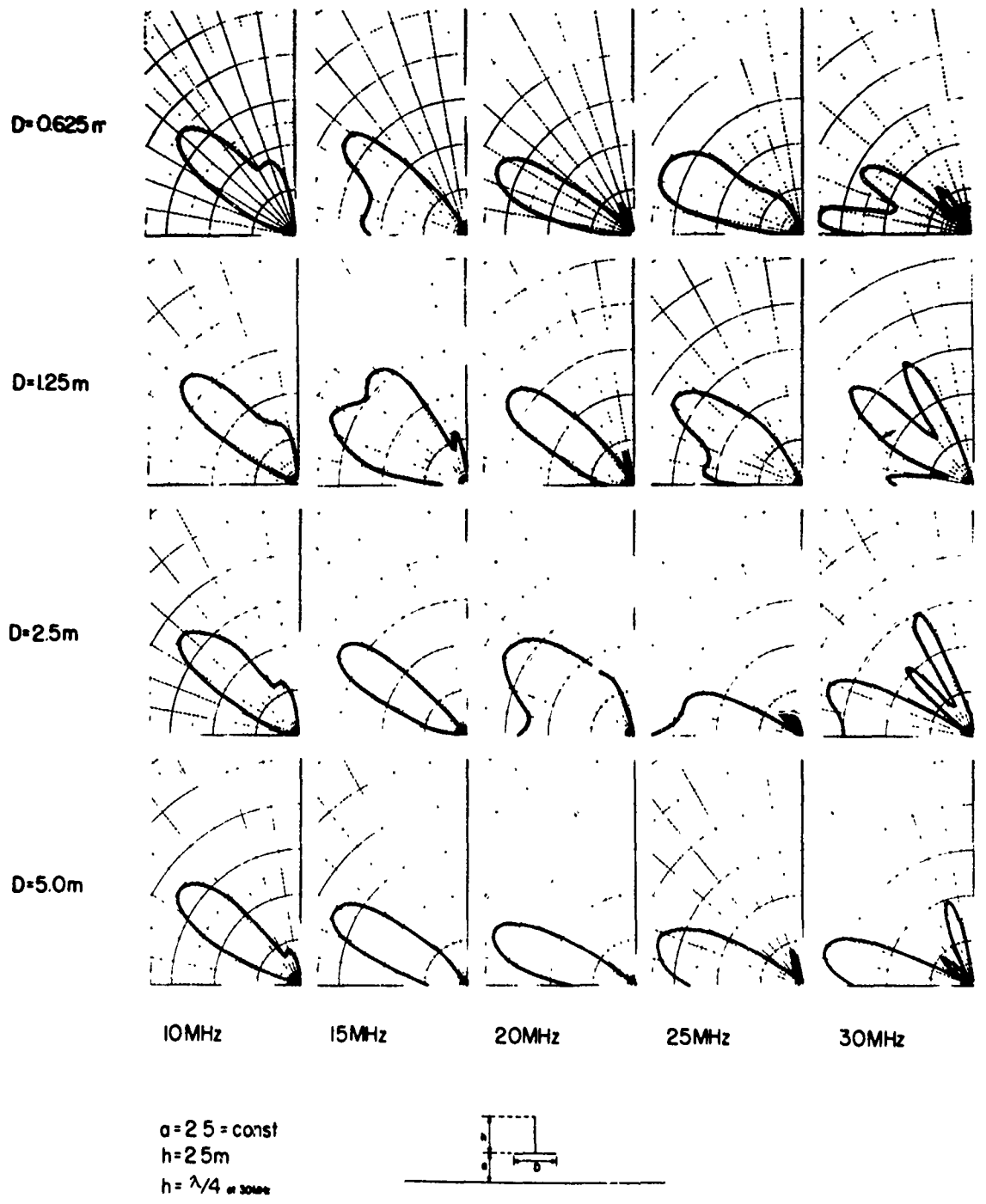

Fig. 4.8. Radiation patterns $|E_\theta|^2$ for various ground plane diameters (D) with a = 2.5m .

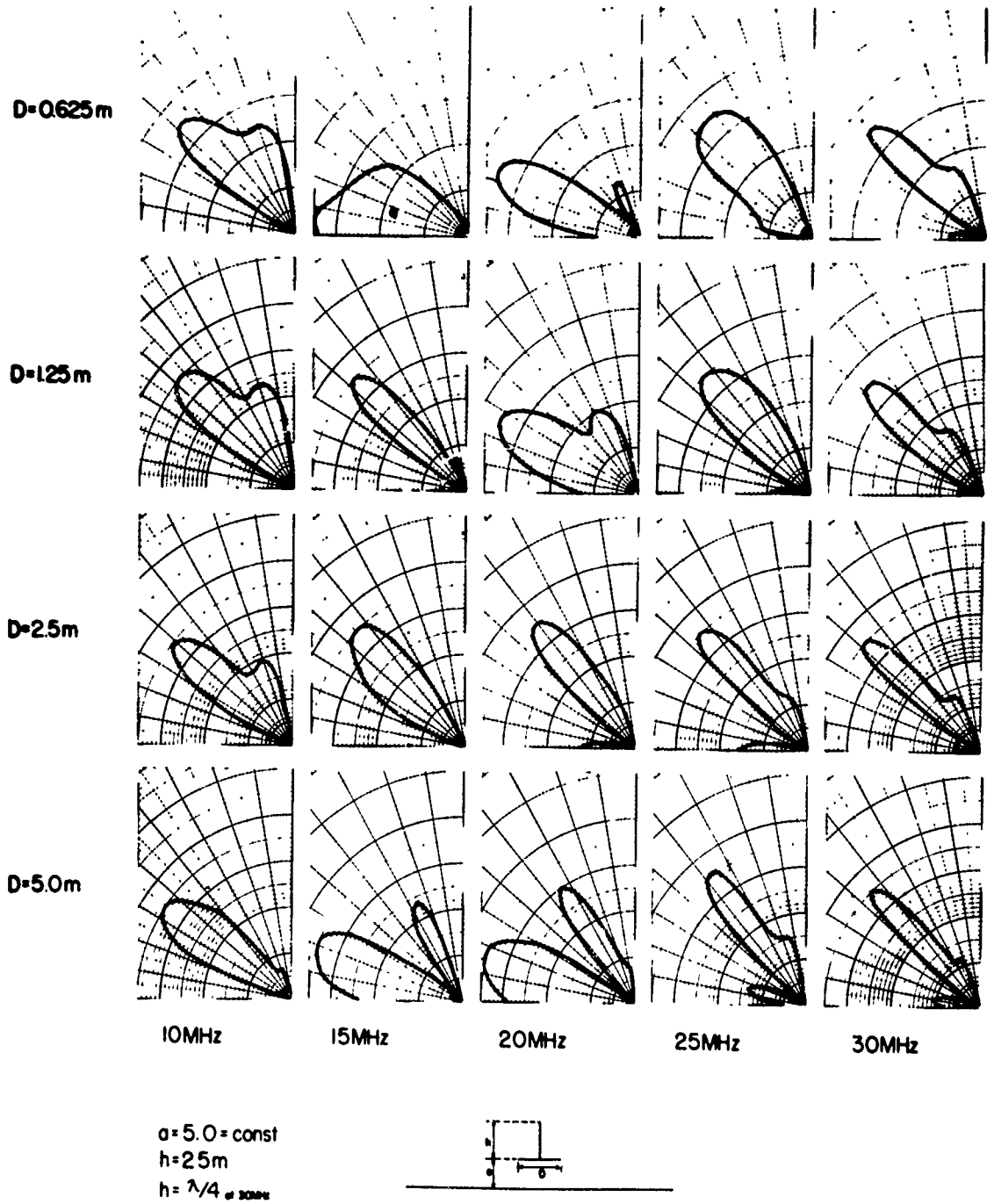

Fig. 4.9. Radiation patterns $|E_\theta|^2$ for various ground plane diameters (D) with a = 5.0m .

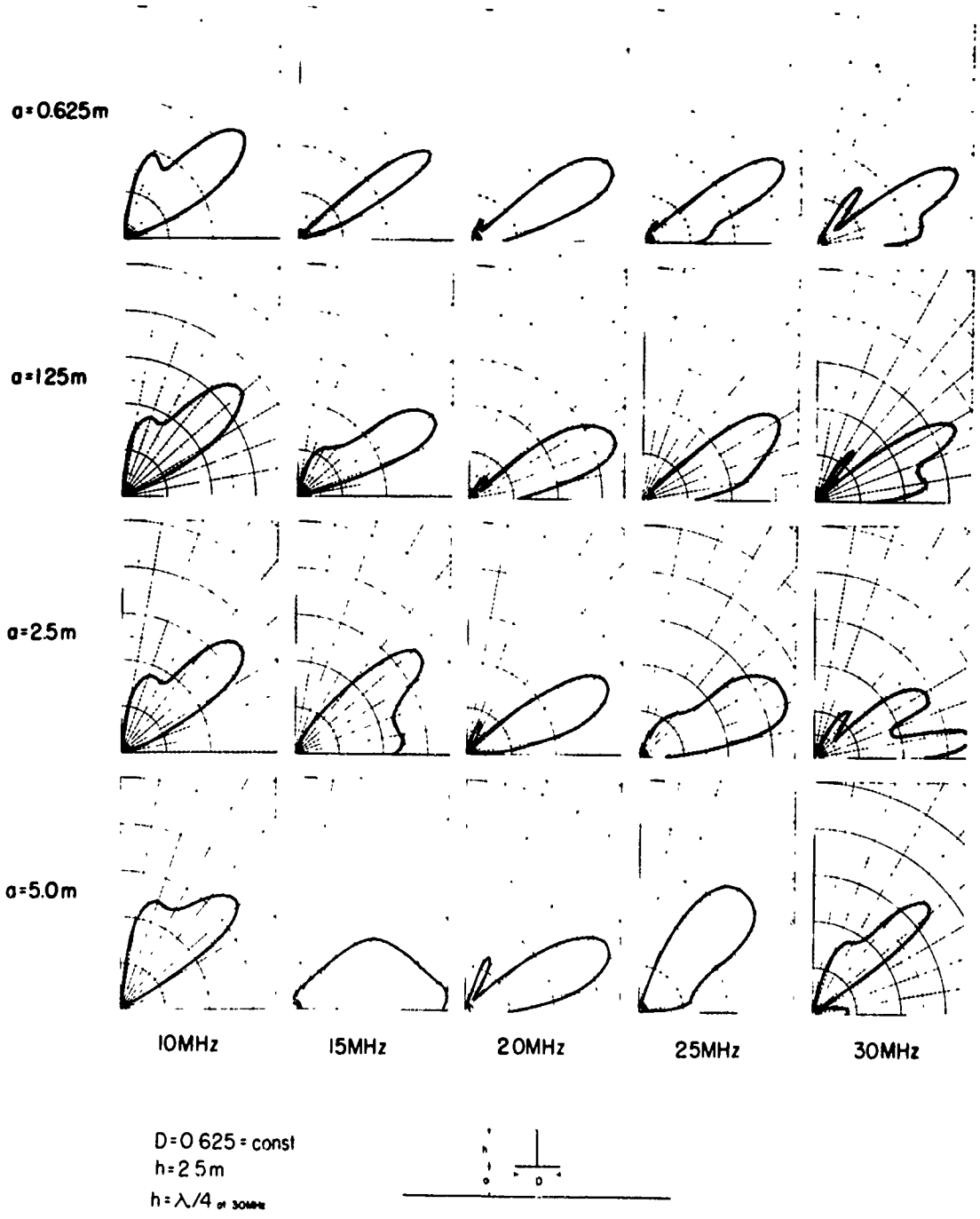

Fig. 4.10. Radiation patterns $|E_\theta|^2$ for various ground plane locations (a) with D = 0.625m

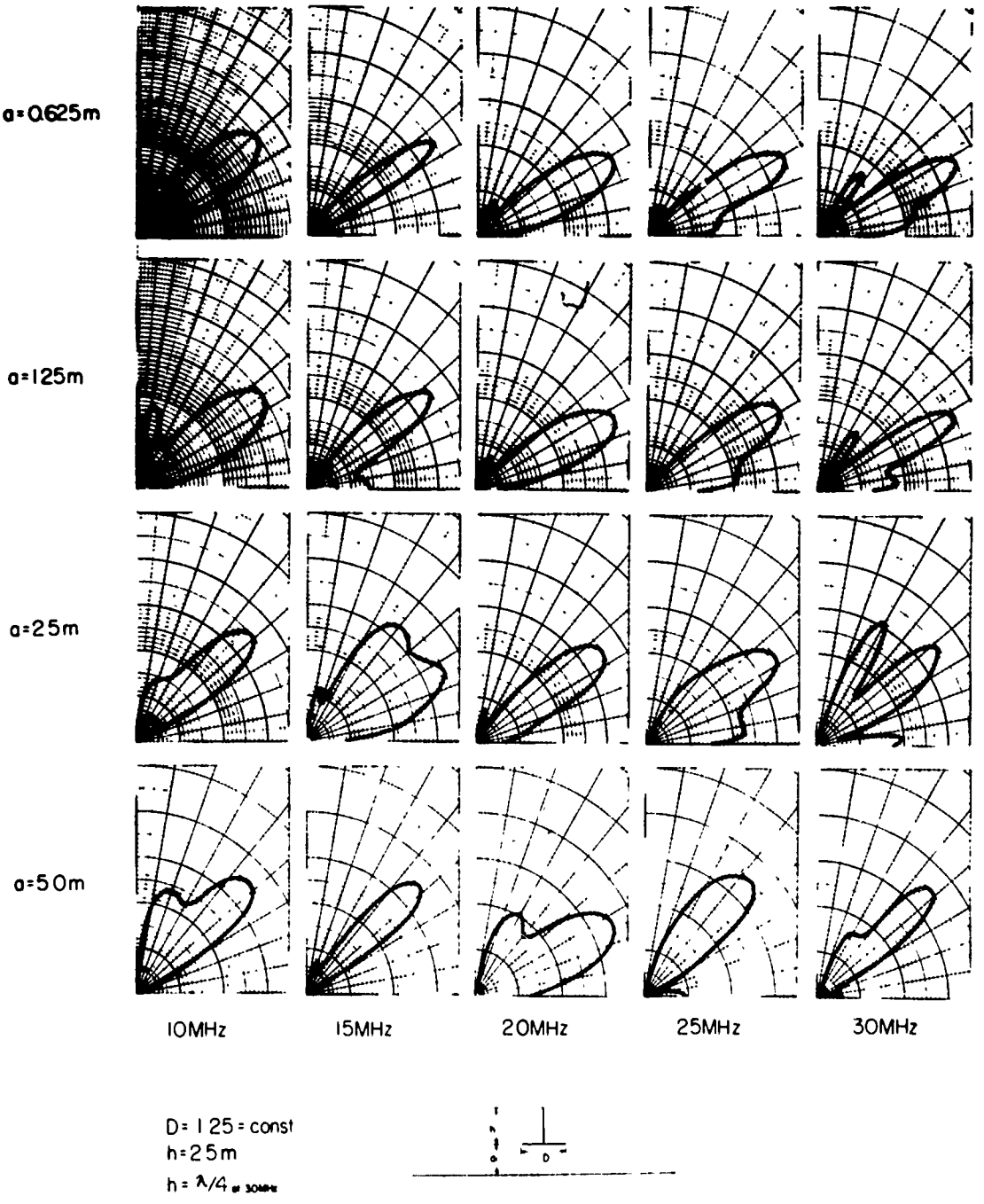

Fig. 4. 11. Radiation patterns $|E_\theta|^2$ for various ground plane locations (a) with D = 1.25m

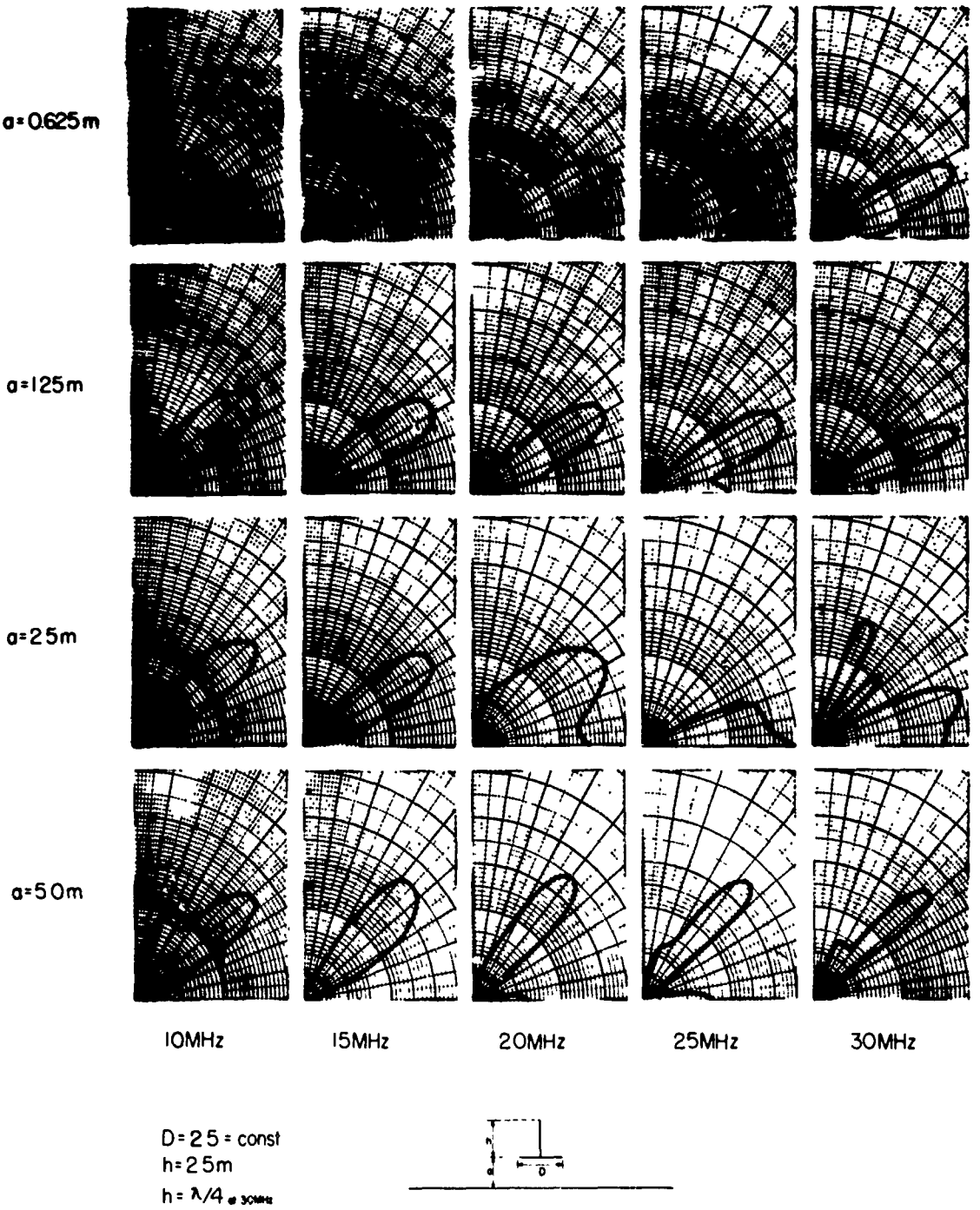

Fig. 4.12. Radiation patterns $|E_\theta|^2$ for various ground plane locations (a) with D = 2.50m

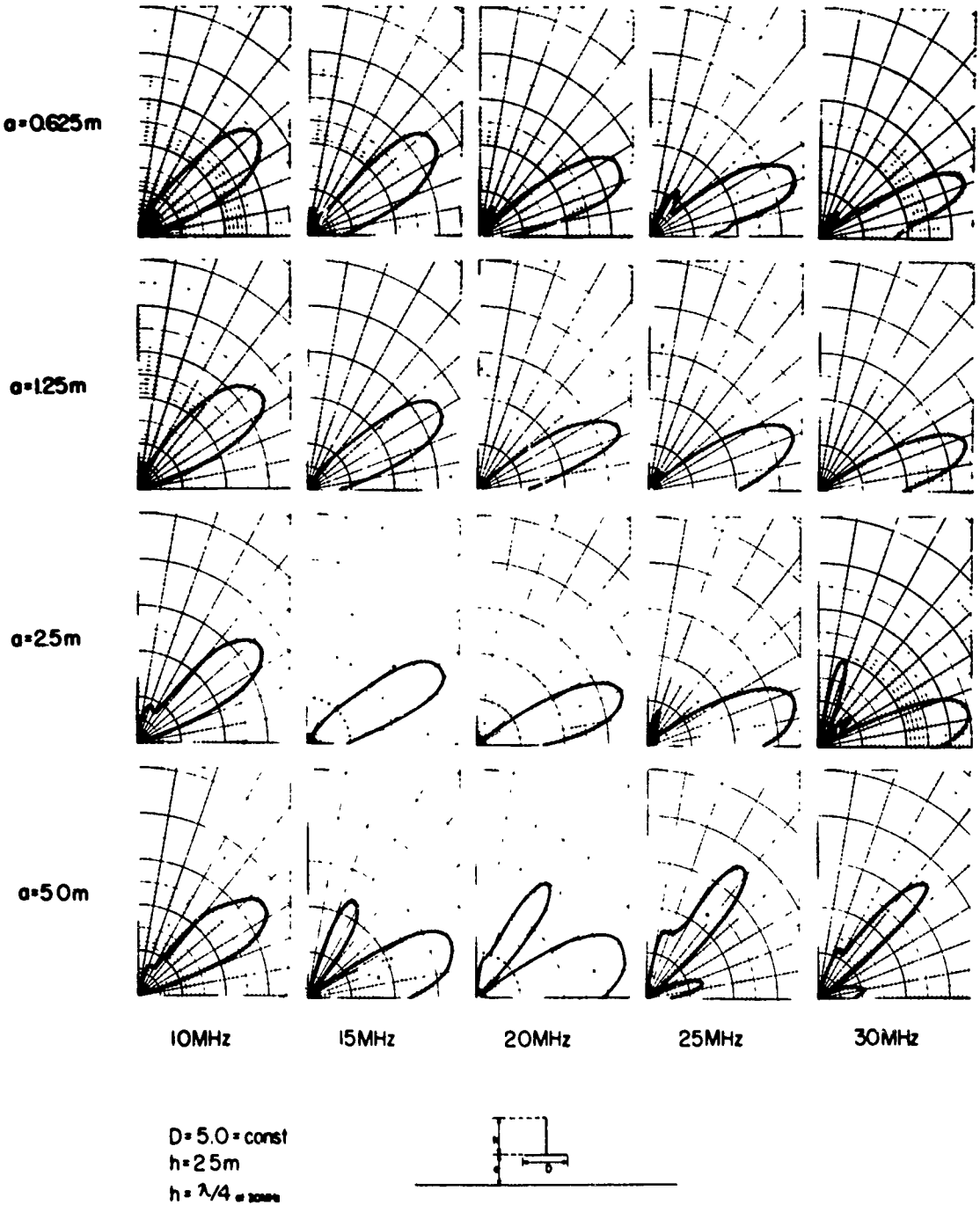

Fig. 4.13. Radiation patterns $|E_\theta|^2$ for various ground plane locations (a) with D = 5.0m

CHAPTER V

THEORETICAL ANALYSIS

5.1 Introduction

In this chapter, the theoretical model analyzed is a monopole antenna on a hemispherical ground plane that is, in turn, above an infinitely large conducting ground. Far zone electromagnetic fields are computed as a function of hemisphere radius and antenna length. The model chosen for the analysis is shown in the Fig. 5.1.

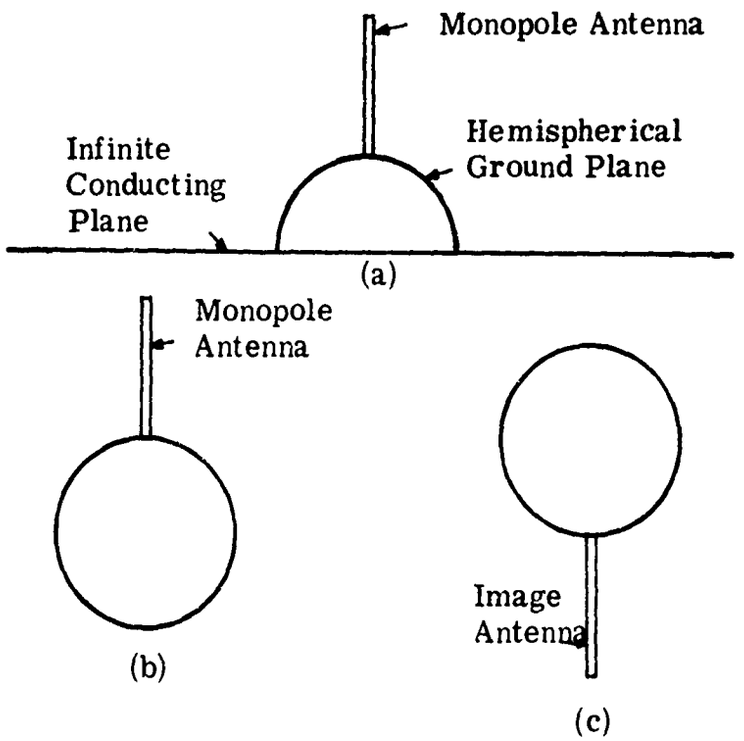

Fig. 5.1. Theoretical model of an antenna system

Using image technique, the original model is divided into two parts as shown in the Fig. 5.1(b) and (c). Each configuration is separately studied and later the far-zone fields due to both antennas and the induced currents on the spherical surfaces are superimposed to obtain the total fields.

The Section 5.2 deals with a development of a general far-zone fields expression from a given source configuration, and the Section 5.3 includes a far-zone field calculation due to two monopoles separated by the diameter of the sphere. The Section 5.4 computes the induced current on the spherical surface due to the monopole and its image. And, the Section 5.5 shows the far-zone field expressions due to the induced surface currents on the sphere, and the total far-zone fields due to the antennas and the surface currents on the hemisphere. Some of the results from the numerical calculation in the forms of radiation patterns are given. Section 5.6 contains results of radiation resistance theoretically obtained for a monopole with a hemispherical ground plane.

5.2 General Far-Zone Field Expressions

5.2.1 Classical Formulation. Let us postulate a new form of Maxwell's equations for harmonically oscillating fields:

$$\nabla \times \bar{E} = -j\omega\mu_0 \bar{H} - \bar{J}_m \qquad \nabla \cdot \bar{J}_m = -j\omega\rho_m$$

$$\nabla \times \bar{H} = \bar{J} + j\omega\epsilon_0 \bar{E} \qquad \nabla \cdot \bar{J} = -j\omega\rho \tag{5.1}$$

where

$\bar{J}_m$ is a fictitious "magnetic current density"

and

ρ_m is a fictitious "magnetic charge density"

From the above equations, the following equations are derived.

$$\nabla \cdot (\epsilon_0 \bar{E}) = \rho \qquad \nabla \cdot (\mu_0 \bar{H}) = \rho_m \tag{5.2}$$

Now define the electric and magnetic fields as sums of two parts, i.e.,

$$\bar{E} = \bar{E}' + \bar{E}''$$

$$\bar{H} = \bar{H}' + \bar{H}'' \tag{5.3}$$

where $\bar{E}'$ and $\bar{H}'$ correspond to the fields arising from the actual current $\bar{J}$ when $\bar{J}_m = 0$ and thus satisfying the equations

$$\nabla \times \bar{E}' = -j\omega\mu_0 \bar{H}' \qquad \nabla \cdot (\epsilon_0 \bar{E}') = \rho$$

$$\nabla \times \bar{H}' = \bar{J} + j\omega\epsilon_0 \bar{E}' \qquad \nabla \cdot (\mu_0 \bar{H}') = 0 \tag{5.4}$$

Similarly, $\bar{E}''$ and $\bar{H}''$ satisfy the equations

$$\begin{aligned} \nabla \times \bar{E}'' &= -j\omega\mu_0 \bar{H}'' - \bar{J}_m & \nabla \cdot (\epsilon_0 \bar{E}'') &= 0 \\ \nabla \times \bar{H}'' &= j\omega\epsilon_0 \bar{E}'' & \nabla \cdot (\mu_0 \bar{H}'') &= \rho_m \end{aligned} \tag{5.5}$$

For the set of equations 5.4 , a vector potential $\bar{A}$ and a scalar potential Φ , can be defined as

$$\mu_0 \bar{H}' = \nabla \times \bar{A} \tag{5.6}$$

and

$$-j\omega\mu_0\epsilon_0\Phi = \nabla \cdot \bar{A} \tag{5.7}$$

where

$$\bar{E}' + j\omega\bar{A} = -\nabla\Phi \tag{5.8}$$

Then the following two differential equations are obtained.

$$\begin{aligned} \nabla^2 \bar{A} + k^2 \bar{A} &= -\mu_0 \bar{J} \\ \nabla^2 \Phi + k^2 \Phi &= -\frac{\rho}{\epsilon_0} \end{aligned} \tag{5.9}$$

where

$$k^2 = \omega^2 \mu_0 \epsilon_0$$

The solutions of these differential equations are

$$\bar{A} = \mu_0 \iiint_{V'} G(\frac{\bar{R}}{\bar{R}'}) \bar{J}(\bar{R}') \, dV'$$

$$\Phi = \frac{1}{\epsilon_0} \iiint_{V'} G(\frac{\bar{R}}{\bar{R}'}) \rho(\bar{R}') \, dV' \qquad (5.10)$$

where

$$G(\frac{\bar{R}}{\bar{R}'}) = \frac{1}{4\pi} \frac{e^{-jk|\bar{R} - \bar{R}'|}}{|\bar{R} - \bar{R}'|} \qquad (5.11)$$

and

$\bar{R}$ and $\bar{R}'$ are the radial distance from the origin of the coordinate system to the observation points and the source points, respectively.

Fields $\bar{E}'$ and $\bar{H}'$ can be written as

$$\bar{E}' = -j\omega \left[\bar{A} + \frac{1}{k^2} \nabla(\nabla \cdot \bar{A}) \right] \qquad (5.12)$$

and

$$\bar{H}' = \frac{1}{\mu_0} \nabla \times \bar{A} \qquad (5.13)$$

Similarly, for the set of equations 5.5 , a new vector potential $\bar{A}_m$ and a scalar potential $\bar{\Phi}_m$ can be defined

$$\epsilon_0 \bar{E}'' = -\nabla \times \bar{A}_m$$

$$-j\omega\mu_0\epsilon_0\Phi_m = \nabla \cdot \bar{A}_m \tag{5.14}$$

The resultant differential equations are

$$\nabla^2 \bar{A}_m + k^2 \bar{A}_m = -\epsilon_0 \bar{J}_m \tag{5.15}$$

and

$$\nabla^2 \Phi_m + k^2 \Phi_m = -\frac{\rho_m}{\mu_0} \tag{5.16}$$

The solutions of these equations are

$$\bar{A}_m = \epsilon_0 \int\int\int G\left(\frac{\bar{R}}{\bar{R}'}\right) J_m(\bar{R}')dV'$$

$$\Phi_m = \frac{1}{\mu_0} \int\int\int G\left(\frac{\bar{R}}{\bar{R}'}\right) \rho_m(\bar{R}')dV' \tag{5.17}$$

The fields $\bar{E}''$ and $\bar{H}''$ can then be expressed

$$\bar{E}'' = -\frac{1}{\epsilon_0} \nabla \times \bar{A}_m \tag{5.18}$$

$$\bar{H}'' = -j\omega \left[\bar{A}_m + \frac{1}{k^2} \nabla(\nabla \cdot \bar{A}_m) \right] \tag{5.19}$$

Therefore, the total $\bar{E}$ and $\bar{H}$ fields due to both electric and magnetic sources can be written in terms of vector potentials as

$$\bar{E} = \bar{E}' + \bar{E}'' = -j\omega\left[\bar{A} + \frac{1}{k^2}\nabla(\nabla \cdot \bar{A})\right] - \frac{1}{\epsilon_0}\nabla \times \bar{A}_m \qquad (5.20)$$

$$\bar{H} = \bar{H}' + \bar{H}'' = \frac{1}{\mu_0}\nabla \times \bar{A} - j\omega\left[\bar{A}_m + \frac{1}{k^2}\nabla(\nabla \cdot A_m)\right] \qquad (5.21)$$

In the region where $\bar{J} = \bar{J}_m = 0$, these equations are simplified to

$$\bar{E} = -\frac{j\omega}{k^2}\nabla \times \nabla \times \bar{A} - \frac{1}{\epsilon_0}\nabla \times \bar{A}_m \qquad (5.22)$$

$$\bar{H} = \frac{j\omega}{k^2}\nabla \times \nabla \times \bar{A}_m + \frac{1}{\mu_0}\nabla \times \bar{A} \qquad (5.23)$$

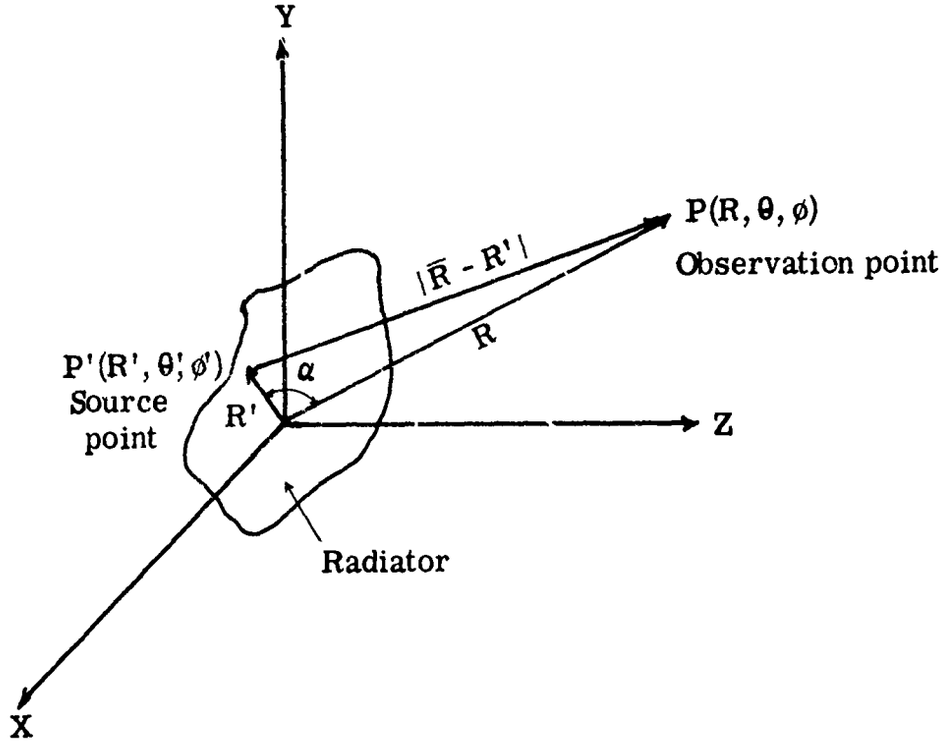

Fig. 5. 2. Coordinate system used to derive far-zone electromagnetic fields

Consider the coordinate system shown above in the Fig. 5.2 for far-zone field $R >> R'$ and $|\bar{R} - \bar{R}'| \doteq R - R' \cos \alpha = |\bar{R}| - (\bar{R}' \cdot \hat{R})$. If the direction of $\hat{R}'$ is denoted by θ, ϕ where $\hat{R}$, and $\hat{R}'$ are the unit vectors, then

$$\cos \alpha = \sin \theta \sin \theta' \cos (\phi' - \phi) + \cos \theta \cos \theta' \tag{5.24}$$

With the approximation shown above

$$|R - R'| \approx R - R' \cos \alpha \tag{5.25}$$

and

$$\bar{A} \doteq \frac{\mu_0 e^{-jkR}}{4\pi R} \int\int\int \bar{J}(R') e^{jkR' \cos \alpha} dV' \tag{5.26}$$

Similarly

$$\bar{A}_m = \frac{\epsilon_0 e^{-jkR}}{4\pi R} \int\int\int \bar{J}_m(R') e^{jkR' \cos \alpha} dV' \tag{5.27}$$

Then

$$\bar{A} = \frac{\mu_0 e^{-jkR}}{4\pi R} \bar{N}(\theta, \phi) \tag{5.28}$$

$$\bar{A}_m = \frac{\epsilon_0 \eta_0 e^{-jkR}}{4\pi R} \bar{M}(\theta, \phi)$$

where

$$\bar{N}(\theta, \phi) = \int\int\int \bar{J}(\bar{R}') e^{jk\bar{R}' \cdot \hat{R}} dV' \tag{5.29}$$

$$\bar{M}(\theta, \phi) = \int\int\int \frac{\bar{J}_m(\bar{R}')}{\eta_0} e^{jk\bar{R}' \cdot \hat{R}} dV'$$

$\bar{N}$ and $\bar{M}$ are only functions of θ and ϕ.

$\bar{N}$ and $\bar{M}$ are called the electric and magnetic radiation vector, respectively.

In general,

$$\bar{N} = N_R \hat{R} + N_\theta \hat{\theta} + N_\phi \hat{\phi} = N_R \hat{R} + \bar{N}_t$$

where $\bar{N}_t$ is a transverse component.

Since

$$\nabla \times \bar{A} = \nabla \times \left[\frac{\mu_0 e^{-jkR}}{4\pi R} \bar{N}(\theta, \phi) \right]$$

$$= \frac{\mu_0 e^{-jkR}}{4\pi R} \left\{ \left[\frac{1}{R \sin\theta} \frac{\partial N_R}{\partial \phi} + jkN_\phi \right] \hat{\theta} + \left[-jkN_\theta - \frac{1}{R} \frac{\partial N_R}{\partial \theta} \right] \hat{\phi} \right.$$

$$\left. + \frac{1}{R \sin\theta} \left[\frac{\partial}{\partial \theta} (\sin\theta \, N_\phi) - \frac{\partial N_\theta}{\partial \phi} \right] \hat{R} \right\} \tag{5.31}$$

in spherical coordinate system, if $R >> \lambda$, then all terms except jkN_θ and jkN_ϕ can be neglected. Therefore,

$$\nabla \times \bar{A} = \frac{\mu_0 e^{-jkR}}{4\pi R} jk \left[N_\phi \hat{\theta} - N_\theta \hat{\phi} \right] = -jk \frac{\mu_0 e^{-jkR}}{4\pi R} (\hat{R} \times \bar{N}) \tag{5.32}$$

Since

$$\nabla \times \bar{A} = \nabla \times \frac{\mu_0 e^{-jkR}}{4\pi R} \bar{N}(\theta, \Phi) = \nabla \times \Phi \bar{N}$$

$$= -jk\Phi (R \times \bar{N})$$

where

$$\Phi = \frac{\mu_0 e^{-jkR}}{4\pi R}$$

$$\nabla \times \nabla \times \bar{A} = \nabla \times (\nabla \times \bar{A})$$

where we can take $\nabla \times \bar{A}$ as a new vector $(\bar{W})$ equivalent to $\bar{N}$ above.

$$\nabla \times \nabla \times \bar{A} = \nabla \times \bar{W} = (-jk)(\hat{R} \times \bar{W})$$

$$= k^2 \left(\frac{\mu_0 e^{-jkR}}{4\pi R} \right) (\hat{R} \times (\hat{R} \times N)) = k^2 \frac{\mu_0 e^{-jkR}}{4\pi R} (\bar{N} - N_R \hat{R}) \tag{5.33}$$

where

$$\bar{N} - N_R \hat{R} = \bar{N}_t$$

Finally, the far-zone field for any antenna is given as

$$\begin{aligned} \bar{E} &= jk\,\eta_o \left[-\bar{N}_t + \hat{R} \times \bar{M}_t \right] \frac{e^{-jkR}}{4\pi R} \\ \bar{H} &= -jk \left[\bar{M}_t + \hat{R} \times \bar{N}_t \right] \frac{e^{-jkR}}{4\pi R} = \frac{1}{\eta_o} \hat{R} \times \bar{E} \end{aligned} \tag{5.34}$$

These expressions show that only the transverse components of $\bar{M}$ and $\bar{N}$ enter into $\bar{E}$ and $\bar{H}$ far-zone expressions.

5.2.2 Stratton-Chu Integral Formulation. In the previous section, a general far-field expression of $\bar{E}$ and $\bar{H}$ have been developed from Maxwell's equations with a given current or source distribution. In this section, the same far-field expressions of electromagnetic fields are developed, using Stratton-Chu integral formulations.

Let $\bar{P}$ and $\bar{Q}$ be two vector functions of position with the proper continuity, then

$$\begin{aligned} &\iiint_V (\bar{Q} \cdot \nabla \times \nabla \times \bar{P} - \bar{P} \cdot \nabla \times \nabla \times \bar{Q})\, dV \\ &= \iint_S (\bar{P} \times \nabla \times \bar{Q} - \bar{Q} \times \nabla \times \bar{P}) \cdot d\bar{S} \end{aligned} \tag{5.35}$$

where S is a regular surface bounding the volume V. The above integral equation is the generalized Stoke's theorem.

If the field vectors $\bar{E}$ and $\bar{H}$ are assumed to be $e^{-j\omega t}$ time dependent, the Maxwell's equations can be written as

$$\nabla \times \bar{E} - j\omega\mu\bar{H} = -\bar{J}_m$$

$$\nabla \times \bar{H} + j\omega\epsilon\,\bar{E} = \bar{J}$$

$$\nabla \cdot \bar{H} = \frac{1}{\mu}\rho_m$$

$$\nabla \cdot \bar{E} = \frac{1}{\epsilon}\rho$$

The medium inside volume V is considered to be homogeneous and isotropic. The quantities $\bar{J}_m$ and ρ_m are the fictitious densities of magnetic current and magnetic charge.

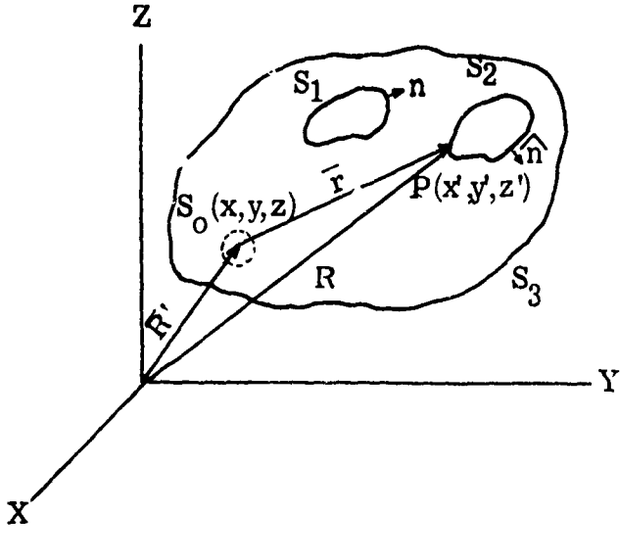

Fig. 5.3 Notations for Stoke's theorem

We consider a volume V bounded by the closed surface S_0, S_1, $S_2 \ldots S_n$, as shown in Fig. 5.3. The notation S in Eq. 5.35 means a sum of S_0, $S_1 \ldots S_n$.

From Maxwell's equation, expressed in Eqs. 5.36, the pair of vector Helmholtz equations can be derived

$$\nabla \times \nabla \times \bar{E} - k^2 \bar{E} = j\omega\mu\bar{J} - \nabla \times \bar{J}_m$$
$$\nabla \times \nabla \times \bar{H} - k^2 \bar{H} = j\omega\epsilon\bar{J}_m + \nabla \times \bar{J} \qquad (5.37)$$

Where currents and charges of each are related by the continuity equations

$$\nabla \cdot \bar{J} - j\omega\rho = 0$$
$$\nabla \cdot \bar{J}_m - j\omega\rho_m = 0 \qquad (5.38)$$

and

$$k^2 = \omega^2 \mu \epsilon$$

In Eq. 5.35, let $\bar{P} = \bar{\bar{E}}$ and $Q = \phi \hat{a}$ where $\hat{a}$ is an arbitrary unit vector and $\phi = e^{ikr}/r$. Distance r is measured from the element at (x', y', z') to the point of observation (x, y, z); i.e.,

$$r = \sqrt{(x - x')^2 + (y - y')^2 + (z - z')^2} = |\bar{R} - \bar{R}'| \tag{5.39}$$

$$R = (x^2 + y^2 + z^2)^{\frac{1}{2}} \text{ and } R' = (x'^2 + y'^2 + z'^2)^{\frac{1}{2}}$$

Then,

$$\nabla \times \bar{Q} = \nabla\phi \times \hat{a}$$

$$\nabla \times \nabla \times \bar{Q} = \hat{a} k^2 \phi + \nabla(\hat{a} \cdot \nabla\phi) \tag{5.40}$$

$$\nabla \times \nabla \times \bar{P} = k^2 \bar{E} + j\omega\mu\bar{J} - \nabla \times \bar{J}_m$$

Substituting Eqs. 5.40 into 5.35 gives

$$\iiint_V [\phi\hat{a} \cdot (k^2 \bar{E} + j\omega\mu\bar{J} - \nabla \times \bar{J}_m) - \bar{E} \cdot (\hat{a} k^2 \phi + \nabla(\hat{a} \cdot \nabla\phi)] \, dV$$

$$= \iint_S [\bar{E} \times \nabla\phi \times \hat{a} - \phi\hat{a} \times \nabla \times \bar{E}] \cdot d\bar{S} \tag{5.41}$$

Since

$$\bar{E} \cdot \nabla(\hat{a} \cdot \nabla\phi) = \nabla \cdot (\hat{a} \cdot \nabla\phi)\bar{E} - (\hat{a} \cdot \nabla\phi)\nabla \cdot \bar{E} \tag{5.42}$$

and

$$\nabla \cdot \bar{E} = \frac{1}{\epsilon} \rho$$

$$\iiint_V \nabla \cdot (\hat{a} \cdot \nabla\phi) \bar{E} \, dV = \iint_S (\hat{a} \cdot \nabla\phi) \bar{E} \cdot d\bar{S}$$

$$= \hat{a} \cdot \iint_S (\hat{n} \cdot \bar{E}) \nabla\phi \, dS \tag{5.43}$$

Equation 5.41 becomes

$$\iiint_V [j\omega\mu\bar{J}\phi - \nabla \times \bar{J}_m \phi + \frac{1}{\epsilon} \rho \nabla\phi] \, dV$$

$$= \iint_S [j\omega\mu(\hat{n} \times \bar{H})\phi + (\hat{n} \times \bar{E}) \times \nabla\phi + (\hat{n} \cdot \bar{E}) \nabla\phi - \hat{n} \times \bar{J}_m \phi] \, dS$$

where

$$d\bar{S} = \hat{n}\, dS$$

Notice that

$$\iint (\bar{E} \times \nabla\phi \times \bar{a}) \cdot \hat{n}\, dS = \iint \hat{n} \times (\bar{E} \times \nabla\phi) \cdot \bar{a}\, dS$$

and

$$\iint (\phi \bar{a} \times \nabla \times \bar{E}) \cdot \hat{n}\, dS = \iint (\phi \bar{a} \times (j\omega\mu\bar{H} - \bar{J}_m) \cdot \hat{n}\, dS$$

$$= -\iint j\omega\mu(\bar{H} \times \hat{n})\phi \cdot \bar{a}\, dS - \iint \hat{n} \times \bar{J}_m \phi \cdot \bar{a}\, dS$$

Equation 5.41 can be further reduced to

$$\iiint_V (j\omega\mu\bar{J}\phi - \bar{J}_m \times \nabla\phi + \frac{1}{\epsilon}\rho\, \nabla\phi)\, dV$$

$$= \iint_S [j\omega\mu(\hat{n} \times \bar{H}) + (\hat{n} \times \bar{E}) \times \nabla\phi + (\hat{n} \cdot \bar{E})\nabla\phi]\, dS \qquad (5.44)$$

with the help of identities:

$$\iiint \nabla \times (\bar{J}_m \phi)\, dV = \iiint \nabla\phi \times \bar{J}_m\, dV + \iiint \phi \nabla \times \bar{J}_m\, dV$$

and

(5.45)

$$\iiint \nabla \times (\bar{J}_m \phi)\, dV = \iint \hat{n} \times \bar{J}_m \phi\, dS$$

Thus

$$-\int\int\int \phi \nabla \times \bar{J}_m dV = -\int\int \hat{n} \times \bar{J}_m \phi \, dS - \int\int\int \bar{J}_m \times \nabla\phi \, dV \qquad (5.46)$$

In Fig. 5.3, the surface S includes S_1, S_2, ... S_n and a volume surface S_0 surrounding the observation point (x, y, z). Since

$$\nabla\phi = \nabla\left(\frac{e^{jkr}}{r}\right) = \left(\frac{1}{r} - jk\right)\frac{e^{jkr}}{r}\hat{r}_0 \qquad (5.47)$$

where $\hat{r}_0$ is a radial unit vector pointed toward the center of the spherical surface S_0. Thus, $\hat{r}_0 = \hat{n}$ for the surface S_0.

Evaluating the surface integral of the Eq. 5.44 over the surface S_0, notice that

$$\begin{aligned}(\hat{n} \times \bar{E}) \times \hat{n} + (\hat{n} \cdot \bar{E})\, n &= -\hat{n} \times (\hat{n} \times \bar{E}) + (\hat{n} \cdot \bar{E})\, n \\ &= -\hat{n}(\bar{E} \cdot \hat{n}) + \bar{E}(\hat{n} \cdot \hat{n}) + (\hat{n} \cdot \bar{E})\hat{n} \qquad (5.48) \\ &= \bar{E}\end{aligned}$$

Also, when the radius of the sphere r_0 represented by S_0 is reduced to zero, the only terms remaining from the surface integral are terms involving $1/r_0^2$:

$$\iint_{S_0} \left[(\hat{n} \times \bar{E}) \times \nabla\phi + j\omega\mu(\hat{n} \times \bar{H})\phi + (\hat{n} \cdot \bar{E}) \nabla\phi \right] dS$$

$$= \int_0^{2\pi} \int_0^{\pi} \left\{ (\hat{r}_0 \times \bar{E}) \times \hat{r}_0 \frac{e^{jkr_0}}{r_0^2} + (\hat{r}_0 \cdot \bar{E})\hat{r}_0 \frac{e^{jkr_0}}{r_0^2} + 0\left(\frac{1}{r_0^2}\right) \right\}$$

$$r_0^2 \sin\theta \, d\theta \, d\phi \tag{5.49}$$

where $0\left(\frac{1}{r_0^2}\right)$ represents other terms involving $\frac{1}{r_0^2}$.

As r_0 approaches zero, the integral becomes

$$\iint_{S_0} \left[(\hat{n} \times \bar{E}) \times \nabla\phi + j\omega\mu(\hat{n} \times \bar{H})\phi + (\hat{n} \cdot \bar{E}) \nabla\phi \right] dS'$$

$$= 4\pi \bar{E}(x, y, z) \tag{5.50}$$

Equation 5.50 then becomes

$$\bar{E}(x, y, z) = \frac{1}{4\pi} \iiint_V (j\omega\mu \bar{J}\phi - \bar{J}_m \times \nabla\phi + \frac{1}{\epsilon} \rho \nabla\phi) \, dV'$$

$$- \frac{1}{4\pi} \iint_{S_1, S_2, \ldots S_n} \left[j\omega\mu(\hat{n} \times \bar{H})\phi \times (\hat{n} \times \bar{E}) \times \nabla\phi + (\hat{n} \cdot \bar{E}) \nabla\phi \right] dS' \tag{5.51}$$

If the volume does not contain any sources, Eq. 5.51 further reduces to

$$\overline{E}(x, y, z) = -\frac{1}{4\pi} \iint_{S_1, S_2, \ldots S_n}$$

$$[j\omega\mu(\hat{n} \times \overline{H})\phi + (\hat{n} \times \overline{E}) \times \nabla\phi + (\hat{n} \cdot \overline{E}) \nabla\phi] \, dS' \qquad (5.52)$$

Also, if all currents and charges can be enclosed within a sphere of finite radius, then the field is regular at infinity and either side of S may be chosen as its interior. The surface integral of Eq. 5.51 represents the contribution of sources located outside S. If, therefore, S recedes to infinity, the contribution from those sources vanishes. Discarding the fictitious magnetic charges $\overline{J}_m$, Eq. 5.51 becomes

$$\overline{E}(x, y, z) = \frac{1}{4\pi} \iiint_V [j\omega\mu \overline{J}\phi + \frac{1}{\epsilon}\rho \nabla\phi] \, dV' \qquad (5.53)$$

Equation 5.52 is the field that would be produced from surface S by electric current density $\overline{K}$, by magnetic current density $\overline{K}_m$, and by surface electric charge of density σ_s; where

$$\hat{n} \times \overline{H} = -\overline{K}, \quad \hat{n} \times \overline{E} = \overline{K}_m, \quad \sigma_s = -\epsilon \hat{n} \cdot \overline{E} \qquad (5.54)$$

If Eqs. 5.52 and 5.53 are applied to the far-zone where $\phi = e^{jkr}/r$, then

$$\phi = \frac{e^{jkR - jk\hat{R} \cdot \overline{R}'}}{R} \qquad (5.55)$$

and Eqs. 5.52 and 5.53 can be written as

$$\overline{E}(x,y,z) = \frac{1}{4\pi} \iint_{S_1, S_2 \ldots S_n} [j\omega\mu(\hat{n} \times \overline{H})\phi + (\hat{n} \times \overline{E}) \times \nabla\phi]_t \, dS' \tag{5.56}$$

and if $S_1, S_2 \ldots S_n$ are perfectly conducting boundary, then $\hat{n} \times \overline{E} = 0$

Therefore,

$$\overline{E}(x,y,z) = \frac{1}{4\pi} \iint_{S_1, S_2, \ldots S_n} [j\omega\mu(\hat{n} \times \overline{H})\phi]_t \, dS' \tag{5.57}$$

where subscript t signifies transverse component to the radial direction. The proof of these equations 5.56 and 5.57 is given in Appendix B. Of course, Eq. 5.56 is equivalent to Eq. 5.34 in Section 5.2.1. Similarly, it can also be shown that in the far-zone,

$$\overline{H}(x,y,z) = \frac{1}{4\pi} \iint_{S_1, S_2 \ldots, S_n} [j\omega\epsilon(\hat{n} \times \overline{E})\phi + (\hat{n} \times \overline{H}) \times \nabla\phi]_t \, dS' \tag{5.58}$$

5.3 Far-Zone Field Expressions for Two Linear Antennas

Consider an antenna and its image with a sinusoidal current distribution as shown in Fig. 5.4.

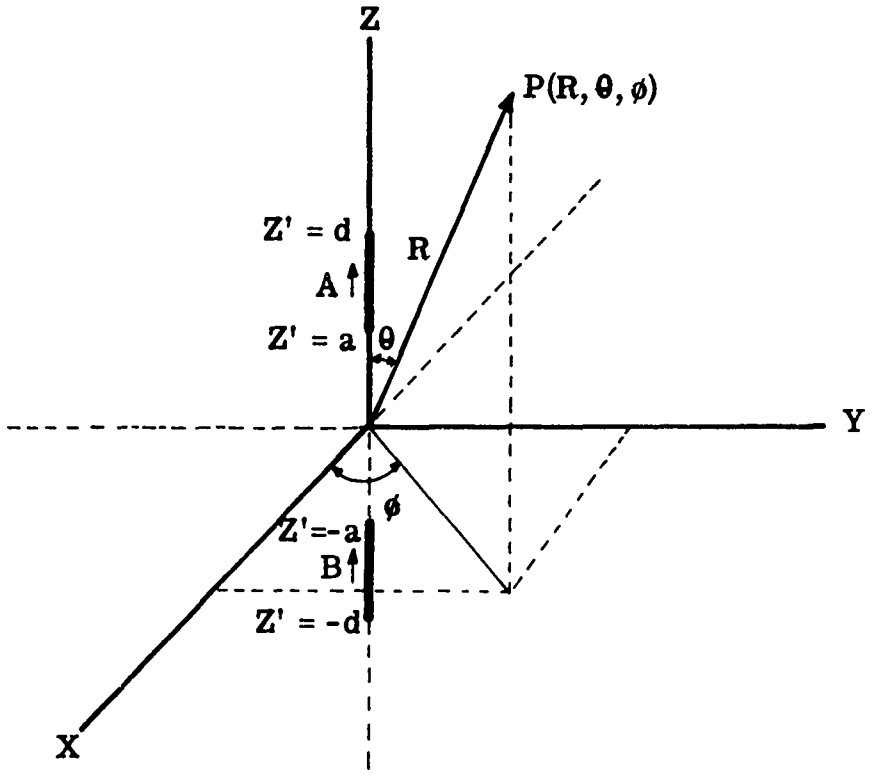

Fig. 5. 4. Collinear dipole

Let the currents on antennas A and B be

$$\bar{I}(z') = I_{max} \sin k(d - z')\,\hat{z} \text{ for } a \leq z' \leq d$$

$$= I_m \sin k(d + z')\,\hat{z} \text{ for } -d \leq z' \leq -a \qquad (5.59)$$

The Antenna B is the image of the Antenna A .

Let us find the expression for the electric radiation vector $\bar{N}$. Since we are only considering the electric source

$$\bar{N} = \iiint \bar{J}(\bar{R}') e^{jk\bar{R}'\cdot\hat{R}} dv' \tag{5.29}$$

where

$$\bar{R}' \cdot \hat{R} = R' \cos\alpha = R' \cos\theta \cos\theta' + \sin\theta \cos(\phi - \phi')$$

$\hat{R}$ = Unit vector in radial direction

In the problem considered only line sources are present. Therefore,

$$\bar{N} = \int \bar{I}(\bar{R}') e^{jk\bar{R}'\cdot\hat{R}} d\ell \tag{5.60}$$

where $\bar{R}' = z'\hat{z}$ and $\bar{R}' \cdot \hat{R} = z' \cos\theta$ for antenna A

and $\bar{R}' = -z'\hat{z}$ and $\bar{R}' \cdot \hat{R} = +z' \cos\theta$ for antenna B

$$N_z = \int_a^d I_m \sin k(d - z') e^{jkz' \cos\theta} dz' + \int_{-d}^{-a} I_m \sin k(d + z') e^{jkz' \cos\theta} dz' \tag{5.61}$$

Changing the variable for the second integral by $z' = -z''$, the integral becomes

$$\int_{-d}^{-a} I_m \sin k(d + z') e^{jkz' \cos\theta} dz' = \int_a^d I_m \sin k(d - z'') e^{-jkz'' \cos\theta} dz'' \tag{5.62}$$

Therefore,

$$N_z = I_m \int_a^d \sin k(d - z') \left[e^{jkz' \cos\theta} + e^{-jkz' \cos\theta} \right] dz'$$

$$= 2 I_m \int_a^d \sin k(d - z') \cos(kz' \cos\theta) dz' \tag{5.63}$$

Since

$$\frac{1}{2}\left[\sin(a+b)+\sin(a-b)\right] = \sin a \cos b$$

$$N_z = I_m \int_a^d \left\{ \sin\left[k(d-z')+kz'\cos\theta\right] + \sin\left[k(d-z')-kz'\cos\theta\right] \right\} dz'$$

$$= I_m \int_a^d \left\{ \sin\left[kd+kz'(\cos\theta-1)\right] + \sin\left[kd-kz'(1+\cos\theta)\right] \right\} dz' \qquad (5.64)$$

Also, using

$$\int \sin(a-bx)dx = \frac{1}{b}\cos(a-bx)$$

$$N_z = I_m \left[\frac{1}{k(1-\cos\theta)} \cos\left[kd-kz'(1-\cos\theta)\right] + \frac{1}{k(1+\cos\theta)} \cos\left[kd-kz'(1+\cos\theta)\right] \right]_a^d$$

$$= I_m \left\{ \frac{1}{k(1-\cos\theta)} \cos\left[kd\cos\theta\right] + \frac{1}{k(1+\cos\theta)} \cos\left[kd\cos\theta\right] \right.$$

$$\left. - \frac{1}{k(1-\cos\theta)} \cos\left[kd-ka(1-\cos\theta)\right] - \frac{1}{k(1+\cos\theta)} \cos\left[kd-ka(1+\cos\theta)\right] \right\}$$

$$N_z = I_m \cos(kd\cos\theta)\left[\frac{1}{k(1-\cos\theta)} + \frac{1}{k(1+\cos\theta)}\right]$$

$$- I_m\left\{\frac{\cos[k(d-a)+ka\cos\theta]}{k(1-\cos\theta)} + \frac{\cos[k(d-a)-ka\cos\theta]}{k(1+\cos\theta)}\right\}$$

$$= \frac{2I_m\cos(kd\cos\theta)}{k\sin^2\theta} - \frac{I_m}{k\sin^2\theta}\Big[(1+\cos\theta)\cos[k(d-a)+ka\cos\theta]$$

$$+ (1-\cos\theta)\cos[k(d-a)-ka\cos\theta]\Big]$$

Using trigonometric identities, Eq. 5.65 can be written as (5.65)

$$N_z = \frac{2I_m\cos(kd\cos\theta)}{k\sin^2\theta} - \frac{2I_m}{k\sin^2\theta}\left[\cos k(d-a)\cos(ka\cos\theta)\right.$$

$$\left. - \cos\theta\sin k(d-a)\sin(ka\cos\theta)\right]$$

$$= \frac{2I_m}{k\sin^2\theta}\left[\cos(kd\cos\theta) - \cos k(d-a)\cos(ka\cos\theta) + \cos\theta\sin k(d-a)\right.$$

$$\left.\sin(ka\cos\theta)\right] \qquad (5.66)$$

When $a = 0$, the expression reduces to the radiation vector of a dipole which is

$$N_z = \frac{2I_m}{k\sin^2\theta}\left[\cos(kd\cos\theta) - \cos kd\right] \qquad (5.67)$$

The θ component of $\bar{N}$ is

$$N_\theta = -N_z \sin\theta = \frac{2 I_m}{k \sin\theta} [\cos(kd\cos\theta) - \cos k(d-a)\cos(ka\cos\theta) + \cos\theta \sin k(d-a)\sin(ka\cos\theta)] \quad (5.68)$$

The far-zone electric field is, from Eq. 5.34,

$$\bar{E} = jk\eta_0 [-\bar{N}_t] \frac{e^{-jkR}}{4\pi R} \quad (5.34)$$

when

$$\bar{M}_t = 0$$

Therefore, the electric field due to two monopoles, E_d, becomes

$$E_{\theta_d} = \frac{j\eta_0 I_m e^{-jkR}}{2\pi R} \left[\frac{\cos(kd\cos\theta) - \cos k(d-a)\cos(ka\cos\theta)}{\sin\theta} + \frac{\cos\theta \sin k(d-a)\sin(ka\cos\theta)}{\sin\theta} \right] \quad (5.69)$$

and

$$\bar{H} = \frac{1}{\eta_0} \hat{R} \times \bar{E} = \frac{1}{\eta_0} E_\theta \hat{\phi} \quad (5.70)$$

The radiation patterns due to the two monopoles discussed above are the plots of angular dependent terms of $\bar{E}$ as a function of θ .

$$F(\theta) = \frac{\cos(kd\cos\theta) - \cos k(d-a)\cos(ka\cos\theta) + \cos\theta \sin k(d-a)\sin(ka\cos\theta)}{\sin\theta} \qquad (5.71)$$

When

$$a = 0$$

$$F(\theta) = \frac{\cos(kd\cos\theta) - \cos kd}{\sin\theta} \qquad (5.72)$$

This expression is the angular term of a far-zone field expression of a dipole.

5.4 Induced Current on a Spherical Surface

5.4.1 Induced Current on a Conducting Sphere Excited by a Monopole.

The induced current on a conducting sphere excited by a monopole antenna erected on its surface was treated by Papas and King (Ref. 16). The current along the antenna was assumed to have a form of sinusoidal distribution and was assumed to be independent of the current on the sphere.

This solution is reviewed here, because the same method will be adopted to calculate the induced current on the spherical surface due to the image antenna located along the negative Z axis.

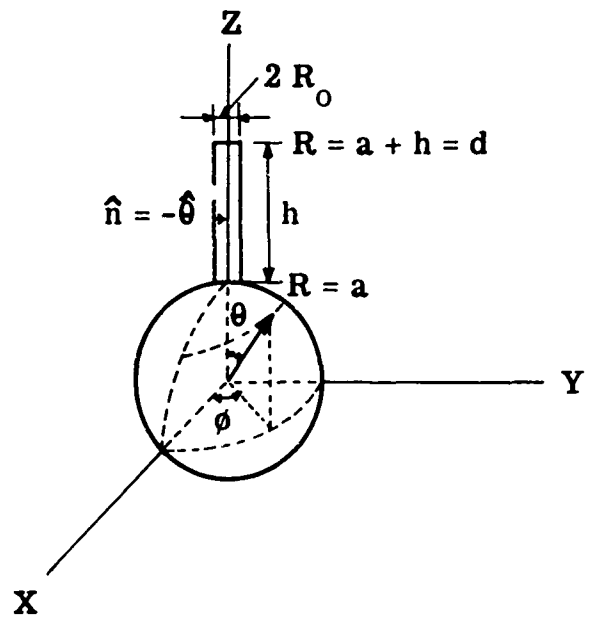

Fig. 5. 5. A monopole antenna above a spherical ground plane.

From the general reciprocity theorem (Appendix A)

$$\int\int_{s} [\,\hat{n}\cdot(\bar{E}_1 \times \bar{H}_2 - \bar{E}_2 \times \bar{H}_1)\,]\, dS = 0 \qquad (5.73)$$

where $\bar{E}_1$ and $\bar{H}_1$ are the electromagnetic fields associated with a current density $\bar{J}_1$ and $\bar{E}_2$, $\bar{H}_2$ with $\bar{J}_2$. Also s is the closed surface of the volume of empty space bounded by the surface of the antenna and the sphere and an imaginary boundary at infinity. $\hat{n}$ is an external normal unit vector of this surface.

The assumption made here is that the two sets of fields, $\bar{E}_1$, $\bar{H}_1$, and $\bar{E}_2$, $\bar{H}_2$, are defined in the free space and are bounded by the same geometrical surfaces, but not necessarily satisfying the same physical properties.

Let fields $\bar{E}_1$ and $\bar{H}_1$ be caused by the actual currents in the antenna located at $\theta = 0$ and $a \leq R \leq a + h$ as shown in Fig. 5.4 and the current on the surface of the sphere.

The boundary conditions for fields $\bar{E}_1$ and $\bar{H}_1$ are:

$\hat{n} \times \bar{E}_1 = 0$ on the spherical surface S_s

$\hat{n} \times \bar{H}_1 = K_{1s}$ " " " " S_s

The current on antennas $\bar{I}_{1A}$ and $\bar{K}_{1s}$ on the sphere is assumed to be maintained by an appropriate generator or a distribution of generators in the antenna in such a way that no current exists in the ϕ direction of the antenna or on the sphere. Therefore,

$$\bar{K}_{1s}(\theta) = \hat{\theta} K_{1s}(\theta) \tag{5.74}$$

and

$$\int_0^{2\pi} K_{1s}(\theta)\, a \sin\theta \, d\phi = I_{1s}(\theta) \tag{5.75}$$

$I_{1s}(\theta)$ is the total current crossing a parallel of latitude on the sphere.

Also, the total current in the antenna at $\theta = 0$ is in radial direction in the spherical coordinate system. Due to the rotational

symmetry about the axis $\vartheta = 0$, the line integral of the tangential component of $\bar{H}_1$ around the surface of the antenna is equal to the total axial current $I_{1A}(R)$ in the antenna.

Thus,

$$\oint \bar{H}_1 \cdot d\bar{\ell} = \int_0^{2\pi} H_{1\phi} R_0 \, d\phi = \iint_{\substack{\text{cross section} \\ \text{of the antenna}}} \bar{i}_{1A} \cdot d\bar{S} = I_{1A}(R) \tag{5.76}$$

The second set of fields $\bar{E}_2$ and $\bar{H}_2$ are not the actual fields that are related to the real currents $\bar{i}_1$ in the antenna or on the sphere. They are, instead, fictitious fields that satisfy the same field equations as the first set and that must be defined over the same geometrical surfaces. Since fields $\bar{E}_2$ and $\bar{H}_2$ are not required to be defined on the boundaries with the same physical properties as set $\bar{E}_1$ and $\bar{H}_1$, let the volume possessed by the antenna for $\bar{E}_1$ and $\bar{H}_1$ be empty space for $\bar{E}_2$ and $\bar{H}_2$. Also, on the surface of the sphere, S_s, fields $\bar{E}_2$ and $\bar{H}_2$ are required to possess the following prescribed form by some appropriate set of generators:

$$\begin{aligned} E_{2\phi} &= 0 \qquad & E_{2\theta} &= U \sin\theta \, P_n(\cos\theta) \\ H_{2\theta} &= 0 \qquad & H_{2R} &= 0 \end{aligned} \tag{5.77}$$

The entire field in empty space, therefore, has the components E_{2R}, $E_{2\theta}$ and $H_{2\phi}$ which must satisfy the field equations and the prescribed boundary conditions.

Returning to Eq. 5.73,

$$\iiint_S [\, n \cdot (\bar{E}_1 \times \bar{H}_2 - \bar{E}_2 \times \bar{H}_1) \,]\, dS = 0 \qquad (5.73)$$

the surface S can be divided into two parts S_s; the surface of the sphere, and S_A, the surface of the antenna.

$$\iint_S [\, \hat{n} \cdot (\bar{E}_1 \times \bar{H}_2 - \bar{E}_2 \times \bar{H}_1)] \, dS = \iint_{S_s} [\, \bar{H}_2 \cdot (\hat{n} \times \bar{E}_1) + \bar{E}_2 \cdot (\hat{n} \times \bar{H}_1)] \, dS$$

$$+ \iint_{S_A} [\, \bar{H}_2 \cdot (\hat{n} \times \bar{E}_1) - \bar{H}_1 \cdot (\hat{n} \times \bar{E}_2)] \, dS \qquad (5.78)$$

Now since $\hat{n} = -\hat{\theta}$ over S_A and since $\hat{n} = -\hat{R}$ over S_s and with the boundary conditions described above, each integral can be rewritten

$$\iint_{S_A} \left\{ \bar{H}_2 \cdot (\hat{n} \times \bar{E}_1) - \bar{H}_1 \cdot (\hat{n} \times \bar{E}_2) \right\} dS = \int_{R=a}^{a+h} E_{1R}\, dR \int_0^{2\pi} H_{2\phi}\, R_0\, d\phi$$

$$- \int_{R=a}^{a+h} E_{2R}\, dR \int_0^{2\pi} H_{1\phi}\, R_0\, d\phi \qquad (5.79)$$

The volume occupied by the antenna is empty space for $H_{2\phi}$. Therefore, for a thin antenna where the radius R_0 goes to zero, the line integral

$$\int_0^{2\pi} H_{2\phi}\, R_0\, d\phi = 0$$

Therefore,

$$\therefore \iint_{S_A} \left\{ \bar{H}_2 \cdot (\hat{n} \times \bar{E}_1) - \bar{H}_1 (\hat{n} \times \bar{E}_2) \right\} dS = - \int_a^{a+h} E_{2R}\, I_{1A}(R)\, dR \tag{5.80}$$

The surface integral on the sphere becomes

$$\iint_S [\, \bar{H}_2 \cdot (\hat{n} \times \bar{E}_1) + \bar{E}_2 \cdot (\hat{n} \times \bar{H}_1)] \; dS = \iint \bar{E}_2 \cdot \bar{K}_{1s}\, dS \tag{5.81}$$

because of the boundary condition $n \times \bar{E}_1 = 0$ on S_s.

From Eqs. 5.75 and 5.77

$$\iint_{S_s} \bar{E}_2 \cdot \bar{K}_{1s}\, dS = \int_0^{\pi} E_{2\theta}\, I_{1s}(\theta)\, a\, d\theta$$

Therefore,

$$\iint_S [\, \hat{n} \cdot (\bar{E}_1 \times \bar{H}_2 - \bar{E}_2 \times \bar{H}_1)] \; dS = 0 \tag{5.73}$$

which implies that

$$\int_0^{\pi} E_{2\theta}\, I_{1s}(\theta)\, a\, d\theta = \int_a^{a+h} E_{2R}\, I_{1A}(R)\, dR \tag{5.82}$$

This is the integral equation to determine $I_{1s}(\theta)$ knowing $I_{1A}(R)$ and the prescribed field $E_{2\theta}$ will assume that the surface

current $I_{1s}(\theta)$ takes the form of

$$I_{1s}(\theta) = \sum_{n=0}^{\infty} B_n P_n(\cos\theta) \qquad (5.83)$$

where the coefficients B_n are to be evaluated from the integral equation.

For the second set of fields $\bar{E}_2$ and $\bar{H}_2$, the volume surrounded by the closed surface S_s, S_A and the boundary at infinity is empty. Furthermore, E_{2R}, $E_{2\theta}$ and $H_{2\phi}$ are the only non-zero components due to currents on the sphere. For TM fields of this type, the fields are found from the scalar wave equation

$$\nabla^2 \left(\frac{u}{R}\right) + k^2 \left(\frac{u}{R}\right) = 0 \qquad (5.84)$$

where

$$k = \omega\sqrt{\mu_0 \epsilon_0}$$

The solution of the equation is

$$u = \sum_{m=0}^{\infty} A_m P_m(\cos\theta)\, \rho_m(kR) \qquad (5.85)$$

where

$P_m(\cos\theta)$ is the Legendre polynomial of order m

$$\rho_m(kR) = \sqrt{\frac{\pi kR}{2}}\, H^{(2)}_{m+\frac{1}{2}}(kR) = (kR)\, h^{(2)}_m(kR)$$

$H^{(2)}_m(kR)$: Hankel function of the 2nd kind

$h^{(2)}_m(kR)$: Spherical Hankel function of the 2nd kind

The components of the fields are obtained from solution u as

$$E_{2R} = \left[k^2 + \frac{\partial^2}{\partial R^2} \right] u$$

$$E_{2\theta} = \frac{1}{R} \left(\frac{\partial^2}{\partial R\, \partial \theta} \right) u \qquad (5.86)$$

$$H_{2\phi} = -j \left(\frac{k}{R} \right) \left(\frac{\partial u}{\partial \theta} \right)$$

From Eq. 5.85 and 5.86 , on the spherical surface R = a,

$$E_{2\theta} = -\left(\frac{k}{a} \right) \sum_{m=0}^{\infty} A_m P_m^1(\cos\theta)\, \rho_m'(ka) \qquad (5.87)$$

Also, we demand that $E_{2\theta}$ take on the spherical surface:

$$E_{2\theta} = U \sin\theta\, P_n(\cos\theta) = U\, \frac{P_{n+1}^1(\cos\theta) - P_{n-1}^1(\cos\theta)}{2n+1} \,. \qquad (5.88)$$

Equating the two equations 5.87 and 5.88 leads to

$$A_{n+1} = -\frac{a\,U}{(2n+1)\cdot k\cdot \rho_{n+1}'(ka)}$$

$$A_{n-1} = \frac{a\,U}{(2n+1)\cdot k\cdot \rho_{n-1}'(ka)} \qquad (5.89)$$

Therefore,

$$E_{2R} = U\left[k^2 + \frac{\partial^2}{\partial R^2}\right]\left[\frac{a\,P_{n-1}(\cos\theta)\,\rho_{n-1}(kR)}{(2n+1)\cdot k\cdot \rho_{n-1}'(ka)} - \frac{a\,P_{n+1}(\cos\theta)\,\rho_{n+1}(kR)}{(2n+1)\cdot k\cdot \rho_{n+1}'(ka)}\right] \qquad (5.90)$$

Assuming that the antenna current takes the sinusoidal form

$$I_{1A}(R) = I_{max}\sin k(d-R) \qquad (5.91)$$

it can be shown that (Appendix C)

$$\int_a^{a+h} E_{2R}\,I_{1A}(R)\,dR = \frac{U\,a\,I_{max}}{2n+1}\left[\frac{\rho_{n-1}(kd)}{\rho_{n-1}'(ka)} - \cos kh\,\frac{\rho_{n-1}(ka)}{\rho_{n-1}'(ka)} - \frac{\rho_{n+1}(kd)}{\rho_{n+1}'(ka)} + \cos kh\,\frac{\rho_{n+1}(ka)}{\rho_{n+1}'(ka)}\right] \qquad (5.92)$$

along $\theta = 0$.

Also

$$\int_0^{\pi} E_{2\theta}\, I_{1s}(\theta)\, a\, d\theta = \int_0^{\pi} E_{2\theta} \sum_{n=0}^{\infty} B_n P_n(\cos\theta)\, a\, d\theta$$

$$= B_n \frac{U\, 2a}{2n+1} \tag{5.93}$$

Finally, the integral equation produces the result

$$B_n = \frac{I_{max}}{2}\left[\frac{\rho_{n-1}(kd)}{\rho_{n-1}'(ka)} - \cos kh\, \frac{\rho_{n-1}(ka)}{\rho_n - 1'(ka)} - \frac{\rho_{n+1}(kd)}{\rho_{n+1}'(ka)} + \cos kh\, \frac{\rho_{n+1}(ka)}{\rho_{n+1}'(ka)}\right] \tag{5.94}$$

The surface current $I_{1s}(\theta)$ is now determined in terms of the coefficients B_n:

$$I_{1s}(\theta) = \sum_{n=0}^{\infty} B_n P_n(\cos\theta) \tag{5.83}$$

5.4.2 Induced Current Due to the Image Antenna. In the Section 5.4.1, the induced current on the spherical surface due to the sinusoidally distributed current on the antenna was found in the form of a modal current. The coefficients B_n of the infinite series that gives the surface current were evaluated in terms of known parameters. In this section, the contribution from the image antenna to the total surface current on the spherical ground plane is obtained following the method

used in the previous section.

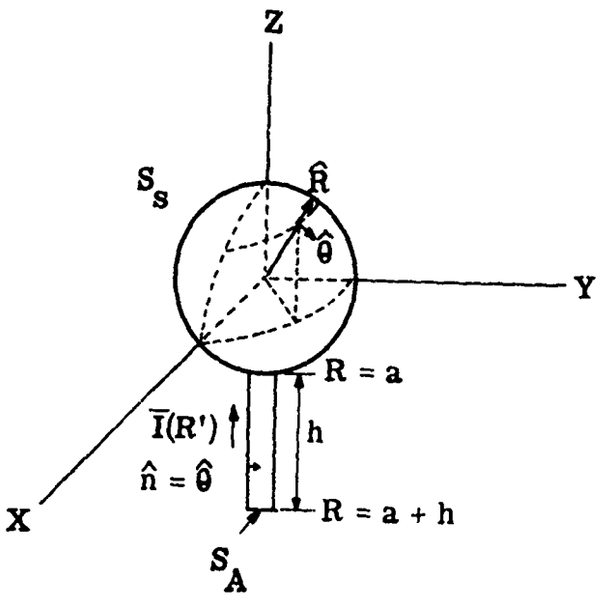

Fig. 5. 6. Image antenna with a spherical ground plane.

The geometrical arrangement of the image antenna and the spherical ground plane is shown in Fig. 5. 6. The center of the spnere is located at the origin of the spherical coordinate system.

The electromagnetic fields and the currents are all expressed in the same way as they were in the previous section except for the prime notation to distinguish the image antenna problem from the real one.

From the reciprocity theorem,

$$\iint_S (\bar{E}_1' \times \bar{H}_2' - \bar{E}_2' \times \bar{H}_1') \cdot d\bar{S} = 0 \qquad (5.95)$$

where surface S is now the closed surface enclosing the volume bounded by the spherical surface, the surface of the image antenna and a boundary at infinity. The surface normal unit vector $\hat{n}$ is the same as was in Section 5.4.1 on spherical surface S_s. However, on the surface of the image antenna S_A the unit vector is in the positive $\hat{\theta}$ direction. The integral equation 5.82 is now modified to become

$$\int_0^{\pi} E_{2\theta}' I_{1s}'(\theta)\, a\, d\theta = -\int_a^{ath} E_{2R}' I_{1A}'(R)\, dR \qquad (5.96)$$

Let the surface current $I_{1s}'(\theta)$ on the sphere due to the image antenna also take a modal form with coefficients of the infinite series B_n'. Then,

$$I_{1s}'(\theta) = \sum_{n=0}^{\infty} B_n' P_n(\cos\theta) \qquad (5.97)$$

Following the steps shown in Section 5.4.1

$$E_{2R}' = U\left[k^2 + \frac{\partial^2}{\partial R^2}\right]\left[\frac{a P_{n-1}(\cos\theta)\rho_{n-1}(kR)}{(2n+1)\cdot k\cdot \rho_{n-1}'(ka)} - \frac{a P_{n+1}(\cos\theta)\rho_{n+1}(kR)}{(2n+1)\cdot k\,\rho_{n+1}'(ka)}\right] \qquad (5.98)$$

Since

$$P_{n-1}(\cos\theta) = (-1)^{n-1} \text{ at } \theta = \pi \tag{5.99}$$

along the image antenna

$$P_{n+1}(\cos\theta) = (-1)^{n+1} \text{ at } \theta = \pi$$

$$E'_{2R} = U\left[k^2 + \frac{\partial^2}{\partial R^2}\right]\left[a(-1)^{n-1}\frac{\rho_{n-1}(kR)}{(2n+1)\,k\rho_{n-1}'(ka)} - (-1)^{n+1}\,a\,\frac{\rho_{n+1}(kR)}{(2n+1)\cdot k\cdot\rho_{n+1}'(ka)}\right]$$

$$= (-1)^{n-1}\,U\left[k^2 + \frac{\partial^2}{\partial k^2}\right]\left[\frac{\rho_{n-1}(kR)}{(2n+1)\,k\rho_{n-1}'(ka)} - a\frac{\rho_{n+1}(kR)}{(2n+1)\cdot k\cdot\rho_{n+1}'(ka)}\right] \tag{5.100}$$

$$\int E_{2R}'\,I_{1A}'\,dR = \int_a^{a+h}(-1)^n\,E_{2R}'\,I_{1A}'\,dR = (-1)^n\,\frac{U\,a\,I_{max}}{2n+1}\left[\frac{\rho_{n-1}(kd)}{\rho_{n-1}'(ka)}\right.$$

$$\left. - \cos k(d-a)\frac{\rho_{n-1}(ka)}{\rho_{n-1}'(ka)} - \frac{\rho_{n+1}(kd)}{\rho_{n+1}'(ka)} + \cos k(d-a)\frac{\rho_{n+1}(ka)}{\rho_{n+1}'(ka)}\right] \tag{5.101}$$

Since

$$\int_a^{a+h} E_{2R}'\,I_{1A}'(R)dR = -\int_{R=a}^{a+h} E_{2\theta}'I_{1s}'(\theta)\,a\,d\theta \tag{5.102}$$

where

$$I'_{1A}(R) = I_{max} \sin k(d - R)$$

and

$$I'_{1s}(\theta) = \sum_{n=0}^{\infty} B_n' P_n(\cos \theta) \qquad (5.97)$$

Also

$$E'_{2\theta} = U \sin \theta P_n(\cos \theta) = U \left[\frac{P'_{n+1}(\cos \theta) - P'_{n-1}(\cos \theta)}{2n + 1} \right] \qquad (5.103)$$

Thus,

$$\int_0^{\pi} E'_{2\theta} \sum_{n=0}^{\infty} B_n' P_n(\cos \theta) \cdot a \, d\theta = B_n' \frac{U 2a}{(2n + 1)} \qquad (5.104)$$

Using the orthogonality relationship for the Legendre function

$$\int_{-1}^{1} P_m(\mu) P_n(\mu) \, d\mu = \left[\frac{2}{2n + 1} \right] \delta_{m,n} \qquad (5.105)$$

$$2 B_n' = \int E'_{2R} I'_{1A}(R) \, dR = (-1)^{n+1} I_{max} \left[\frac{\rho_{n-1}(kd)}{\rho'_{n-1}(ka)} - \cos k(d - a) \frac{\rho_{n-1}(ka)}{\rho'_{n-1}(ka)} \right.$$

$$- \frac{\rho_{n+1}(ka)}{\rho_{n+1}'(ka)} + \cos k(d-a) \frac{\rho_{n+1}(ka)}{\rho_{n+1}'(ka)}]$$

Or

$$B_n' = \frac{(-1)^{n+1} I_{max}}{2} \left[\frac{\rho_{n-1}(kd)}{\rho_{n-1}'(ka)} - \cos k h \frac{\rho_{n-1}(ka)}{\rho_{n-1}'(ka)} - \frac{\rho_{n+1}(kd)}{\rho_{n+1}'(ka)} + \cos k h \frac{\rho_{n+1}(ka)}{\rho_{n+1}'(ka)} \right] \tag{5.106}$$

Finally, the total surface current induced by the antenna and its image can be written as

$$\left(I_{ls}(\theta) \right)_{Total} = \sum_{n=0}^{\infty} B_n P_n(\cos\theta) + \sum_{n=0}^{\infty} B'_n P_n(\cos\theta) \tag{5.107}$$

where

$$B_n' = (-1)^{n+1} B_n \tag{5.108}$$

Therefore, the total surface current due to both antennas is expressed as

$$\left[I_{ls}(\theta) \right]_{Total} = 2 \sum_{n=odd} B_n P_n(\cos\theta) \tag{5.109}$$

where

$$B_n = \frac{I_{max}}{2}\left[\frac{\rho_{n-1}(kd)}{\rho_{n-1}'(ka)} - \cos k h \frac{\rho_{n-1}(ka)}{\rho_{n-1}'(ka)} - \frac{\rho_{n+1}(kd)}{\rho_{n+1}'(ka)} + \cos k h \frac{\rho_{n+1}(ka)}{\rho_{n+1}'(ka)}\right] \tag{5.110}$$

Finally,

$$I_S(\theta) = I_{max} \sum_{n=odd} \left[\frac{\rho_{n-1}(kd)}{\rho_{n-1}'(ka)} - \cos kh \frac{\rho_{n-1}(ka)}{\rho_{n-1}'(ka)} - \frac{\rho_{n+1}(kd)}{\rho_{n+1}'(ka)} + \cos k h \frac{\rho_{n+1}(ka)}{\rho_{n+1}'(ka)}\right] \rho_n(\cos\theta) \tag{5.111}$$

5.5 Far-Field Expressions Due to a Spherical Surface Current Distribution

The radiation vector $\bar{N}$ due to an electrical source $\bar{I}'$ is found to be

$$\bar{N} = \iiint_V \bar{I}' e^{jk R' \cos\psi} dv' \tag{5.112}$$

where ψ is the angle between the radial lines to the source point and the observation point.

The far-zone electromagnetic fields are obtained from radiation vector $\bar{N}$:

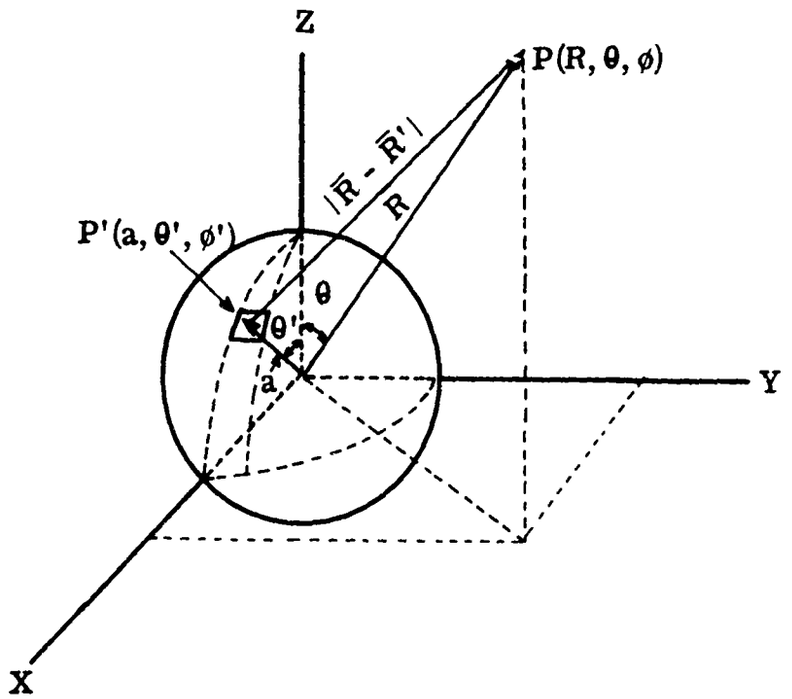

Fig. 5.7. Fields due to a surface current on a spherical ground plane.

$$\left.\begin{aligned} E_\theta &= -\frac{j\omega\mu}{4\pi R} e^{-jk\,R} N_\theta \\ E_\phi &= \frac{j\omega\mu}{4\pi R} e^{-jk\,R} N_\phi \end{aligned}\right\} \qquad (5.34)$$

Since $R' = a$ at the surface of the sphere, the term $e^{ik\,R'\cos\psi}$ in Eq. 5.112 can be written as

$$e^{jk\,R'\cos\psi} = e^{jk\,a[\cos\theta\cos\theta' + \sin\theta'\sin\theta\cos(\phi - \phi')]} \qquad (5.113)$$

The current density $\bar{I}'$ inside the volume integral is the surface current per unit width and flowing in $\hat{\theta}$ direction. Therefore,

$$\bar{I}' = k(\theta')\hat{\theta} = k(\theta')\,[\cos\theta'\cos\phi'\,\hat{x} + \cos\theta'\sin\phi'\,\hat{y} - \sin\theta'\,\hat{z}] \qquad (5.114)$$

where $\hat{x}$, $\hat{y}$, and $\hat{z}$ are unit vectors of the Cartesian coordinate system. The radiation vector $\bar{N}$ can be written

$$\bar{N} = \int_0^{2\pi}\int_0^{\pi} k(\theta')[\cos\theta'\cos\phi'\,\hat{x} + \cos\theta'\sin\phi'\,\hat{y} - \sin\theta'\,\hat{z}]$$

$$e^{jka[\cos\theta'\cos\theta' + \sin\theta'\sin\theta\cos(\phi - \phi')]}\; a^2\sin\theta'\,d\theta'\,d\phi' \qquad (5.115)$$

Breaking $\bar{N}$ into three components

$$N_x = \int_0^{2\pi} \int_0^{\pi} k(\theta') \cos\theta' \cos\phi'$$

$$e^{jka[\cos\theta\cos\theta' + \sin\theta'\sin\theta\cos(\phi - \phi')]}\ a^2 \sin\theta'\, d\theta'\, d\phi'$$

$$N_y = \int_0^{2\pi} \int_0^{\pi} k(\theta') \cos\theta' \sin\phi'$$

$$e^{jka[\cos\theta\cos\theta' + \sin\theta'\sin\theta\cos(\phi - \phi')]}\ a^2 \sin\theta'\, d\theta'\, d\phi' \qquad (5.116)$$

$$N_z = -\int_0^{2\pi} \int_0^{\pi} k(\theta') \sin\theta'$$

$$e^{jka[\cos\theta\cos\theta' + \sin\theta'\sin\theta\cos(\phi - \phi')]}\ a^2 \sin\theta'\, d\theta'\, d\phi'$$

Also

$$\int_0^{2\pi} k(\theta')\, a \sin\theta'\, d\phi' = I(\theta') \qquad (5.76)$$

Since $k(\theta')$ is independent of ϕ'

$$k(\theta') = \frac{I(\theta')}{2\pi a \sin\theta'} = \frac{\sum^{n=odd} B_n P_n(\cos\theta')}{\pi a \sin\theta'} \qquad (5.117)$$

Using the identity(Ref. 14, p. 407)

$$e^{jk R \cos\psi} = \sum_{n=0}^{\infty} (j)^n (2n + 1)\, j_n(kR)\, P_n(\cos\psi) \qquad (5.118)$$

where

$$j_n(kR) = \sqrt{\frac{\pi}{2kR}}\, J_{n+\frac{1}{2}}(kR) \tag{5.119}$$

and expanding $P_n(\cos\psi)$ into a finite series of the form

$$P_n(\cos\psi) = \frac{c_o}{2} P_n(\cos\theta) + \sum_{m=1}^{n} (c_m \cos m\phi + d_m \sin m\phi)\, P_n^m(\cos\theta) \tag{5.120}$$

and evaluating the coefficients c_m and d_m by using the orthogonal relationship of the Legendre polynomials such as

$$\int_0^{2\pi}\int_0^{\pi} P_n(\cos\psi)\, P_n^m(\cos\theta)\cos m\phi \sin\theta\, d\theta\, d\phi = \frac{2\pi}{2n+1}\frac{(n+m)!}{(n-m)!} c_m \tag{5.121}$$

and

$$\int_0^{2\pi}\int_0^{\pi} Y_n(\theta,\phi)\, P_n(\cos\theta)\sin\theta\, d\theta\, d\phi = \frac{4\pi}{2n+1}\left[Y_n(\theta,\phi)\right]_{\phi=o} \tag{5.122}$$

where

$$Y_n(\theta,\phi) = P_n(\cos\theta)\cos m\phi \tag{5.123}$$

$$\cos\psi = \sin\theta' \sin\theta \cos(\phi - \phi') + \cos\theta \cos\theta$$

it can be shown that

$$\int_0^{2\pi}\int_0^{\pi} P_n(\cos\psi)\, P_n^m(\cos\theta)\cos m\phi \sin\theta\, d\theta\, d\phi = \frac{4\pi}{2n+1} P_n^m(\cos\theta')\cos m\phi' \tag{5.124}$$

The coefficients c_m and d_m are evaluated to be

$$c_m = 2\frac{(n-m)!}{(n+m)!} P_n^m(\cos\theta')\cos m\phi'$$

$$d_m = 2\frac{(n-m)!}{(n+m)!} P_n^m(\cos\theta')\sin m\phi' \tag{5.125}$$

Therefore,

$$P_n(\cos\psi) = P_n(\cos\theta')\, P_n(\cos\theta) + 2\sum_{m=1}^{n}\frac{(n-m)!}{(n+m)!} P_n^m(\cos\theta')\, P_n^m(\cos\theta)\cos m(\phi-\phi') \tag{5.126}$$

$$N_x = \int_0^{2\pi}\int_0^{\pi} \frac{\sum_{\ell} B_{2\ell+1} P_{2\ell+1}(\cos\theta')}{2\pi a \sin\theta'} \cos\theta'\cos\phi' \; e^{jka[\cos\theta\cos\theta' + \sin\theta\sin\theta'\cos(\phi-\phi')]}\, a^2 \sin\theta'\, d\theta'\, d\phi' \tag{5.127}$$

Since

$$e^{jka\cos\psi} = \sum_{n=0}^{\infty}(j)^n(2n+1)\, j_n(ka)\left[P_n(\cos\theta')\, P_n(\cos\theta) + 2\sum_{m=1}^{n}\frac{(n-m)!}{(n+m)!} P_n^m(\cos\theta')\, P_n^m(\cos\theta)\cos m(\phi-\phi')\right] \tag{5.128}$$

and

$$\cos m(\phi - \phi') = \cos m\phi' \cos m\phi + \sin m\phi \sin m\phi'$$

the contribution of the first integral with respect to ϕ' reduces the double integral to

$$N_x = \int_0^{\pi} \frac{\sum_{\ell} B_{2\ell+1} P_{2\ell+1}(\cos\theta')}{\pi a} \sum_{n=0}^{\infty} j^n (2n+1) \dot{j}_n(ka)$$

$$2 \frac{(n-1)!}{(n+1)!} P_n'(\cos\theta') P_n'(\cos\theta) \pi \cdot \cos\phi \, a^2 \cos\theta' \, d\theta'$$

$$= \left[2a \int_0^{\pi} \sum_{\ell} B_{2\ell+1} P_{2\ell+1}(\cos\theta') \sum_{n=0} j^n \frac{2n+1}{n(n+1)} \right.$$

$$\left. \dot{j}_n(ka) P_n'(\cos\theta') P_n'(\cos\theta) \cos\theta' \, d\theta' \right] \cos\phi \qquad (5.129)$$

because

$$\int_0^{2\pi} \cos m\phi' \cos\phi' \, d\phi' = 0 \quad \text{for } m \neq 1$$

$$= \pi \quad \text{for } m = 1$$

$$\int \sin m\phi' \cos\phi' \, d\phi' = 0 \quad \text{for all } m$$

Similarly, for the evaluation of N_y, we obtain

$$N_y = \left[a \int_0^{\pi} \sum_{\ell} B_{2\ell+1} P_{2\ell+1}(\cos\theta') \sum_{n} j^n \frac{2n+1}{n(n+1)} \right.$$

$$\left. 2 \dot{j}_n(ka) P_n'(\cos\theta') P_n'(\cos\theta) \cos\theta' \, d\theta' \right] \sin\phi \qquad (5.130)$$

If we let

$$\eta = a \int_0^{\pi} \sum_{\ell} B_{2\ell+1} P_{2\ell+1}(\cos\theta') \sum_n j^n \frac{2n+1}{n(n+1)} \cdot 2 j_n(ka) P'_n(\cos\theta') P'_n(\cos\theta) \cos\theta' \, d\theta' \tag{5.131}$$

then

$$N_x = \eta \cos\phi$$
$$N_y = \eta \sin\phi \tag{5.132}$$

Finally, the $\hat{z}$ component of the radiation vector $\bar{N}$ can be written as

$$N_z = -\int_0^{2\pi}\int_0^{2\pi} k(\theta') \sin\theta' e^{jka[\cos\theta\cos\theta' + \sin\theta\sin\theta'\cos\phi']} a^2 \sin\theta' d\theta' d\phi'$$

$$= -\int_0^{2\pi}\int_0^{\pi} \frac{\sum B_{2\ell+1} P_{2\ell+1}(\cos\theta')}{\pi a} \left\{ \sum_{n=0}^{\infty} j^n (2n+1) j_n(ka) \right.$$

$$\left. [P_n(\cos\theta')P_n(\cos\theta) + 2\sum_{m=1}^{n} \frac{(n-m)!}{(n+m)!} P_n^m(\cos\theta')P_n^m(\cos\theta)\cos m\phi'] \right\}$$

$$a^2 \sin\theta' d\theta' d\phi' \tag{5.133}$$

Since

$$\int_0^{2\pi} \cos m\phi' d\phi' = 0$$

for

$$m \neq 0$$

$$N_z = -2a \int_0^{\pi} \sum_{\ell=0}^{\infty} B_{2\ell+1} P_{2\ell+1}(\cos\theta')$$

$$\left[\sum_{n=0}^{\infty} j^n (2n+1) \; {}_n(ka) P_n(\cos\theta') P_n(\cos\theta) \right] \sin\theta' d\theta' \tag{5.134}$$

From the orthogonality relationship of the Legendre functions,

$$\int_0^{\pi} P_m(\cos\theta) P_n(\cos\theta) (-\sin\theta) d\theta = 0 \qquad m \neq n$$

$$= \frac{2}{2n+1} \qquad m = n \tag{5.135}$$

Therefore,

$$N_z = a \sum_{\ell=0}^{\infty} 2B_{2\ell+1} (j^{2\ell+1}) j_{2\ell+1}(ka) P_{2\ell+1}(\cos\theta) \left(\frac{2}{4\ell+3}\right) (4\ell+3)$$

$$= 4a \sum_{\ell=0}^{\infty} B_{2\ell+1} (j)^{2\ell+1} j_{2\ell+1}(ka) P_{2\ell+1}(\cos\theta) \tag{5.136}$$

Radiation vector $\bar{N}$ in a spherical coordinate system is related to the Cartesian components by

$$N_\theta = (N_x \cos\phi + N_y \sin\phi) \cos\theta - N_z \sin\theta$$

$$N_\phi = -N_x \sin\phi + N_y \cos\phi \tag{5.137}$$

Therefore, the transverse component of $\bar{N}$ becomes

$$N_\theta = \eta \cos\theta - N_z \sin\theta$$

$$N_\phi = 0 \qquad (5.138)$$

Due to the symmetry of the problem with respect to z axis, it was anticipated that there be no ϕ component of $\bar{E}$ fields, at far-zone. The result shown in equations 5.137 and 5.138 confirms the physical phenomena. Since the direction of the $\bar{E}$ fields coincided with that of the $\bar{N}$, and it was shown that $N_\phi = 0$, only the θ component of $\bar{E}$ exists.

Finally,

$$\bar{E}_s = -\frac{jk\eta_o e^{-jkR}}{4\pi R}\,\bar{N}_t$$

$$= -\frac{jk\eta_o e^{-jkR}}{4\pi R}\,[\eta\cos\theta - N_z \sin\theta]\,\hat{\theta} \qquad (5.139)$$

Equation 5.139 is the expression for the far-zone electric field $\bar{E}_s$ due to the spherical surface current that was; in turn, induced by the monopole and its image.

5.5.1 Evaluation of $\mathcal{N}$. From Eq. 5.131, $\mathcal{N}$ is defined as

$$\mathcal{N} = 2a \int_0^{\pi} \sum_{\ell=0} B_{2\ell+1} P_{2\ell+1}(\cos\theta') \sum_{n=0} j^n \frac{2n+1}{n(n+1)} \mathcal{J}_n(ka)$$

$$P_n^1(\cos\theta') P_n^1(\cos\theta) \cos\theta' \, d\theta' \qquad (5.131)$$

since

$$\mathcal{P}_n^m(x) = (-1)^m (1-x)^{m/2} \frac{d^m P_n(x)}{dx^m}$$

$$P_n^1(\cos\theta') \, d\theta' = \frac{d P_n(\cos\theta')}{d(\cos\theta')} \, d(\cos\theta') ,$$

if we let $x = \cos\theta'$, the integral can be rewritten as

$$\mathcal{N} = 2a \int_{-1}^{1} \sum_{\ell=0} B_{2\ell+1} P_{2\ell+1}(x) \sum_{n=0} j^n \frac{2n+1}{n(n+1)} \mathcal{J}_n(ka)$$

$$P_n^1(\cos\theta) \frac{d P_n(x)}{dx} x \, dx \qquad (5.140)$$

The evaluation of this integral depends upon the evaluation of the integral I

$$I = \int_{-1}^{1} x \, P_{2\ell+1}(x) \frac{d P_n(x)}{dx} \, dx \qquad (5.141)$$

From Ref. 17

$$\frac{d P_n(x)}{dx} = (2n-1) P_{n-1}(x) + (2n-5) P_{n-3}(x) + (2n-9) P_{n-5}(x) + \ldots \tag{5.142}$$

also

$$(2n-1)\, x\, P_{n-1}(x) = n P_n(x) + (n-1) P_{n-2}(x) \tag{5.143}$$

From (5.142) and (5.143)

$$\begin{aligned} x \frac{d P_n(x)}{dx} &= [n P_n(x) + (n-1) P_{n-2}(x)] + [(n-2) P_{n-2}(x) + (n-3) P_{n-4}(x)] \\ &\quad + [(n-4) P_{n-4}(x) + (n-5) P_{n-5}(x)] + \ldots\ldots \\ &= n P_n(x) + (2n-3) P_{n-2}(x) + (2n-7) P_{n-4}(x) + (2n-11) P_{n-6}(x) + \ldots \\ &= n P_n(x) + \sum_{q=1}^{\leq n/2} (2n - 4q + 1) P_{n-2q}(x) \end{aligned} \tag{5.144}$$

Thus

$$I = \int_{-1}^{1} P_{2\ell+1}(x) \left[n P_n(x) + (2n-3) P_{n-2}(x) + (2n-7) P_{n-4}(x) + \ldots\ldots \right] dx \tag{5.145}$$

From the orthogonal relationship of the legendre polynomials,

$$\begin{aligned} \int_{-1}^{1} P_m(x) P_n(x)\, dx &= 0 \qquad \text{for} \quad m \neq n \\ &= \frac{2}{2n+1} \quad \text{for} \quad m = n \ . \end{aligned} \tag{5.135}$$

Using the orthogonality shown above, the integral I can be written as

$$I = \int_{-1}^{1} n P_{2\ell+1}(x)\, P_n(x)\, dx + \int_{-1}^{1} \sum_{q=1}^{\leq n/2} (2n - 4q + 1)\, P_{2\ell+1}(x)\, P_{n-2q}(x)\, dx$$

$$= (2\ell+1)\, \frac{2\,\delta_{n-(2\ell+1)}}{2(2\ell+1)+1} + \left(2n - 4\,\frac{n-2\ell-1}{2} + 1\right) \frac{2}{2(2\ell+1)+1}$$

$$= \frac{2(2\ell+1)\,\delta_{n-(2\ell+1)}}{4\ell+3} + 2 \sum_{q=0}^{\leq n/2} \delta_{n-2q-(2\ell+1)} \qquad (5.146)$$

where

$$\delta_m = 1 \quad \text{for} \quad m = 0$$

$$0 \quad \text{for} \quad m \neq 0 \ .$$

Then,

$$\eta = 2a \sum_{\ell} B_{2\ell+1}\, j^{2\ell+1}\, \frac{2(2\ell+1)+1}{(2\ell+1)(2\ell+2)}\, j_{2\ell+1}(ka)\, P^1_{2\ell+1}(\cos\theta)\, \frac{2(2\ell+1)}{4\ell+3}$$

$$+ 4a \sum_{n,\ell} B_{2\ell+1}\, j^n\, \frac{2n+1}{n(n+1)}\, j_n(ka)\, P^1_n(\cos\theta)$$

$$= 2a \sum_{\ell=0}^{\infty} B_{2\ell+1} (j)^{2\ell+1}\, \frac{1}{\ell+1}\, j_{2\ell+1}(ka)\, P^1_{2\ell+1}(\cos\theta)$$

$$+ 4a \sum_{\ell=0} B_{2\ell+1} \sum_{n=0} j^n\, \frac{2n+1}{n(n+1)}\, j_n(ka)\, P^1_n(\cos\theta) \ . \qquad (5.147)$$

Also from the orthogonality condition of the second integral in I; i.e.,

$$q = \frac{n - 2\ell - 1}{2}$$

it follows that

$$n = 2\ell + 2q + 1$$

where

$$\ell = 0, 1, 2, \ldots$$

$$q = 1, 2, \quad \ldots$$

$$n = 2\ell+3, 2\ell+5, \ldots, \infty \ .$$

Finally,

$$\eta = 2a \sum_{\ell=0}^{\infty} B_{2\ell+1} j^{2\ell+1} \frac{j_{2\ell+1}(ka)}{\ell+1} P^1_{2\ell+1}(\cos\theta)$$

$$+ \sum_{\ell=0}^{\infty} B_{2\ell+1} \sum_{m=\ell+1}^{\infty} j^{2m+1} \frac{(4m+3)}{(2m+1)(m+1)} j_{2m+1}(ka) P^1_{2m+1}(\cos\theta) \tag{5.148}$$

The far-zone electric field E_θ, due to the surface current on the conducting sphere induced by two monopoles, is:

$$E_{\theta_s} = \frac{-jk\,\eta_o\, e^{-jkR}}{2\pi R}\left[a\cos\theta\left(\sum_{\ell=0}^{\infty} B_{2\ell+1}\, j^{2\ell+1}\,\frac{j_{2\ell+1}(ka)}{\ell+1}\,P_{2\ell+1}^{1}(\cos\theta)\right.\right.$$

$$+\left.\sum_{\ell=0}^{\infty} B_{2\ell+1}\sum_{m=\ell+1}^{\infty} j^{2m+1}\,\frac{(4m+3)}{(2m+1)(m+1)}\,j_{2m+1}(ka)\,P_{2m+1}^{1}(\cos\theta)\right)$$

$$+\left.2a\sin\theta\sum_{\ell=0} B_{2\ell+1}\, j^{2\ell+1}\, j_{2\ell+1}(ka)\,P_{2\ell+1}(\cos\theta)\right]$$

which becomes

$$E_{\theta_s} = \frac{\eta_o\, e^{-jkR}}{\pi R}\left\{\frac{ka\cos\theta}{2}\left[B_1\, j_1(ka)\,P_1^1(\cos\theta) - \frac{B_3}{2}\, j_3(ka)\,P_3^1(\cos\theta)\right.\right.$$

$$+\left.\frac{B_5}{3}\, j_5(ka)\,P_5^1(\cos\theta)\ldots.\right]$$

$$+\frac{ka\cos\theta}{2}\left[B_1\left(\frac{-7}{6}\, j_3(ka)\,P_3^1(\cos\theta) + \frac{11}{15}\, j_5(ka)\,P_5^1(\cos\theta)\right.\right.$$

$$-\left.\frac{15}{28}\, j_7(ka)\,P_7^1(\cos\theta) + \ldots..\right)$$

$$+ B_3\left(\frac{11}{15}\, j_5(ka)\,P_5^1(\cos\theta) - \frac{15}{28}\, j_7(ka)\,P_7^1(\cos\theta) + \ldots\right)$$

$$+\left. B_5\left(-\frac{15}{28}\, j_7(ka)\,P_7^1(\cos\theta) + \ldots\right)\right] + ka\sin\theta\left[B_1\, j_1(ka)\,P_1(\cos\theta)\right.$$

$$-\left. B_3\, j_3(ka)\,P_3(\cos\theta) + B_5\, j_5(ka)\,P_5(\cos\theta) - \ldots\right]\Bigg\} \qquad (5.149)$$

The ratio of the first term to second term is, in general, much greater than 1 as was shown in Tables 5.1 and 5.2 so the series converges rapidly. To simplify the expression, an initial term is

taken to approximate the infinite series. It will be shown later than the subsequent terms do not contribute significantly toward the exact value of the series.

The simplified form of E_{θ_S} is

$$E_{\theta_S} = \frac{I_m \eta_o e^{-jkR}}{\pi R} \left(\frac{(ka)\, B_1'' \cos\theta \sin\theta}{4}\right)\left(3\, j_1(ka) - \frac{7}{4}(5\cos^2\theta - 1)\, j_3(ka)\right) \tag{5.150}$$

where

$$B_n'' = \frac{2\, B_n}{I_{max}}$$

The numerical calculation of the far-zone fields E_{θ_S} are performed with the above equation (5.150).

5.5.2 Numerical Evaluation of a Radiation Pattern. Since, in Section 5.3, it was shown that the far-zone electric field due to two monopoles separated by $d = 2a + h$, measured between center to center, has an expression as shown in equation (5.69); i.e.,

$$E_{\theta_d} = \frac{j \eta_o I_m e^{-jkR}}{2\pi R} \left(\frac{\cos(kd\cos\theta) - \cos k(d-a)\cos(ka\cos\theta) + \cos\theta \sin k(d-a)\sin(ka\cos\theta)}{\sin\theta}\right) \tag{5.69}$$

The total electric field E_θ at far-zone is

$$E_\theta = E_{\theta_S} + E_{\theta_d} \tag{5.151}$$

This theoretical evaluation of a far-zone electric field due to the monopole above a semi-spherical ground plane on an infinite ground plane was conducted mainly to evaluate the effect of the detailed size of the semi-spherical ground plane, although its radius was much smaller than a wavelength. Here, a majority of experimental studies were performed with models that have the dimensions of a, corresponding to the radius of the sphere, less than or equal to a quarter of a wavelength of interest.

The expression E_θ is in the form of an infinite series where the coefficient B_n and $\overset{s}{j}_n(ka)$ are constants for a given geometrical size of the ground plane and a given frequency. B_n is a complex function of the radius of the sphere and the antenna height in terms of wavelength; i.e., ka and kh.

When the argument of a spherical Bessel function is much smaller than 1, it can be evaluated using the formula

$$\overset{s}{j}_n(z) \approx \frac{z^n}{1 \cdot 3 \cdot 5 \ldots (2n+1)} \quad \text{for } n = 0, 1, 2 \ldots \quad z \ll 1 \qquad (5.152)$$

Although the above formula is for $z \ll 1$, the ratio of these functions between $n = 1$, and $n = 3$ or $n = 5$ are fairly close to the actual ratio of these functions evaluated with exact values of $\overset{s}{j}_n(z)$.

Since the far-zone electric field E_θ due to the spherical surface current is in the form of an infinite series with only odd n's,

the ratio of the successive terms and the nature of its convergence is important to justify taking only the first few terms in the actual evaluation of the field and the radiation resistance.

Ratios of the $j_1(x)$ to $j_3(x)$ and $j_3(x)$ to $j_5(x)$ are evaluated by using the approximate formula (5.152), and by using the exact values for $x = 0.5$, 1. and 1.5. Results are tabulated in Table 5.1.

Because the ground plane sizes used in the study were limited to $ka \leq \frac{\pi}{2}$ which corresponds to the diameter of a semi-spherical ground plane equal to or less than one half of a wavelength, the ratios only of those spherical Bessel functions with an argument less than or equal to $\frac{\pi}{2}$ are of interest to us.

Ratio \ Arguments		x = 0.5	x = 1.0	x = 1.5
$\left(\frac{j_1(x)}{j_3(x)}\right)$	Approx.	144	35.0	15.55
	Exact	138	33.4	14.0
$\left(\frac{j_3(x)}{j_5(x)}\right)$	Approx.	396	99.0	44.0
	Exact	395	97.2	42.4

Table 5.1. Ratios of $j_n(x)$.

Further study is necessary to determine the magnitude of each term of the series. Each term, in addition to $j_n(x)$, contains B_n -- the constants evaluated for each given size of the ground plane radius and the antenna height. Ratios of B_1'' to B_3'' and B_3'' to B_5'' can be obtained from Table 2 for several typical values of ka and kh.

	ka = $\pi/2$, kh = $\pi/2$	ka = $\pi/3$, kh = $\pi/3$	ka = $\pi/6$, kh = $\pi/6$
B_1''	$1.298 - j0.742$	$0.808 - j0.078$	$0.342 - j\,1.30 \times 10^{-3}$
B_3''	$-0.247 + j0.738$	$-0.057 + j0.078$	$0.052 + j\,1.30 \times 10^{-3}$
B_5''	$-0.046 + j\,4.28 \times 10^{-3}$	$0.0287 + j\,9.66 \times 10^{-5}$	$0.031 + j\,1.11 \times 10^{-7}$

Table 5.2. Coefficients B_n''

Finally, the behavior of $P_n(\cos\theta)$ and $P_n^1(\cos\theta)$ are graphically shown in Figs. 5.8 and 5.9 for $0 \leq \theta \leq 90^o$. From Fig. 5.8, the magnitude of $P_n(x)$ is to be always less than or equal to 1, and the ratios of $P_n^1(\cos\theta)$ for $n = 1$ and 3 or $n = 3$ and 5 are always less than 6.

It can be concluded, with the considerations given above, that the ratio of the successive terms of the series between $n = 1$ and $n = 3$ is always less than 0.1. Therefore, it is jusitifed using only the initial term from each infinite series in Eq. (5.149) or (5.153)

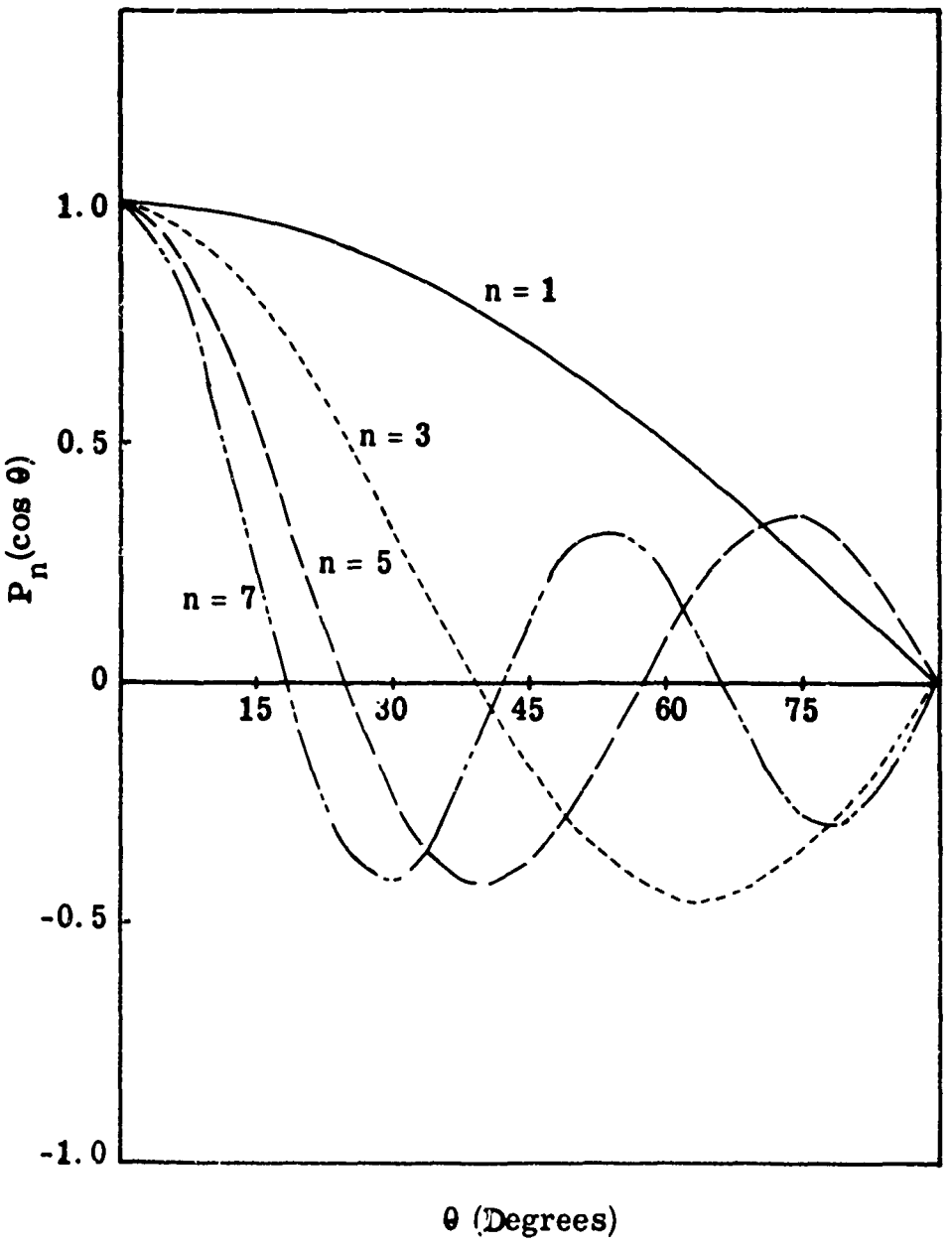

Fig. 5.8. $P_n(\cos\theta)$ versus θ.

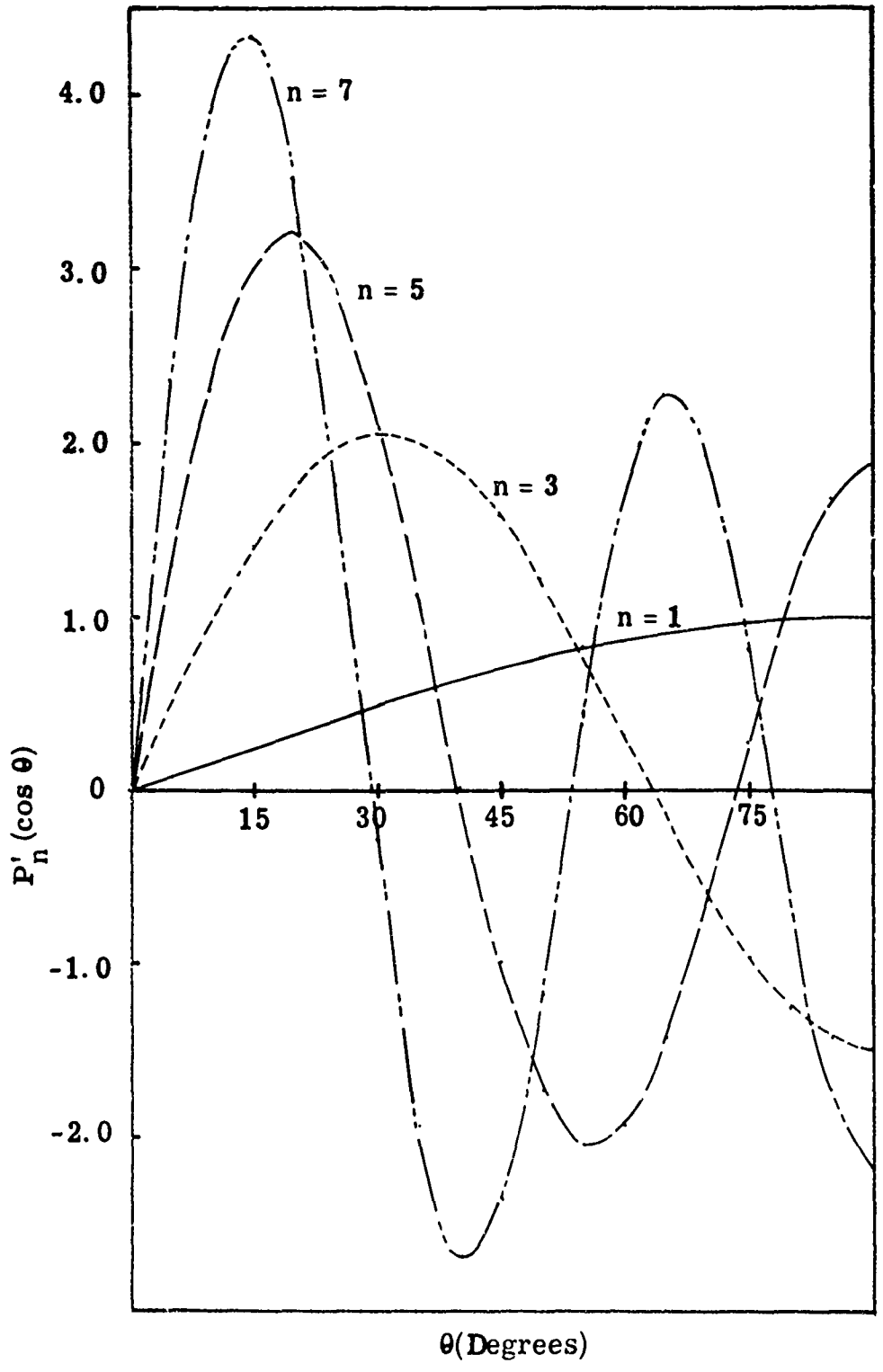

Fig. 5.9. $P_n^1(\cos\theta)$ versus θ.

$$\sum_{\ell=0}^{\infty} j^{2\ell+1} B_{2\ell+1} \frac{\dot{j}_{2\ell+1}(ka)}{\ell+1} P^{1}_{2\ell+1}(\cos\theta)$$

$$\sum_{\ell=0}^{\infty} B_{2\ell+1} \sum_{m=\ell+1}^{\infty} j^{2m+1} \frac{(4m+3)}{(2m+1)(m+1)} \dot{j}_{2m+1}(ka) P^{1}_{2m+1}(\cos\theta) \tag{5.153}$$

$$\sum_{\ell=0}^{\infty} B_{2\ell+1} j^{2\ell+1} \dot{j}_{2\ell+1}(ka) P_{2\ell+1}(\cos\theta)$$

Thus,

$$E_\theta \approx \frac{j\eta_o I_m e^{-jkR}}{2\pi R} \left\{ \left[\frac{\cos(kd\cos\theta) - \cos k(d-a)\cos(ka\cos\theta) + \cos\theta \sin k(d-a)\sin(ka\cos\theta)}{\sin\theta} \right] - j\left[\frac{(ka) B_1'' \cos\theta \sin\theta}{2} \right] \left[3\dot{j}_1(ka) - \frac{7}{4}(5\cos^2\theta - 1)\dot{j}_3(ka) \right] \right\} \tag{5.154}$$

The plot of the magnitude of the term inside the bracket is a function of θ and is a radiation pattern for a particular a and h.

A few of the patterns are calculated and are plotted below in Fig. 5.10 in order to compare with the experimental results.

Figure 5.10 displays a set of theoretical radiation patterns E_θ for a monopole and for its image in the upper hemisphere. This is the plot of Eq. 5.154. Since the radiation patterns are symmetrical along the $\theta = 0^o$ axis, only the right half of the complete radiation

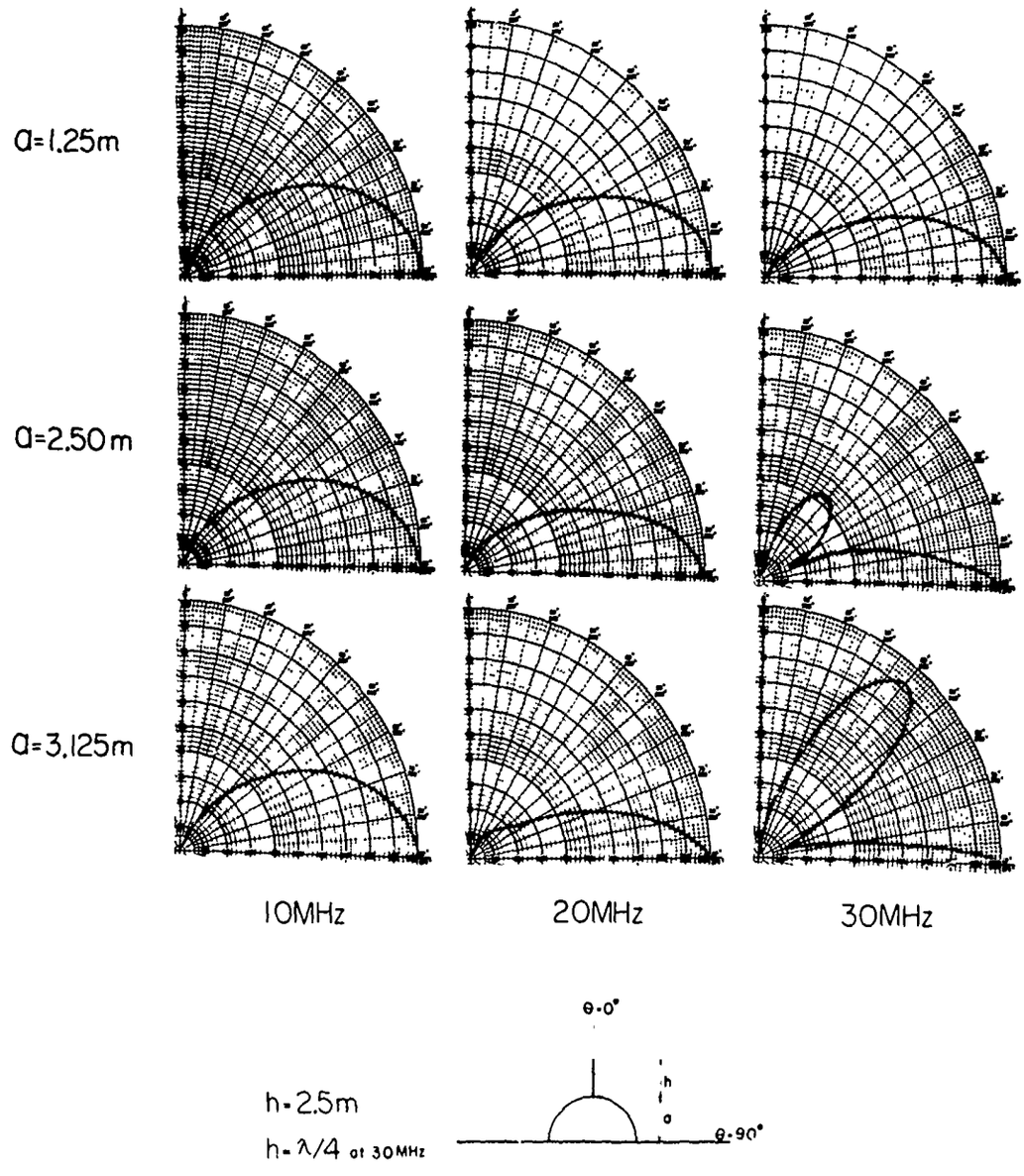

Fig. 5.10. Theoretical radiation patterns $|E_\theta|^2$

pattern on the x - z plane is plotted in the polar coordinates.

A minor lobe off $\theta = 0^{o}$ axis increases with the size of ground diameter. The changes in the ratio of the intensity of the major to minor lobe is shown in this figure.

There are a total of 9 patterns plotted in Fig. 5.10. Each row is a plot with a constant distance of separation, and each column with a constant frequency. The monopole antenna was fixed at a quarter wavelength for the highest frequency in the band. Each pattern contains information on the antenna length and the separation distance between the two antennas.

Comparison between the patterns theoretically obtained for a monopole and its image separated by a diameter of the spherical ground plane, but without the presence of the ground plane, to those with the ground plane shows that adding the ground plane moved the null position between the major and minor lobes toward $\theta = 90^{o}$ axis at higher frequencies. Also at lower frequencies, the beam width was made to become broader by adding the ground plane. Comparing the theoretical results to the experimental results also show that the general behaviours of radiation patterns are similar even though actual amplitude do not seem to match exactly. This can be explained by pointing out the fact that the initial assumptions made concerning the current distributions on the antenna do not quite agree with the actual current distributions. Also a finite ground plane used to simulate an infinite ground in the scale models caused the whole pattern to be shifted toward $\theta = 0^{o}$ axis. These facts are theoretically shown by Leitner and Spence (Ref. 3) in their study on a monopole with a finite ground plane.

5.6 Radiation Resistance

In this section, the radiation resistance is calculated as a function of the antenna length and ground plane diameter. The radiated power is calculated using the far-zone field expression that was obtained through an approximation of the infinite series. The far-zone field E_θ was given in Eq. 5.154.

The convergence of Eq. 5.153 for $ka \leq \pi$, justifies using only the first few terms to obtain E_{θ_s}. The far-zone electric field due to a monopole of length h and a hemispherical ground plane of radius a is

$$E_\theta = \frac{j\eta_o e^{-jkR}}{2\pi R} I_m \left\{ \left\{ \frac{\cos(kd\cos\theta) - \cos k(d-a)\cos(ka\cos\theta)}{\sin\theta} + \cos\theta \sin k(d-a)\sin(ka\cos\theta) \right\} - j \left[\frac{(ka) B_1'' \cos\theta \sin\theta}{2} \right] \left[j_1(ka) - \frac{7}{4}(5\cos^2\theta - 1) j_3(ka) \right] \right\} \quad (5.154)$$

The first and second terms of the equation in the brackets are due to contributions from the currents on the two monopoles and a spherical ground plane, respectively.

Let

$$F_1(\theta) = \frac{\cos(kd\cos\theta) - \cos k(d-a)\cos(ka\cos\theta)}{\sin\theta}$$

$$\frac{+\cos\theta \sin k(d-a)\sin(ka\cos\theta)}{\sin\theta} \qquad (5.71)$$

and

$$F_2(\theta) = \frac{(ka)\cos\theta\sin\theta\left[\, j_1(ka) + \frac{7}{4}(5\cos^2\theta - 1)\, j_3(ka)\right]}{2} \qquad (5.155)$$

Then, the Eq. 5.154 can be written as

$$E_\theta = \frac{j\eta_o e^{-jkR}}{2\pi R} I_m\left[F_1(\theta) + j B_1'' F_2(\theta)\right] \qquad (5.156)$$

Letting $B_1'' = \alpha_1 + j\beta_1$, E_θ can be written as

$$E_\theta = \frac{j\eta_o e^{-jkR}}{2\pi R} I_m\left[F_1(\theta) + (\alpha_1 + j\beta_1) F_2(\theta)\right]$$

$$= \frac{j\eta_o e^{-jkR}}{2\pi R} I_m\left[\left[F_1(\theta) + \beta_1 F_2(\theta)\right] - j\alpha_1 F_2(\theta)\right] \qquad (5.157)$$

The far-zone magnetic field intensity is, from $\bar{H} = \frac{1}{\eta_o}(\hat{R} \times \bar{E})$,

$$H_\phi = \frac{j e^{-jkR}}{2\pi R} I_m\left[\left[F_1(\theta) + \beta_1 F_2(\theta)\right] - j\alpha_1 F_2(\theta)\right] \qquad (5.158)$$

$$\therefore H_{\phi}^{*} = \frac{-j\, e^{jkR}}{2\pi R}\, I_m \left[\left[F_1(\theta) + \beta_1 F_2(\theta) \right] + j\, \alpha_1 F_2(\theta) \right] \qquad (5.159)$$

Radiation resistance R_r is defined as

$$R_r = \frac{1}{I_{rms}^2} \oint R_e \left\{ \frac{1}{2} (\bar{E} \times \bar{H}^*) \cdot d\bar{S} \right\}$$

$$= \frac{1}{2 I_{rms}^2} \oint R_e \left\{ E_\theta H_\phi^* \right\} R^2 \sin\theta \, d\theta \, d$$

$$= \frac{1}{2 I_{rms}^2} \oint \frac{\eta_o I_m^2}{4\pi^2 R^2} \left[\left[F_1(\theta) + \beta_1 F_2(\theta) \right]^2 + \alpha_1^2 F_2^2(\theta) \right] R^2 \sin\theta \, d\theta \, d\phi$$

$$= \frac{\eta_o}{4\pi^2} \oint \left[F_1^2(\theta) + 2\beta_1 F_1(\theta) F_2(\theta) + \beta_1^2 F_2^2(\theta) + \alpha_1^2 F_2^2(\theta) \right]$$

$$\sin\theta \, d\theta \, d\phi$$

$$= \frac{\eta_o}{2\pi} \int_0^{\pi} \left[F_1^2(\theta) + 2\beta_1 F_1(\theta) F_2(\theta) + (\alpha_1^2 + \beta_1^2) F_2^2(\theta) \right] \sin\theta \, d\theta \qquad (5.160)$$

Since $\eta_o = 120\pi$ in free-space,

$$R_r = 60 \int_0^{\pi} \left[F_1^2(\theta) \right] \sin\theta \, d\theta + 120\beta_1 \int_0^{\pi} F_1(\theta) F_2(\theta) \sin\theta \, d\theta$$

$$+ 60(\alpha_1^2 + \beta_1^2) \int_0^{\pi} F_2^2(\theta) \sin\theta \, d\theta \qquad (5.161)$$

Let

$$R_r = R_{r_1} + R_{r_2} + R_{r_3} \tag{5.162}$$

where

$$R_{r_1} = 60 \int_0^{\pi} F_1^2(\theta) \sin\theta \, d\theta$$

$$R_{r_2} = 120 \beta_1 \int_0^{\pi} F_1(\theta) F_2(\theta) \sin\theta \, d\theta \tag{5.163}$$

$$R_{r_3} = 60(\alpha_1^2 + \beta_1^2) \int_0^{\pi} F_2^2(\theta) \sin\theta \, d\theta$$

5.6.1 Evaluation of R_{r_1}. From Eq. $F_1(\theta)$ is given as

$$F_1(\theta) = \frac{\cos(kd\cos\theta) - \cos k(d-a)\cos(ka\cos\theta)}{\sin\theta} + \frac{\cos\theta \sin k(d-a)\sin(ka\cos\theta)}{\sin\theta} \tag{5.71}$$

Therefore,

$$F_1^2 = \left(\frac{1}{\sin^2\theta}\right)\Big[\cos^2(kd\cos\theta) + \cos^2 k(d-a)\cos^2(ka\cos\theta)$$

$$+ \cos^2\theta \sin^2 k(d-a)\sin^2(ka\cos\theta)$$

$$- 2\cos k(d-a)\cos(kd\cos\theta)\cos(ka\cos\theta)$$

$$+ 2\cos\theta \sin k(d-a)\sin(ka\cos\theta)$$

$$- 2\cos\theta \sin k(d-a)\cos k(d-a)\cos(ka\cos\theta)\sin(ka\cos\theta)\Big] \qquad (5.164)$$

$$R_{r_1} = 60 \int_0^{\pi} \left[F_1^2(\theta)\right] \sin\theta \, d\theta$$

Let

$$(1) = \int_0^{\pi} \frac{\cos^2(kd\cos\theta)}{\sin\theta} \, d\theta$$

$$(2) = \cos^2 k(d-a) \int_0^{\pi} \frac{\cos^2(ka\cos\theta)}{\sin\theta} \, d\theta$$

$$(3) = \sin^2 k(d-a) \int_0^{\pi} \frac{\cos^2\theta \sin^2(ka\cos\theta)\, d\theta}{\sin\theta}$$

$$(4) = -2\cos k(d-a) \int_0^{\pi} \frac{\cos(kd\cos\theta)\cos(ka\cos\theta)\, d\theta}{\sin\theta}$$

$$(5) = 2\sin k(d-a) \int_0^{\pi} \frac{\cos\theta \cos(kd\cos\theta)\sin(ka\cos\theta)\, d\theta}{\sin\theta}$$

$$(6) = -2\cos k(d-a)\sin k(d-a) \int_0^{\pi} \frac{\cos\theta \cos(ka\cos\theta)\sin(ka\cos\theta)}{\sin\theta} \, d\theta$$

Let $\mu = \cos\theta$, $d\mu = -\sin\theta\, d\theta$ and $d = a + h$ and solve integrals from ① through ⑥ separately. Then sum of the results will give R_{r_1}. In evaluating each integral, logarithmic singularities appear. These singularities will later cancel. However, in order to show the convergence of the integrals, the limits of the integration have been changed from $\mu = -1$ and $\mu = 1$ to $\mu = -1 + \epsilon$ and $\mu = 1 - \epsilon$ and then ϵ was made vanishingly small.

Then,

$$① = \lim_{\epsilon \to 0} \int_{-1+\epsilon}^{1-\epsilon} \frac{\cos^2 k(a + h)\,\mu}{1 - \mu^2}\, d\mu$$

Since

$$\frac{1}{1 - \mu^2} = \frac{1}{2}\left(\frac{1}{1 + \mu} + \frac{1}{1 - \mu}\right)$$

and

$$\cos^2 k(a + h)\,\mu = \frac{1}{2}\left(1 + \cos 2k(a + h)\,\mu\right)$$

$$① = \frac{1}{4} \lim_{\epsilon \to 0} \int_{-1+\epsilon}^{1-\epsilon} \left[\frac{1}{1 + \mu} \quad \frac{1}{1 - \mu}\right] \left(1 + \cos 2k(a + h)\,\mu\right) d\mu$$

When

$$F(\mu) = F(-\mu)$$

$$\int_a^b \frac{F(\mu)}{1+\mu}\, d\mu = \int_a^b \frac{F(\mu)}{1-\mu}\, d\mu$$

Therefore,

$$\textcircled{1} = \frac{1}{2} \lim_{\epsilon \to 0} \int_{-1+\epsilon}^{1} \frac{1 + \cos 2k(a+h)\mu}{1+\mu}\, d\mu$$

$$= \frac{1}{2} \lim_{\epsilon \to 0} \left[\int_{-1+\epsilon}^{1} \frac{d\mu}{1+\mu} + \int_{-1+\epsilon}^{1} \frac{\cos 2k(a+h)\,\mu}{1+\mu}\, d\mu \right]$$

After the change of variables, $1 + \mu = u$ for the first integral and $1 + \mu = u$ and $2k(a+h)u = v$ for the second integral, $\textcircled{1}$ can be written as

$$\textcircled{1} = \frac{1}{2} \lim_{\epsilon \to 0} \left[\int_{\epsilon}^{2} \frac{du}{u} + \cos 2k(a+h) \int_{2k(a+h)\epsilon}^{4k(a+h)} \frac{\cos v}{v}\, dv \right.$$

$$\left. + \sin 2k(a+h) \int_{2k(a+h)\epsilon}^{4k(a+h)} \frac{\sin v}{v}\, dv \right] = \frac{1}{2} \left\{ \ln 2 - \lim_{\epsilon \to 0} \ln \epsilon + \cos 2k(a+h) \right.$$

$$\left. \left[\mathrm{Ci}\left(4k(a+h)\right) - \lim_{\epsilon \to 0} \mathrm{Ci}\left(2k(a+h)\epsilon\right) \right] + \sin 2k(a+h)\, \mathrm{Si}\left(4k(a+h)\right) \right\}$$

where

$$\mathrm{Si}(x) = \int_0^x \frac{\sin v}{v}\, dv = \text{sine integral}$$

$$\mathrm{Ci}(x) = \int_\infty^x \frac{\cos v}{v}\, dv = \text{cosine integral}$$

In the solution for (1) , singularities associated with logarithm and cosine integral are left as they are and it will be shown later that they cancel.

Using a similar technique, it can be shown that

$$(2) = \cos^2(kh) \lim_{\epsilon \to 0} \int_{-1+\epsilon}^{1-\epsilon} \frac{\cos^2 ka\,\mu}{1-\mu^2}\, d\mu$$

$$= \frac{1}{2}\cos^2(kh) \left\{ \ell n\, 2 - \lim_{\epsilon \to 0} \ell n\, \epsilon + \cos 2ka \left[\mathrm{Ci}(4ka) - \lim_{\epsilon \to 0} \mathrm{Ci}(2ka\,\epsilon) \right] \right.$$

$$\left. + \sin 2ka\, \mathrm{Si}(4ka) \right\}$$

$$\textcircled{3} = (\sin^2 kh) \lim_{\epsilon \to 0} \int_{-1+\epsilon}^{1-\epsilon} \frac{\mu^2 \sin^2(ka\,\mu)\, d\mu}{1-\mu^2}$$

adding and subtracting $\sin^2(ka\,\mu)$ in the numerator.

$$= (\sin^2 kh) \lim_{\epsilon \to 0} \int_{-1+\epsilon}^{1-\epsilon} \frac{\sin^2(ka\,\mu) - (1-\mu^2)\sin^2 ka\,\mu}{1-\mu^2}\, d\mu$$

$$= (\sin^2 kh) \lim_{\epsilon \to 0} \left[\int_{-1+\epsilon}^{1-\epsilon} \frac{\sin^2 ka\,\mu}{1-\mu^2}\, d\mu - \int_{-1+\epsilon}^{1-\epsilon} \sin^2 ka\,\mu\, d\mu \right]$$

The result of the integration is

$$\textcircled{3} = \frac{1}{2}(\sin^2 kh) \left\{ \ell n\, 2 - \lim_{\epsilon \to 0} \ell n\, \epsilon - 2\left(1 - \frac{\sin 2ka}{2ka}\right) \right.$$

$$\left. - \cos 2ka \left[Ci(4ka) - \lim_{\epsilon \to 0} Ci(2ka\,\epsilon) \right] - \sin 2ka\, Si(4ka) \right\}$$

$$\textcircled{4} = -2\cos(kh) \lim_{\epsilon \to 0} \int_{-1+\epsilon}^{1-\epsilon} \frac{\cos k(a+h)\,\mu \cos(ka\,\mu)}{1-\mu^2}\, d\mu$$

using an identity that

$$\cos A \cos B = \frac{1}{2}\left[\cos(A+B) + \cos(A-B)\right]$$

$$(4) = -\cos(kh) \lim_{\epsilon \to 0} \left\{ \int_{-1+\epsilon}^{1} \frac{\cos k(2a+h)\mu}{1+\mu}\, d\mu + \int_{-1+\epsilon}^{1} \frac{\cos kh\, \mu}{1+\mu}\, d\mu \right\}$$

$$= -\cos(kh) \left\{ \cos k(2a+h) \left[Ci\Big(2k(2a+h)\Big) - \lim_{\epsilon \to 0} Ci\Big(k(2a+h)\,\epsilon\Big) \right] \right.$$

$$+ \sin k(2a+h)\, Si\Big(2k(2a+h)\Big) + \cos kh \left[Ci(2\,kh) - \lim_{\epsilon \to 0} Ci(kh\,\epsilon) \right]$$

$$\left. + \sin kh\, Si(2\,kh) \right\}$$

$$(5) = 2 \sin kh \lim_{\epsilon \to 0} \int_{-1+\epsilon}^{1-\epsilon} \frac{\mu \cos k(a+h)\,\mu \sin ka\,\mu\, d\mu}{1-\mu^2}$$

using the identities

$$\frac{\mu}{1-\mu^2} = \frac{1}{2}\left(\frac{1}{1-\mu} - \frac{1}{1+\mu}\right)$$

and $\cos A \sin B = \frac{1}{2}\left[\sin(A+B) - \sin(A-B)\right]$

and also $\int_a^b \frac{F(\mu)}{1-\mu}\, d\mu = -\int_a^b \frac{F(\mu)}{1+\mu}\, d\mu$ when $F(\mu) = -F(-\mu)$

the result of the integral (5) becomes

$$(5) = \sin kh \left\{ \sin k(2a+h) \left[Ci\Big(2k(2a+h)\Big) - \lim_{\epsilon \to 0} Ci\Big(k(2a+h)\,\epsilon\Big) \right] \right.$$

$$- \cos k(2a+h)\, Si\Big(2k(2a+h)\Big) - \sin kh \left[Ci(2kh) - \lim_{\epsilon \to 0} Ci(kh\,\epsilon) \right]$$

$$\left. + \cos kh\, Si(2kh) \right\}$$

Similarly,

$$\textcircled{6} = -2 \cos kh \sin kh \lim_{\epsilon \to 0} \int_{-1+\epsilon}^{1-\epsilon} \frac{\mu \cos ka\,\mu \sin ka\,\mu}{1-\mu^2}\, d\mu$$

$$= \frac{1}{2} \sin 2kh \left\{ \cos 2ka\, Si(4ka) - \sin 2ka \left[Ci(4ka) - \lim_{\epsilon \to 0} Ci(kh\,\epsilon) \right] \right\}$$

Cosine integral Ci(x) can be expanded into a power series such as (Ref. 18, p. 232).

$$Ci(z) = \gamma + \ell n\, Z + \sum^{\infty} \frac{(-1)^n Z^{2n}}{2n(2n)!} \qquad (5.165)$$

If argument of the cosine integral, z, is small

$$\lim_{z \to 0} Ci(z) \approx \gamma + \ell n\, z \qquad (5.166)$$

where

$$\gamma = 0.577 = \text{Euler's constant}$$

Therefore, $\lim_{\epsilon \to 0} Ci(2k\,a\epsilon)$, for instance, can be broken up into two terms; i.e.,

$$\lim_{\epsilon \to 0} Ci(2\,ka\,\epsilon) \approx \gamma + \ell n(2\,ka) + \lim_{\epsilon \to 0} \ell n(\epsilon) \qquad (5.167)$$

Applying the technique shown in Eq.5.166and adding the results (1) through (6), it can be shown (Appendix E) that

$$R_{r_1} = 30 \Bigg\{ 2\gamma + 2\ell n(2\,kh) - 2\,Ci(2\,kh) - 2\sin^2 kh\,(1 - \frac{\sin 2\,ka}{2\,ka}) + \cos 2k(a+h) \Big[Ci(4\,ka) + Ci\Big(4k(a+h)\Big) + 2\,\ell n\,k(2a+h) - \ell n(2\,ka) - \ell n\,2k(a+h) - 2\,Ci\Big[2k(2a+h)\Big]\Big] + \sin 2k(a+h)\Big[Si(4\,ka) + Si\Big(4k\,(a+h)\Big) - 2\,Si\Big(2k(a+h)\Big)\Big]\Bigg\} \qquad (5.168)$$

If we impose a condition that $a = 0$ and $h = m\,\frac{\lambda}{4}$ where m is an odd integer, the result matches with that of Stratton's (Ref. 14, p. 444) where he found a radiation resistance of a linear dipole at resonance.

When $a = 0$ and $h = \frac{\lambda}{4}$, Eq. 5.168 reduces to

$$R_{r_1} = 30\Big[\gamma + \ell n\,2\pi - Ci(2\pi)\Big] \qquad (5.169)$$

which is the exact replica of Stratton's expression

$$R = 30\Big[\ell n\,2\pi\,\gamma^* - Ci\,2m\,\pi\Big] \quad \text{with} \quad m = 1 \qquad (5.170)$$

$$\gamma^* = 1.7811$$

It can further be shown that when $h = 0$, $R_{r_1} = 0$. This, of course, must be true for physical reasons and this gives another confirmation of the correctness of this theoretical result.

5.6.2 Evaluation of R_{r_2}.

From Eq. 5.163,

$$R_{r_2} = 120\beta_1 \int_0^{\pi} F_1(\theta)\, F_2(\theta) \sin\theta\, d\theta$$

$$= 120\beta_1 \int_0^{\pi} \left[\frac{\cos(kd\cos\theta) - \cos k(d-a)\cos(ka\cos\theta)}{\sin\theta} \right.$$

$$\left. + \frac{\cos\theta \sin k(d-a)\sin(ka\cos\theta)}{\sin\theta} \right]$$

$$\left[\frac{ka\cos\theta\sin\theta \left\{ 3 j_1(ka) - \frac{7}{4}(5\cos^2\theta - 1)\, j_3(ka) \right\}}{2} \right] \sin\theta\, d\theta \qquad (5.171)$$

Let

$$G(ka) = \frac{ka}{2}\left[j_1(ka) - \frac{7}{4} j_3(ka) \right] \qquad (5.172)$$

$$H(ka) = \left(\frac{ka}{2}\right)\left(\frac{35}{4} j_3(ka)\right) = \frac{35}{16}(ka)\, j_3(ka)$$

Then

$$F_2(\theta) = G(ka)\sin\theta\cos\theta + H(ka)\sin\theta\cos^3\theta$$

R_{r_2} can now be expressed as

$$R_{r_2} = 120\,\beta_1 \int_{-1}^{1} \Big[\cos kd\,x - \cos k(d-a)\cos ka\,x + x \sin k(d-a)\sin(ka\,x) \Big]$$

$$\Big[G(ka)\,x + H(ka)\,x^3 \Big]\, dx$$

Every term in the above integral is an odd function of x with respect to $x = 0$. Therefore, the result of integration becomes zero.

Therefore

$$R_{r_2} \equiv 0 \tag{5.174}$$

5.6.3 Evaluation of R_{r_3}.

$$R_{r_3} = 60(\alpha_1^2 + \beta_1^2) \int_0^{\pi} F_2^2(\theta) \sin\theta\, d\theta$$

$$= 60(\alpha_1^2 + \beta_1^2) \int_0^{\pi} \Big[G(ka) \sin\theta\cos\theta + H(ka) \sin\theta \cos^3\theta \Big]^2 \sin\theta\, d\theta$$

$$= 60(\alpha_1^2 + \beta_1^2) \int_0^{\pi} \Big[G^2(ka) \sin^2\theta \cos^2\theta + 2G(ka)\,H(ka) \sin^2\theta \cos^4\theta$$

$$+ H^2(ka) \sin^2\theta \cos^6\theta \Big] \sin\theta\, d\theta \tag{5.175}$$

Letting

$$\cos\theta = x \qquad -\sin\theta\, d\theta = dx$$

$$\sin^2\theta = 1 - x^2$$

$$R_{r_3} = 60(\alpha_1^2 + \beta_1^2) \int_{-1}^{1} \Big[G^2(ka)(1 - x^2)\, x^2 + 2G(ka)\, H(ka)(1 - x^2)\, x^4 + H^2(ka)(1 - x^2)\, x^6 \Big] dx$$

$$= 60(\alpha_1^2 + \beta_1^2) \int_{-1}^{1} \Big| G^2(ka)\, x^2 + \Big[2G(ka)\, H(ka) - G^2(ka) \Big] x^4 + \Big[H^2(ka) - 2G(ka)\, H(ka) \Big] x^6 - H^2(ka)\, x^8 \Big| dx$$

$$= 60(\alpha_1^2 + \beta_1^2) \Big| G^2(ka)\, (\tfrac{2}{3}) + \Big[2G(ka)\, H(ka) - G^2(ka) \Big]\, (\tfrac{2}{5}) + \Big[H^2(ka) - 2G(ka)\, H(ka) \Big] (\tfrac{2}{7}) - H^2(ka)\, (\tfrac{2}{9}) \Big|$$

$$= 60(\alpha_1^2 + \beta_1^2) \left| \frac{4}{15}\, G^2(ka) + \frac{8}{35}\, G(ka)\, H(ka) + \frac{4}{63}\, H^2(ka) \right|$$

$$= 240(\alpha_1^2 + \beta_1^2) \left| \frac{G^2(ka)}{15} + \frac{2G(ka)\, H(ka)}{35} + \frac{H^2(ka)}{63} \right| \qquad (5.176)$$

Finally, the total radiation resistance of the system with a monopole and a hemispherical ground plane is obtained by summing R_{r_1}, R_{r_2} and R_{r_3}. However, this sum represents a radiation resistance of the actual antenna system and its image. Because only a half of the power evaluated previously is actually radiated, monopole and hemispherical ground plane radiating into a half space, the final radiation resistance is

$$\text{Rad. Resistance} = \frac{1}{2}(R_{r_1} + R_{r_2} + R_{r_3})$$

$$= 15 \left\{ 2\gamma + 2\,\ell n(2\,kh) - 2\,Ci(2kh) - 2\sin^2 kh \left(1 - \frac{\sin 2\,ka}{2\,ka}\right) \right.$$

$$+ \cos 2k(a+h) \left[Ci(4\,ka) + Ci\Big(4k(a+h)\Big) + 2\,\ell n\, k(2a+h) \right.$$

$$\left. - \ell n(2\,ka) - \ell n\, 2k(a+h) - 2\,Ci\left[2k(2a+h)\right] \right]$$

$$\left. + \sin 2k(a+h) \left[Si(4\,ka) + Si\Big(4k(a+h)\Big) - 2\,Si\Big(2k(a+h)\Big) \right] \right\}$$

$$+ 120(\alpha_1^2 + \beta_1^2) \left\{ \frac{G^2(ka)}{15} + \frac{2G(ka)\,H(ka)}{35} + \frac{H^2(ka)}{63} \right\} \qquad (5.177)$$

From Eq. 5.177, radiation resistances of several different combinations of ka and kh are numerically calculated and tabulated.

The result of numerical evaluation of Eq. 5.177 is given in a graphical form in Fig. 5.11, where radiation resistance is plotted as a function of frequency. Each curve represents a different size of semi-spherical ground plane. When the radius of a ground plane is zero, the resulting radiation resistance corresponds to that of a monopole on an infinite ground plane.

Results shown in Fig. 5.11 indicates that there exists definitely a peaking effect on the radiation resistance as the radius of the ground plane is changed. Comparing with the monopole resonating at 30 MHz over an infinite ground plane the radiation resistance becomes larger with a semi-spherical ground plane well below the resonant frequency. The peaking seems to occur at $ka = 1$ and this conclusion has been drawn mainly from the results of numerical calculations.

Fig. 5.12 and 5.13 compare these theoretical results with experimentally obtained input resistances. Of course, we are not comparing the same resistances, namely the radiation resistances. However, assuming that the loss is small, the input resistance should be similar to the radiation resistances. Some of the discrepancies shown in this comparison can also be explained with the discrepancies in the assumed current and the actual current on the antenna. However, the peaking effect is shown to exist using a small semi-spherical ground plane with a monopole.

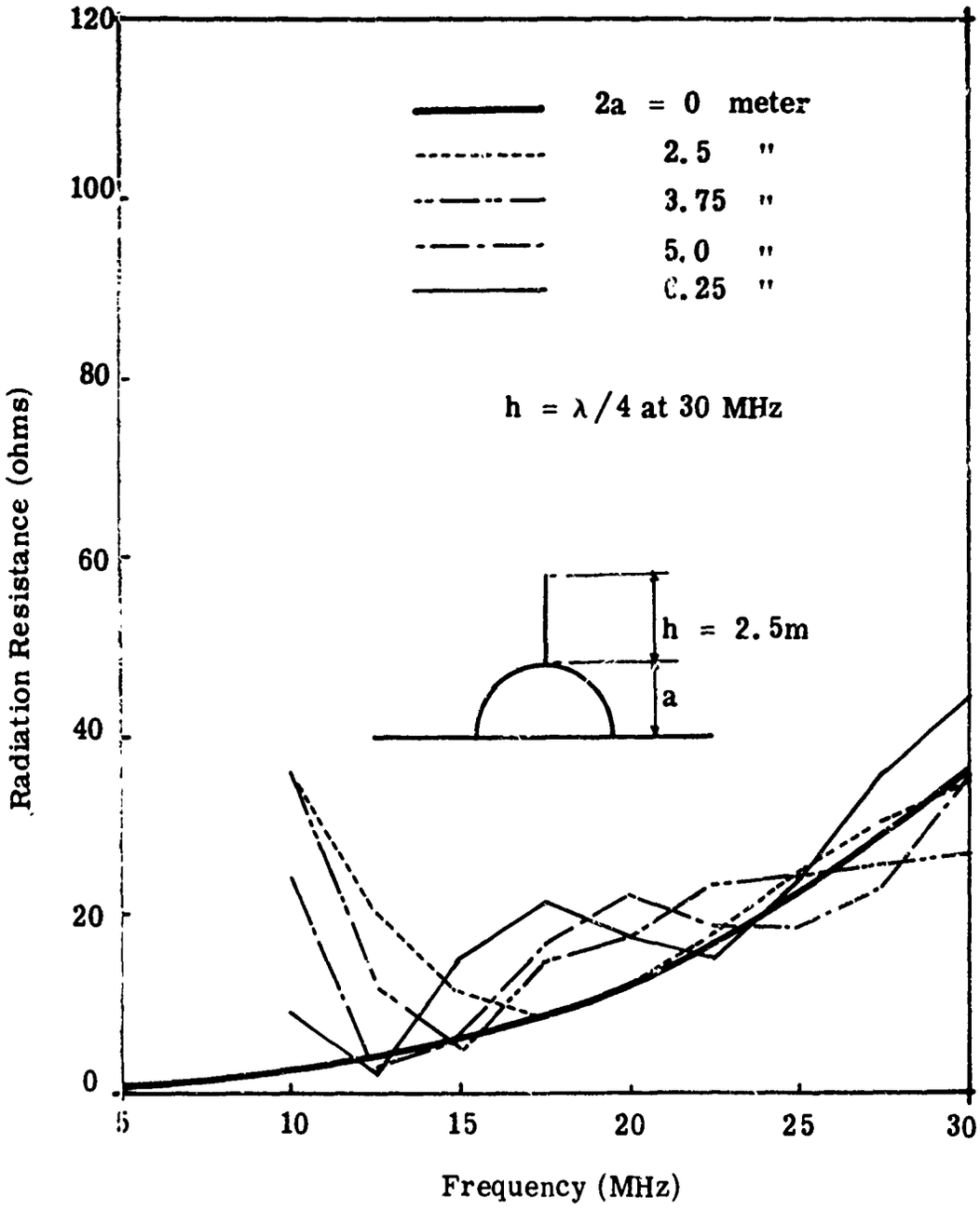

Fig. 5.11. Theoretical radiation resistances for various values of ground plane size

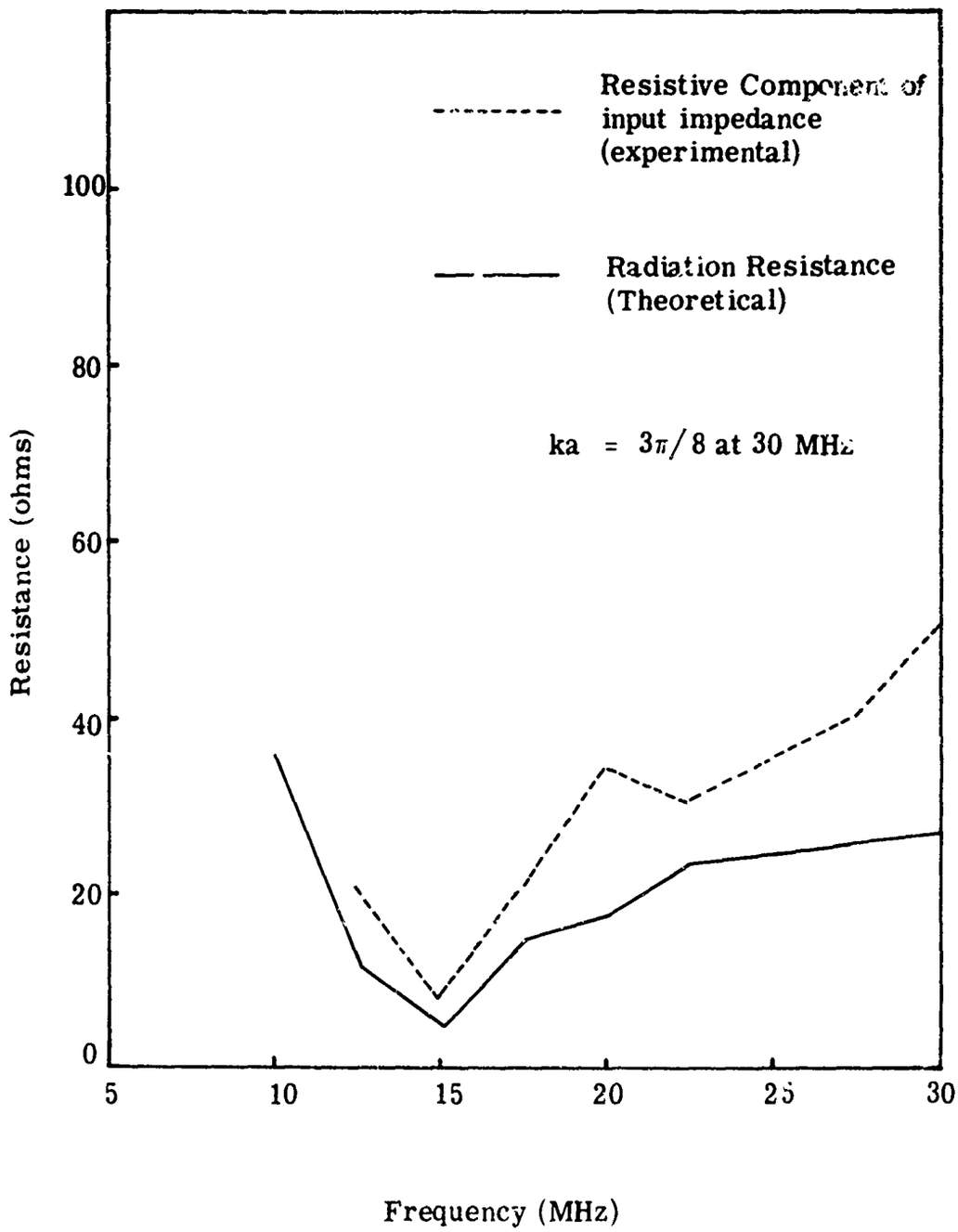

Fig. 5.12. Theoretical radiation resistance and experimental input resistance for a monopole with a hemispherical ground plane

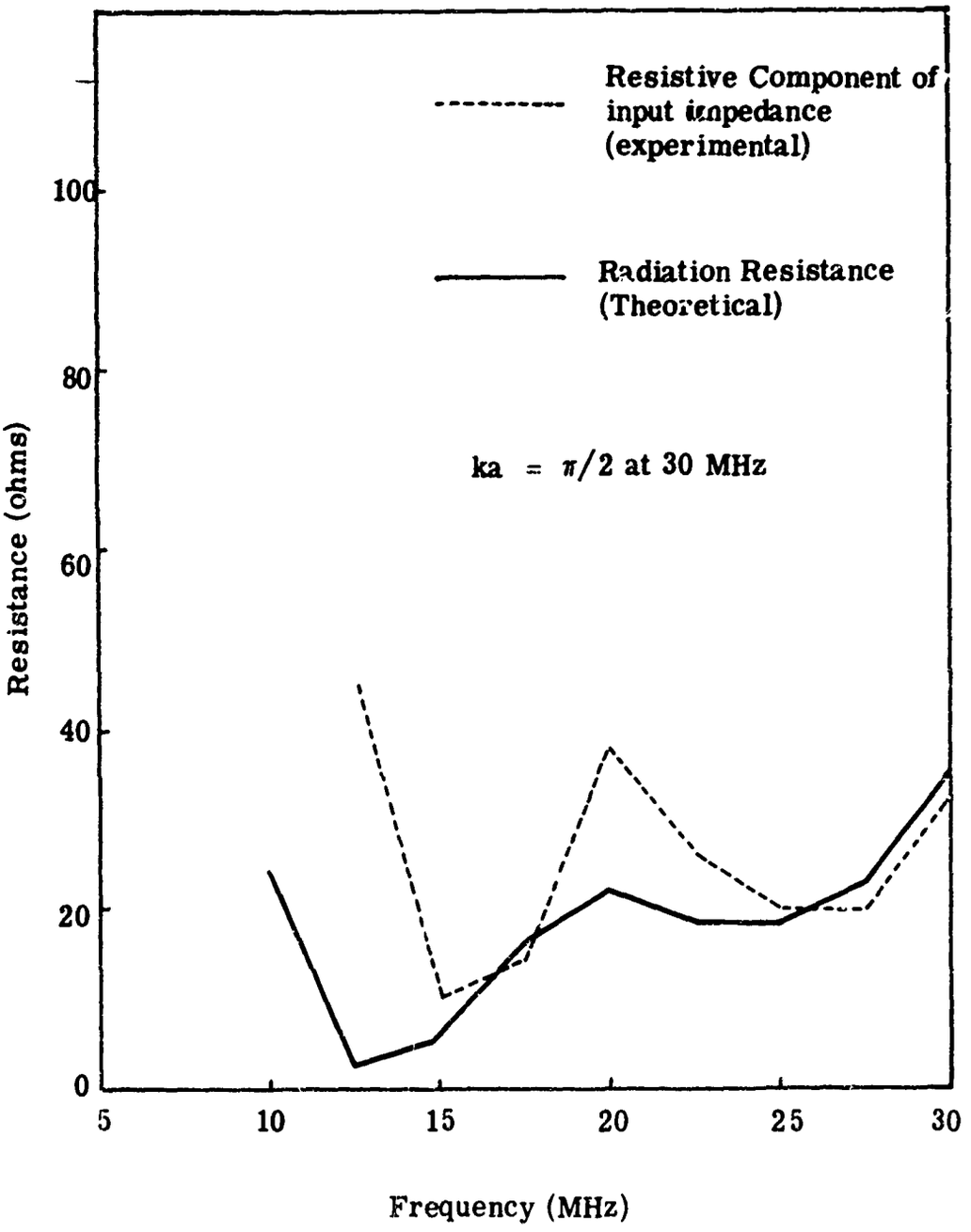

Fig. 5.13. Theoretical radiation resistance and experimental input resistance for a monopole with a hemispherical ground plane

Since radiation resistance is defined as the ratio of radiated power to a square of the input current at the terminal where it is measured, the current must be that current at the terminal and resulting radiation resistance will be the radiation resistance at that point.

At the beginning of the theoretical analysis for this problem, it was assumed that the current distribution on the antenna itself is in the sinusoidal form.

From Eq. 5. 59 , the current on the antenna is given as

$$I(z) = I_{max} \sin k(d - z)$$

where at $z = a$, $\sin k(d - z) = 1$ at 30 MHz.

Therefore, the input currents at the base of the antenna ($z = a$) would be different from I_{max} for frequencies lower than 30 MHz. We must use these currents to evaluate the radiation resistance at the input terminal for each frequency.

It seems as though one can have a radiation resistance as large as desired by making the feedpoint located at a point where current is approximately zero. One example would be a full wave dipole which has a zero input current at the center of the dipole. Theoretically, then, it has an infinitely large radiation resistance. However, in practice an actual antenna is not infinitesimally thin, which was the assumption used for deriving a theoretical result, and the current at a minimum point is not zero. Nevertheless, the radiation resistance

at a current minimum may in practice be very large, possibly thousands of ohms.

In view of the above argument, the radiation resistance cannot be used as a sole measure of an antenna performance. The reactive component of an input impedance is another factor which should be considered. When an input current is fixed at a certain value, both the resistive and reactive components of the input impedance determine the voltage required to maintain the current. Therefore, it is necessary to consider a ratio of reactive component and resistive components, or the Q of the antenna in order to decide whether increases in radiation resistance actually increase the antenna efficiency. Input current and voltage determines the input power and radiation resistance determines the radiated power. The ratio of these quantities determines the efficiency of the antenna.

In addition to the efficiency considerations, the Q of the antenna system determines broadband tuning possibilities of the antenna. When the antenna is electrically short, in particular, the reactive component is usually very large and the resistive component is very small giving very high Q values. When the reactive component is large, a wideband tuning becomes very difficult, because one has to find a way for a wide range variation in the conjugate reactive component to cancel out the large radiative reactances. Also, a small value of resistive component will cause a difficulty in transforming up to a characteristic impedance of transmission lines normally available.

The ratio of a capacitive reactance to a resistance of the antenna is defined as Q, for a monopole above an infinite ground plane, Q of the antenna increases rapidly as frequencies go down below resonance. Typically, for a monopole one quarter wavelength long at 30 MHz, with the antenna or diameter ratio of approximately 400, Q at 5MHz becomes 1400 and gradually reduces to 0 at 30MHz. The resistive component increases from 2 ohms at 5 MHz to 36 ohms at 30Mhz. However, from the experimentally obtained data, Q of a monopole one quarter wavelength long at 30 MHz placed above a finite circular disc ground plane of 2.5 meters in diameter which is placed 1.25 meters above an infinite natural ground is shown to vary between 43 to 0. It is mainly due to smaller reactive components and large resistive components over the frequency range of SMHz through 30MHz for a monopole over a finite ground plane.

The resistive component of the input impedance contains loss due to several sources in addition to radiation resistance. In order to make an educated judgment on the variation of the resistive component as a function of frequency whether it can be attributed to an increase in radiation resistance or not, a theoretical result of a radiation resistance for a mon pole over semi-spherical ground planes has been obtained. Using these theoretical results of radiation, resistance and the experimentally obtained reactive components, Q of the antenna has been obtained between 5MHz and 30MHz. It shows

that the Q of the antenna varies between 25 to 1 with X_c at 10MHz of 850 ohms compared with 900 ohms for a monopole above an infinite ground plane.

A conclusion can be drawn from the above studies that by using a monopole with a finite ground plane above an infinitely large ground plane , a significant advantage can be realized in radiation resistance as well as a broad band matching at the input terminals. Through this study, a qualitative conclusion of an antenna behavior with two ground planes has been possible. However, an exact behavior of a monopole with a disc ground plane above an infinite ground can only be predicted with a new mathematical model.

CHAPTER VI

CONCLUSIONS AND RECOMMENDATIONS

6.1 Conclusion

One of the major objectives of this study was to determine how a finite ground plane used in addition to an infinite lossly ground affects performance of a monopole antenna. Attention was mainly directed toward the effect of ground planes equal to, or smaller than, a half wavelength in diameter. If there is to be any advantage in using these finite ground planes, they cannot be physically bulky. At frequencies 5MHz to 30 MHz, where the study was performed, a half wavelength at the upper end of the frequency band is equal to 5 meters.

In studying this antenna system, the length of monopole was fixed at 2.5 meters, which is a quarter wavelength at 30 MHz. Impedance measurements show that the real part is a strong function of both the ground plane diameter and its location. Also it shows a peaking effect at particular frequencies, which depends upon the diameter of the ground plane and its location above the infinite ground.

Using a theoretical model with hemispherical ground planes substituted for flat discs, it was established that the sharp increase in resistive component was largely due to an increase in radiation resistance. From the theory, it seems that at least one peak exists at frequencies where $ka \sim 1$. It was not possible to draw a clear conclusion of this nature for an antenna with a finite disc ground

plane. When $ka \approx 1$, the distance from the base of the antenna to an infinite ground along the path of the spherical surface is a quarter wavelength. This provides a voltage maximum or current minimum point at the base of the antenna, regarding the infinite ground plane as a zero potential surface. Therefore, a larger input impedance or larger resistive component is realized at $ka = 1$. However, based on the experimental results, a general conclusion that a peaking effect occurs at frequencies approximately determined by $k\left(\frac{D}{2} + a\right) \approx C$ where C is a function of the ratio $\frac{D}{2}$:a. It can also be concluded that the Q of the antenna is generally much lower than that of the same antenna over an infinite ground plane, providing some advantage in designing a tuning network at frequencies well below resonance.

Curves showing the input reactance with a finite disc-ground plane of various sizes exhibit a region where the reactance variation as a function of frequency is remarkably small. This phenomenon is usually associated with a resistive maximum. Clearly, this type of frequency response is very much better, from the point of view of broad-band operation, than the response of either a half-wave or a full-wave dipole. With an appropriately designed reactive matching network the standing wave ratio on a line terminated in the antenna with a finite ground plane over an infinite ground can be minimized over a wide frequency range.

Because of the assumption made in the theoretical studies that the current distribution on the monopole is in sinusoidal form

and independent of the surface current on the ground plane, actual current measurements were performed using scale models. Current distribution at the higher end of the frequency band approximated closely the initial assumption of a sinusoidal distribution. However, as frequency is decreased, particularly for the monopole with a hemispherical ground, the actual current deviates appreciably from the original assumption. At the lower end of the frequency band, the current measurement shows almost a constant amplitude similar to Hertzian dipole.

The theoretical results obtained here for the radiation resistance assumed that the current distribution had a triangular form at low frequencies. These results would be improved by assumption, in the theory, of a current distribution more closely approximating that observed experimentally. This effect is much more noticeable at the lower end of frequency band. Experimentally measured input resistances confirm these facts. In Chapter 5, a comparison is made between the theoretical and experimental radiation and input resistances. The experimental values are always larger than the theoretical values.

From the results of a theoretical study using a hemispherical ground plane and the experimental results obtained for a monopole with a finite disc ground plane above an infinite natural ground, it can be concluded that a marked increase in radiation resistance results with a finite disc ground plane, below the resonant

frequency.

The major effect of the finite ground plane upon the antenna radiation pattern is an emergence of side lobes when the ground plane diameter becomes appreciable compared with a wavelength. In general, the appearance of a side lobe is not desirable, because the power radiated is actually deviated from the main lobe where it should be concentrated. Also the beam width measured between 3db points from the position of the maximum amplitude is generally broader than that of an antenna on an infinite ground plane. Theoretically, it has been found that a spherical surface current makes only a very slight contribution to the far-zone electromagnetic field.

In summarizing the results of this study, it is concluded that definitely improved performance can be obtained with an electrically-short monopole antenna by operating it with a physically small finite ground plane above natural ground. This improvement occurs in the radiation resistance and with respect to matching network design for a broad-band operation. These results have bearing on the design of short monopole antennas for operation of ground-based vehicles, in which case the antenna may be considered to be mounted on a small ground plane above natural ground.

6.2 Recommendation for Future Work

First, in the analysis of this problem, the infinite ground below the finite hemispherical ground was assumed to be perfectly

conducting, permitting use of a conventional image technique for solving the problem. The loss due to the finite conductivity of the natural ground has also been neglected. However, in order to isolate an exact radiation resistance from the measured impedance shown in Chapter 2, it is necessary to take the loss due to the natural ground into account.

Also, a new theoretical model consisting of an antenna on a small ground plane above a larger ground plane, could possibly give more accurate results than have been obtained here through assumption of a hemispherical ground plane.

Second, since the current distribution measured shows deviation from the original sinusoidal form, the measured current may be taken as a given current distribution and may be decomposed into Fourier Series to add an effect of each term. In this way, the experimental result may be made to match better against theoretical results.

Third, because the ultimate application of this analysis is for a vehicular mounted antenna where a body of a vehicle can be taken as an equivalent ground plane of a finite diameter, it is necessary to study further to determine how a particular size of a vehicular body and shape and location of the antenna correspond with an antenna on a finite disc or semispherical ground plane above an infinite natural gound.

Finally, a detailed study of the measured input impedance

given in Chapter 2 and deriving equivalent circuits for each case may be useful for design of tuning networks for vehicular mounted antennas.

APPENDIX A

RECIPROCITY THEOREM

Let a source or a distribution of sources maintain a current density $\bar{J}_1$ with associated electromagnetic fields $\bar{E}_1$ and $\bar{H}_1$. A second source maintains a current density $\bar{J}_2$ with associated fields $\bar{E}_2$ and $\bar{H}_2$. Then, according to Lorentz's reciprocal theorem:

$$\nabla \cdot (\bar{E}_1 \times \bar{H}_2) - \nabla \cdot (\bar{E}_2 \times \bar{H}_1) = \bar{J}_1 \cdot \bar{E}_2 - \bar{J}_2 \cdot \bar{E}_1 \qquad \text{(A. 1)}$$

Let's assume that the two sets of fields are defined in free space and are bounded by the same geometrical surfaces. Applying volume integration on both sides of Eq. A. 1 with dV as volume element, the integration performed over a volume V in empty space that is bounded by a closed surface S can be written as

$$\iiint_V \nabla \cdot (\bar{E}_1 \times \bar{H}_2)\, dV = \iiint_V \nabla \cdot (\bar{E}_2 \times \bar{H}_1)\, dV \qquad \text{(A. 2)}$$

where

$$\iiint (\bar{J}_1 \cdot \bar{E}_2 - \bar{J}_2 \cdot \bar{E}_1)\, dV = 0 \qquad \text{(A. 3)}$$

because all volume densities of current vanish in empty space.

From the divergence theorem

$$\iiint_V \nabla \cdot (\bar{E}_1 \times \bar{H}_2) - (\bar{E}_2 \times \bar{H}_1) \, dV = \oiint_S (\bar{E}_1 \times \bar{H}_2 - \bar{E}_2 \times \bar{H}_1) \cdot dS = 0 \tag{A.4}$$

Where $d\bar{S} = \hat{n}\, dS$ and $\hat{n}$ is an external unit normal vector of the surface toward volume V. The only restrictions of the two sets of fields $(\bar{E}_1, \bar{H}_1)$ and $(\bar{E}_2, \bar{H}_2)$ are that they satisfy Maxwell's equations, the volume integration is performed in empty space V and the boundary surfaces are in the same geometrical shape for both sets, but not necessarily the same physical properties.

APPENDIX B

PROOF AND DERIVATION OF EQ. 5.56

Equation 20 was written as

$$\overline{E}(x.\ y,\ z) = -\frac{1}{4\pi}\int\int_S [j\omega\mu(n \times \overline{H})\,\phi + (n \times \overline{E}) \times \nabla'\,\phi + (n \cdot \overline{E})\,\nabla'\,\phi]\,dS' \tag{5.50}$$

At far-zone,

$$r = \sqrt{(x - x')^2 + (y - y')^2 + (z - z')^2} = |\overline{R} - \overline{R}'| \tag{5.39}$$

can be simplified as

$$r \cong R - \frac{\overline{R} \cdot \overline{R}'}{R} = R - \hat{R} \cdot \overline{R}'$$

Therefore,

$$\phi \cong \frac{e^{jkR - jk\hat{R} \cdot \overline{R}'}}{R} \tag{5.55}$$

when

$$|R| >> |R'|$$

Then

$$\nabla'\phi \triangleq \frac{e^{ikR}}{R} \nabla' e^{-jk\hat{R}\cdot\bar{R}'} = -jk \frac{e^{ikR}}{R} e^{-jk\hat{R}\cdot\bar{R}'} \hat{R} \tag{5.47}$$

where the prime notation on operator ∇ indicates that ∇ is operated on the primed coordinate system.

In Eq. 5.50, the radial component of $\bar{E}$ (x, y, z) can be written as

$$E_R(x, y, z) = -\frac{1}{4\pi} \iint_S \hat{R} \cdot \left\{ j\omega\mu(\hat{n} \times \bar{H}) - jk(\hat{n} \cdot \bar{E})\hat{R} \right\} \frac{e^{jkR - jk\hat{R}\cdot\bar{R}'}}{R} dS' \tag{B.1}$$

Consider the following integral

$$\oint_S \nabla' \times \left(\bar{H} e^{-jk\hat{R}\cdot\bar{R}'} \right) \cdot d\bar{S}' = 0 \tag{B.2}$$

Where S is a closed surface bounding a volume V.

Since

$$\nabla \times (\phi \bar{a}) = \nabla\phi \times \bar{a} + \phi \nabla \times \bar{a}$$

$$\nabla' \times \left(\bar{H} e^{-jk\hat{R}\cdot\bar{R}'} \right) = \nabla' \left(e^{-jk\hat{R}\cdot\bar{R}'} \right) \times \bar{H} + e^{-jk\hat{R}\cdot\bar{R}'} \nabla' \times \bar{H} \tag{B.3}$$

Therefore, Eq. B.2 becomes

$$\iint_S \left[\hat{n} \cdot (\nabla' \times \bar{H}) e^{-jk\hat{R} \cdot \bar{R}'} + \hat{n} \cdot (\nabla' e^{-jk\hat{R} \cdot \bar{R}'} \times \bar{H})\right] dS = 0 \tag{B.4}$$

where

$$d\bar{S} = \hat{n}\, dS$$

Knowing

$$\nabla' e^{-jk\hat{R} \cdot \bar{R}'} = -jk\, e^{-jk\hat{R} \cdot \bar{R}'}\, \hat{R}$$

and

$$\hat{n} \cdot (\hat{R} \times \bar{H}) = -\hat{R} \cdot (\hat{n} \times \bar{H})$$

Equation B.4 can be written as

$$\iint \left[\hat{n} \cdot (\nabla' \times \bar{H})\, e^{-jk\hat{R} \cdot \bar{R}'} + \hat{R} \cdot (\hat{n} \times \bar{H})\, jk\, e^{-jk\hat{R} \cdot \bar{R}'}\right] dS' = 0 \tag{B.5}$$

Also, from Maxwell's equation

$$\nabla' \times \bar{H} = -j\omega\epsilon_0 \bar{E}$$

in a source free region.

Thus,

$$\oint \left[(\hat{n} \cdot \bar{E}) (-j\omega\epsilon_0) e^{-jk\hat{R} \cdot \bar{R}'} + \hat{R} \cdot (\hat{n} \times \bar{H}) jk e^{-jk\hat{R} \cdot \bar{R}'} \right] dS'$$

$$\sqrt{\frac{\epsilon_0}{\mu_0}} \oint \left[j\omega\mu_0 \hat{R} \cdot (\hat{n} \times \bar{H}) - jk (\hat{n} \cdot \bar{E}) \right] e^{-jk\hat{R} \cdot \bar{R}'} dS' = 0$$

It is, therefore, true that

$$\oint \left[j\omega\mu_0 \hat{R} \cdot (\hat{n} \times \bar{H}) - jk(\hat{n} \cdot \bar{E}) \right] e^{-jk\hat{R} \cdot \bar{R}'} dS' = 0 \quad (B.6)$$

From Eq. B.1 and B.6, the radial component of $\bar{E}(x, y, z')$ is proved to be zero at far-zone.

At far-zone, consequently,

$$\bar{E}(x, y, z) = -\frac{1}{4\pi} \iint_S \left[j\omega\mu (\hat{n} \times \bar{H}) \phi \right]_t dS' \qquad (5.56)$$

APPENDIX C

PROOF OF EQ. 5.92

The purpose of this appendix is to show the steps involved in arriving at Eq. 5.92 from Eqs. 5.90 and 5.91. The same steps were also taken to get the expression (Eq. 5.106).

From Eq. 5.90 and Eq. 5.91,

$$E_{2R} = U(k^2 + \frac{\partial^2}{\partial R^2}) \left[\frac{a P_{n-1}(\cos\theta)\rho_{n-1}(kR)}{(2n+1)\cdot k\cdot \rho_{n-1}'(ka)} - \frac{a P_{n+1}(\cos\theta)\rho_{n+1}(kR)}{(2n+1)\cdot k\cdot \rho_{n+1}'(ka)} \right] \tag{5.90}$$

$$I_{1A}(R) = I_{max} \sin k(d - R) \tag{5.91}$$

where

$$d = a + h$$

Therefore,

$$\int_{R=a}^{d} E_{2R} I_{1A}(R)\, dR = \frac{U a I_{max}}{(2n+1)\cdot k\cdot \rho_{n-1}'(ka)} \int_{a}^{d} \sin k(d - R)(k^2 + \frac{\partial^2}{\partial R^2})\rho_{n-1}(kR)dR$$

$$- \frac{U a I_{max}}{(2n+1)\cdot k\cdot \rho_{n+1}'(ka)} \int_{a}^{d} \sin k(d-R)(k^2 + \frac{\partial^2}{\partial R^2})\rho_{n+1}(kR)dR \tag{C.1}$$

Let

$$I_1 = \int_a^d \sin k(d-R)\left(k^2 + \frac{\partial^2}{\partial R^2}\right) \rho_{n-1}(kR)\, dR$$

$$I_2 = \int_a^b \sin k(d-R)\left(k^2 + \frac{\partial^2}{\partial R^2}\right) \rho_{n+1}(kR)\, dR \qquad (C.2)$$

Changing a variable kR to z,

$$kR = z \qquad \therefore \; kdR = dz$$

$$\frac{\partial^2}{\partial R^2} = k^2 \frac{\partial^2}{\partial z^2}$$

The integral I_1 becomes

$$I_1 = \int_{ka}^{kd} \sin k(d-z)\left(k^2 + k^2 \frac{\partial^2}{\partial z^2}\right) \rho_{n-1}(z)\, \frac{dz}{k}$$

$$= k \int_{ka}^{kd} \sin k(d-z)\, \rho_{n-1}(z)\, dz + k \int_{ka}^{kd} \sin k(d-z) \frac{\partial^2}{\partial z^2} \rho_{n-1}(z)\, dz \qquad (C.3)$$

Let

$$I_{11} = k \int_{ka}^{kd} \sin k(d-z)\, \rho_{n-1}(z)\, dz \qquad (C.4)$$

and

$$I_{12} = k \int_{ka}^{kd} \sin k(d - z) \frac{\partial^2}{\partial z^2} \rho_{n-1}(z)\, dz \qquad (C.5)$$

Then

$$I_{11} = k \int_{ka}^{kd} \sin k(d - z)\, \rho_{n-1}(z)\, dz\,.$$

Let

$$\rho_{n-1}(z) = u \qquad \sin k(d - z)\, dz = dv$$

$$\frac{\partial}{\partial z} \rho_{n-1}(z) = du \qquad \cos k(d - z) = v$$

By part integration

$$I_{11} = k \left[\cos k(d - z)\, \rho_{n-1}(z) - \int \cos k(d - z) \frac{\partial \rho_{n-1}(z)}{\partial z} dz \right]_{z = ka}^{kd}$$

Integrating the second term of I_{11} by part again, we get

$$\int_{ka}^{kd} \cos k(a - z) \frac{\partial \rho_{n-1}(z)}{\partial z} dz$$

$$= \left[-\sin k(d - z) \frac{\partial \rho_{n-1}(z)}{\partial z} + \int \sin k(d - z) \frac{\partial^2 \rho_{n-1}(ka)}{\partial z^2} dz \right]_{z=ka}^{kd}$$

The second integral of the above equation is exactly the same as I_{12}.

Rewriting I_{11} we obtain

$$I_{11} = k \left[\cos k(d - z) \rho_{n-1}(z) + \sin k(d - z) \rho_{n-1}'(z) \right]_{z=ka}^{kd} - I_{12} \tag{C.6}$$

$$I_1 = I_{11} + I_{12} = k \left[\rho_{n-1}(kd) - \cos k(d - a) \rho_{n-1}(ka) - \sin k(d - a) \rho_{n-1}'(ka) \right] \tag{C.7}$$

and

$$I_2 = k \left[\rho_{n+1}(kd) - \cos k(d - a) \rho_{n+1}(ka) - \sin k(d - a) \rho_{n+1}'(ka) \right] \tag{C.8}$$

Finally,

$$\int_a^d E_{2R}\, I_{1A}(R)\, dR = \frac{U\, a\, I_{max}}{2n+1} \left[\frac{\rho_{n-1}(kd)}{\rho_{n-1}'(ka)} - \cos k(d-a) \frac{\rho_{n-1}(ka)}{\rho_{n-1}'(ka)} \right.$$

$$\left. - \frac{\rho_{n+1}(kd)}{\rho_{n+1}'(ka)} + \cos k(d-a) \frac{\rho_{n+1}(ka)}{\rho_{n+1}'(ka)} \right] \qquad (5.92)$$

APPENDIX D

NUMERICAL EVALUATION OF B_n

The functions shown in the evaluation of the coefficients B_n of an infinite series expressing an induced surface current on a hemispherical ground plane are the weighted spherical Hankel functions of the second kind andtheir derivatives.

These functions $\rho_n(x)$ can be expressed in the form of a series such as

$$\rho_n(x) = x\, h_n^{(2)}(x) = (j)^{n+1}\, e^{-jx} \sum_{k=o}^{n} (n+\frac{1}{2}, k)\, \frac{1}{(2jx)^k} \qquad (D.1)$$

where

$$(n+\frac{1}{2}, k) = \frac{(n+k)!}{k!\,\Gamma(n-k+1)}$$

$$\Gamma(z+1) = z! \qquad z: \text{ integers}$$

$$h_n^{(2)}(x) = \sqrt{\frac{\pi}{2x}}\, H_{n+\frac{1}{2}}^{(2)}(x) \qquad \text{and} \quad j = \sqrt{-1}$$

Also, from the recurrence relations of Hankel functions, the following relationship between the spherical Hankel functions and their derivatives can be obtained (Ref. 18).

$$\frac{d}{dx} h_n^{(2)}(x) = h_{n-1}^{(2)}(x) - \frac{n+1}{x} h_n^{(2)}(x) \qquad \text{(D. 2)}$$

and

$$\frac{d\rho_n(x)}{dx} = \frac{d}{dx}\left(x\, h_n^{(2)}(x)\right) = h_n^{(2)}(x) + x \frac{d}{dx} h_n^{(2)}(x) \qquad \text{(D. 3)}$$

From Eqs. D. 2 and D. 3, the following relationships are derived

$$\rho'_o(x) = \frac{d\,\rho_o(x)}{dx} = h_o^{(2)}(x) - x\, h_1^{(2)}(x) \qquad \text{(D. 4)}$$

$$\rho'_n(x) = \frac{d\,\rho_n(x)}{dx} = x\, h_{n-1}^{(2)}(x) - n\, h_n^{(2)}(x) \qquad \text{(D. 5)}$$

$$\rho_n(x) = x\, h_n^{(2)}(x) \qquad \text{(D. 6)}$$

Equations D. 4, D. 5, and D. 6 are used with a table for spherical Hankel functions to evaluate the coefficients B_n.

APPENDIX E

EVALUATION OF R_{r_1} in Eq. 5.168

From the power series representation of cosine integral Ci(z), Eq. 5.165, the terms associated with cosine integral of a small argument can be written as

$$\lim_{\epsilon \to 0} \mathrm{Ci}\Big(2k(a+h)\,\epsilon\Big) \approx \gamma + \ell n\, 2k(a+h) + \lim_{\epsilon \to 0} \ell n(\epsilon) \qquad \text{(E.1)}$$

$$\lim_{\epsilon \to 0} \mathrm{Ci}(2ka\,\epsilon) \approx \gamma + \ell n(2ka) + \lim_{\epsilon \to 0} \ell n(\epsilon) \qquad \text{(E.2)}$$

$$\lim_{\epsilon \to 0} \mathrm{Ci}\, k(2a+h)\,\epsilon \approx \gamma + \ell n\Big(k(2a+h)\Big) + \lim_{\epsilon \to 0} \ell n(\epsilon) \qquad \text{(E.3)}$$

$$\lim_{\epsilon \to 0} \mathrm{Ci}(kh\epsilon) \approx \gamma + \ell n(kh) + \lim_{\epsilon \to 0} \ell n(\epsilon) \qquad \text{(E.4)}$$

Substituting Eq. E.1 through Eq. E.4 into appropriate places in (1) through (6)

$$R_{r_1} = 60 \Bigg\{ \ell n\, 2 - \lim_{\epsilon \to 0} \ell n\, \epsilon + \gamma + \lim_{\epsilon \to 0} \ell n(\epsilon) + \ell n(kh) - \frac{1}{2} \cos 2k(a+h)\, \ell n(2ka)$$

$$- \frac{1}{2} \cos 2k(a+h)\, \ell n\, 2k(a+h) + \cos 2k(a+h)\, \ell n(2a+h)k - \mathrm{Ci}(2kh)$$

$$+ \frac{1}{2} \cos 2k(a+h)\, \mathrm{Ci}(4ka) + \frac{1}{2} \sin 2k(a+h)\, \mathrm{Si}(4ka) - \Big(1 - \frac{\sin 2ka}{2ka}\Big) \sin 2kh$$

$$- \cos 2k(a + h)\, \mathrm{Ci}\Big(2k(a + h)\Big) - \sin 2k(a + h)\, \mathrm{Si}\Big(2k(2a + h)\Big)$$

$$+ \frac{1}{2} \cos 2k(a + h)\, \mathrm{Ci}\Big(4k(a + h)\Big) + \frac{1}{2} \sin 2k(a + h)\, \mathrm{Si}\Big(4k(a + h)\Big) \qquad \text{(E. 5)}$$

It should be noticed that the coefficients of γ and $\ell n(\epsilon)$ associated with the cosine integrals add up to 1. This can be shown easily after some algebraic manipulation with trigonometric identities.

After cancelling out the logarithmic singularities in Eq. E. 5 and collecting terms, the final form of Eq. E. 5 can be shown as Eq. 5. 168.

REFERENCES

1. S. J. Bardeen, "The Diffraction of a Circularly Symmetrical Electromagnetic Wave by a Coaxial Circular Disc of Finite Conductivity," Physical Review, Vol. 36, Nov. 1930, p. 1482.

2. G. H. Brown & O. M. Woodward, Jr., "Experimentally Determined Impedance Characteristics of Cylindrical Antennas," Proc. IRE, April 1945, p. 257.

3. A. Leitner & R. D. Spence, "Effect of a Circular Ground Plane on Antenna Radiation," J. Appl. Phys., Vol. 21, Oct. 1950, p. 1001.

4. J. E. Storer, "The Impedance of an Antenna Over a Large Circular Screen," J. Appl. Phys., Vol. 22, No. 8, Aug. 1951, p. 1058.

5. C. L. Tang, "On the Radiation Pattern of a Base-Driven Antenna Over a Circular Conducting Screen," J. Soc. Indust. Appl. Math., Vol. 10, No. 4, Dec. 1962, p. 695.

6. J. R. Wait & W. A. Pope, "Input Resistance of L. F. Unipole Aerials," Wireless Engineers, May 1955, p. 131.

7. G. H. Brown, R. F. Lewis, & J. Epstein, "Ground Systems as a Factor in Antenna Efficiency," Proc. IRE, Vol. 25, 1937, p. 753.

8. F. R. Abbot, "Design of Buried R. F. Ground Systems," Proc. IRE, Vol. 40, 1952, p. 846.

9. R. King & C. W. Harrison, "The Distribution of Current Along a Symmetrical Center-Driven Antenna," Proc. IRE, Oct. 1943, p. 548.

10. H. Whiteside & R. King, "The Loop Antenna as a Probe," IEEE Trans. Antennas & Propagation, Vol. AP-12, May 1964, p. 291.

11. H. Jasik (Editor), Antenna Engineering Handbook, McGraw-Hill Book Co., Inc., New York, 1961.

12. R. W. King, Fundamental Electromagnetic Theory, Dover Publication, Inc., New York, 1963.

REFERENCES (CONT.)

13. J. E. Storer, "Impedance of Thin Wire Loop Antennas," Trans. AIEE (Comm. and Electronics), November 1956, p. 606.

14. J. A. Stratton, Electromagnetic Theory, McGraw-Hill Book Co., Inc., New York, 1941.

15. O. Norgorden & A. W. Walters, "Experimentally Determined Characteristics of Cylindrical Sleeve Antennas," J. Am. Naval Engrs., May 1950, p. 365.

16. C. H. Papas & R. King, "Surface Currents on a Conducting Sphere Excited by a Dipole," J. Appl. Phys., Vol. 19, Sept. 1948, p. 808.

17. W. Magnus & F. Oberhettinger, Formulas and Theorems for the Functions of Mathematical Physics, Chelsea Publishing Co., New York, 1954.

18. M. Abramowitz & I. Stegun (Editors), Handbook of Mathematical Functions With Formulas, Graphs, and Mathematical Tables, NBS Applied Math. Series 55, June 1964.